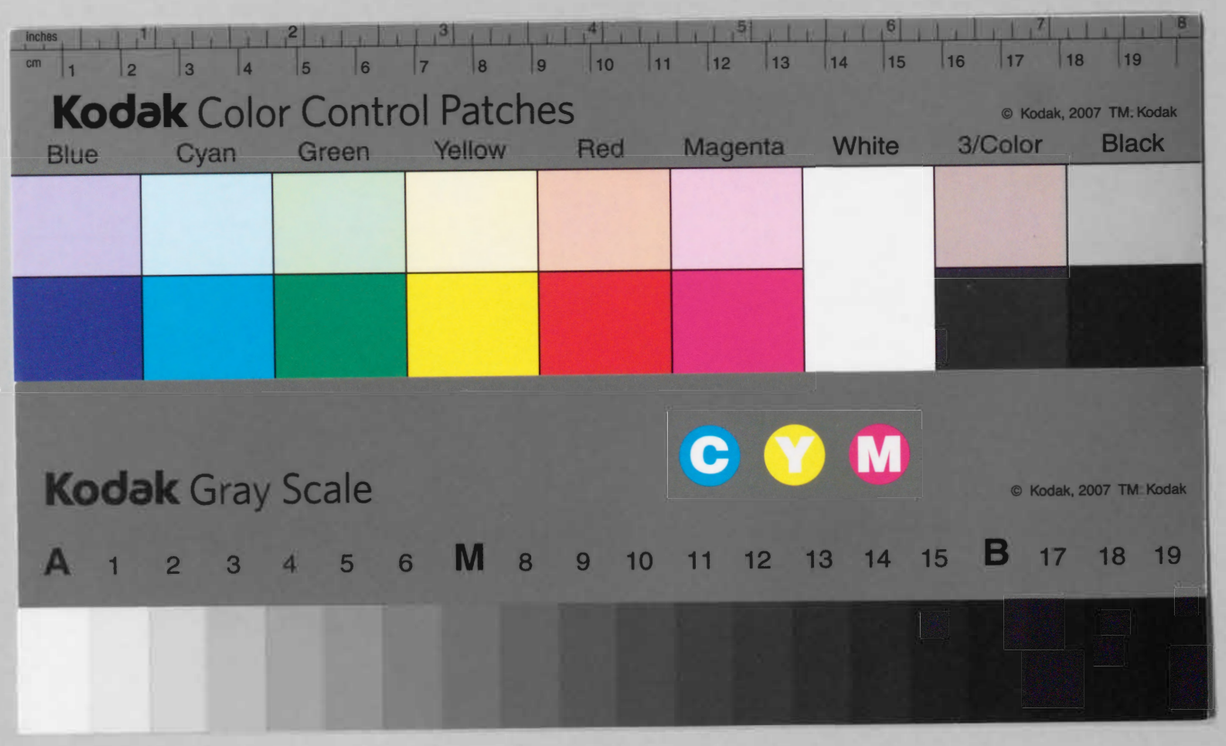
inches
cm
Kodak Color Control Patches
© Kodak, 2007 TM: Kodak
Blue
Cyan
Green
Yellow
Red
Magenta
White
3/Color
Black
C
Y
M
Kodak Gray Scale
© Kodak, 2007 TM: Kodak
A 1 2 3 4 5 6 M 8 9 10 11 12 13 14 15 B 17 18 19

様式6

論　文　目　録

報告番号	甲　工 (乙　工)　第 **22** 号 工　修	氏名	上 田 哲 史
学位論文題目	Bifurcation and Controlling Chaos in Nonlinear Dynamical Systems		

論文の目次

参考論文

主論文

1. 上田哲史, 川上 博. “ジョセフソン接合素子を含む回路に生じるヘテロクリニック軌道の分岐”. 電子情報通信学会論文誌, Vol. J76-A, No.10, pp. 1450–1456, 1993.
2. Tetsushi UETA and Hiroshi KAWAKAMI. “Bifurcation of an Inductively Coupled Josephson Junction Circuit”. IEICE Trans. Fundamentals, Vol. E77-A, No.11, pp. 1758–1763, 1994.
3. Tetsushi UETA and Hiroshi KAWAKAMI. “Composite Dynamical System for Controlling Chaos”. IEICE Trans. Fundamentals, Vol. E78-A, No.6, pp. 708–714, 1995.
4. Tetsushi UETA, Hiroshi KAWAKAMI, Ikuro MORITA. “A Study of the Pendulum Equation with a Periodic Impulsive Force — Bifurcation and Control —”. IEICE Trans. Fundamentals, Vol. E78-A, No.10, pp. 1269–1275, 1995.

副論文

1. 田中芳夫, 上田哲史, 川上 博. “球面振子を有するクレーンのシミュレーション法”. 日本機械学会論文集, Vol.59, No. 559–C, pp. 186–190, 1993.
2. Yoshio TANAKA, Yasuo YOSHIDA, Tetsushi UETA, and Hiroshi KAWAKAMI. “Vibration Suppressing Control of Flexible Rotary Crane Using Tip Position Sensor”. Journal of Robotics and Mechatronics, Vol.4, No.6, pp. 520–525, 1993.
3. Yoshio TANAKA, Tetsushi UETA, Hiroshi KAWAKAMI and Takashi SUMITOMO, “A Robotic Truck Crane with Vibration Sensors”, Journal of Robotics and Mechatronics, Vol.7, No.3, pp.213–217, 1995.
4. 高坂拓司, 上田哲史, 川上 博, “不安定化制御によるカオスの一生成法”. 電子情報通信学会論文誌, Vol. J79-A, 1996(印刷中)

備考
1　論文目録は，用語が英語以外の外国語のときは日本語訳をつけて，外国語，日本語の順に列記すること．
2　参考論文は，論文題目，著者名，公刊の方法及び時期を順に明記すること．
3　参考論文は，博士論文の場合に記載すること．

様式7

論 文 内 容 要 旨

報告番号	甲　工 (乙　工) 工　修　第 **22** 号	氏名	上 田 哲 史
学位論文題目	Bifurcation and Controlling Chaos in Nonlinear Dynamical Systems		

本論文は，非線形常微分方程式で記述された力学系の分岐現象の解析，およびカオス制御の問題と応用について述べている．

強制外力を加えた振り子結合系，ジョセフソン接合素子の結合系（超電導量子干渉計）などの力学系は，常微分方程式に三角関数を含んでいる．そのため，状態空間とパラメータ空間との積空間において周期性を有し，観測される現象もその周期性を反映して複雑になっている．これら力学系にみられる平衡点，周期解の分岐現象を解析し，解の振舞いの定性的性質を検討する．

第2章では，回転方向に弾性復元力をもつ振り子を取り上げ，パラメータの変化に伴い発生するヘテロクリニック軌道の分岐構造を解明した．また，2個の振り子を，弾性復元力のある梁で接続した場合と，クラッチを有する剛体で接続した場合について，定トルクを加えたとき発生する平衡点，周期解の分岐の詳細を検討した．これらの解析により，従来知られていなかった，高次元回転系の大域的な解の振舞いを定性的に説明することができている．

連続系においてカオス応答がみられるとき，そのカオスアトラクタ中に埋め込まれている不安定な周期軌道を安定化する問題をカオス制御という．第3章では，カオス制御理論についての新手法，およびその応用を述べている．従来のカオス制御系の手法の多くは，離散系に対してのみ制御器を構成していたが，本手法では，ポアンカレ写像から導かれる離散系の周期点を安定化する制御器を設計し，状態フィードバックを極配置法で構成する．その制御入力を元の微分方程式系のパラメータへ摂動として加える．つまり，差分方程式系と微分方程式との組合せによる合成力学系での制御系設計を提案している．応用例としてステッピングモータにみられる脱調現象の制御問題を取り上げた．この脱調現象は周期倍分岐連鎖によって引き起こされるカオスであり，実用上望ましくない運転状態である．まずステッピングモータが周期インパルス列で駆動される振り子と等価であることを導出し，第2章の結果を踏まえ，ポアンカレ写像の構成と分岐の解析を行なった．また，分岐を抑制する制御器の設計とその制御系の数値シミュレーションを行ない，提案した制御方法の有用性を示した．

Bifurcation and Controlling Chaos in Nonlinear Dynamical Systems

April 1996

Tetsushi Ueta

Bifurcation and Controlling Chaos in Nonlinear Dynamical Systems

Tetsushi Ueta

April, 1996

Contents

Acknowledgement

The works presented in this dissertation has been carried out at The University of Tokushima under the advice of Professor Hiroshi Kawakami for 1993–1996.

First of all, I wish to express my great gratitude to Professor Hiroshi Kawakami for his precise direction, continuous encouragement and careful guidance.

I would like to express my appreciation to Professor Yoshizo Takahashi and Professor Shun'ichiro Oe of The University of Tokushima, the members of my thesis committee, for their comments and suggestions, especially for their helpful and critical reading of the dissertation.

I also wish to thank Assistant Professor Tetsuya Yoshinaga of The University of Tokushima. He is also my advisor and his valuable comments are great help for me to proceed my studies.

I would like to acknowledge Associate Professor Yoshifumi Nishio, Tohru Kawabe of The University of Tokushima and their wives for tenderly encouragements and helpful advice together my life.

I am indebted to Dr. Toshio Shoman, Ex-Professor of The University of Tokushima, for his encouragements and financial supports.

I am also indebted to Associate Professor Yuuji Katsuta of Ube National College of Technology and Associate Professor Ikuro Morita of The University of Tokushima for their fruitful discussions.

I would like to thank Professor Ken'ichi Yoshikawa of Nagoya University and Professor Akio Ushida of The University of Tokushima for their encouragements.

I have been influenced from discussions at periodic workshop of Kansai NLP Konshinkai (Ozashiki). Particularly, I would like to thank for valuable comments and encouragements from Associate Professor Toshimitsu Ushio of Osaka University, Associate Professor Takashi Hikihara of Kansai University, Assistant Professor Hiroyuki Nakajima of Kyoto University, for their valuable comments and encouragements.

I would like to thank Associate Professor Kazuyuki Aihara of University of Tokyo, Associate Professor Toshimichi Saito of Hosei University, and Associate Professor Naohiko Inaba of Utsunomiya University for his helpful advice.

I would like to express my appreciation to Associate Professor Tomohiro Kubo and Associate Professor Kenji Ikeda of The University of Tokushima for their technical comments of computations.

Finally my thanks are also due to a number of my colleagues at Department of Information Science and Intelligent Systems, The University of Tokushima.

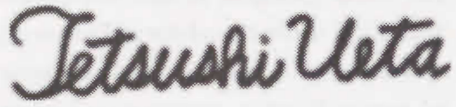

Tetsushi UETA

Chapter 1

Introduction

1.1 Background

During the last few decades topics on nonlinear dynamical systems, especially chaotic phenomena, have been studied by many scientists with great interest. Presently, the chaotic phenomena were reported from wide theoretical and experimental fields; mathematical maps[1], mechanical oscillating system, electric circuits or devices[2], optical electronics, chemical reaction systems[3], biological systems[4], and so on. By mathematician, much attentions are being also paid to clarify what mechanism does chaos occur, many investigations and analyses have been established until today. In the whole of this dissertation we fix our attention on mathematical models derived from physical systems.

Suppose that a physical system is described by a differential equation as :

$$\frac{d\boldsymbol{x}}{dt} = \boldsymbol{f}(t, \boldsymbol{x}, \boldsymbol{\lambda}) \tag{1.1}$$

where $t \in \boldsymbol{R}$ is the time, $\boldsymbol{x}$ is an n-dimensional state, and $\boldsymbol{\lambda} \in \boldsymbol{R}^m$ is a system parameter. If the function $\boldsymbol{f}$ depends explicitly on t, Eq.(1.1) is called *non-autonomous system.* If $\boldsymbol{f}$ has no explicit dependence on t, Eq.(1.1) is called *autonomous system.* It must be emphasized that although Eq.(1.1) does not have unknown, random or stochastic factors, i.e., Eq.(1.1) is derived from deterministic physical processes, however, the system would often behave "complicated and nose-like phenomena — chaos"[5]. As is well known chaotic phenomena are caused by bifurcations, which means changing qualitative characteristics of equilibria, periodic solutions (limit cycles) or the flows on the phase space as the parameter varies continuously. Therefore, in order to understand chaos, it is important to investigate the route along which the periodic solution is bifurcated and the outline of the bifurcations

generated in the system. Thus bifurcation diagrams are quite useful to grasp qualitative properties of the solutions in the parameter region.

Several methods to obtain the bifurcation parameter for Eq.(1.1) are developed. Particularly a mixed qualitative and numerical method is convenient to calculate a fixed point of the Poincaré mapping and the bifurcation parameter simultaneously. The method uses only the solution of Eq. (1.1) and a solution of variational equation with respect to Eq.(1.1). There are many analyses of nonlinear systems described by Eq.(1.1) by using the mixed method. Bifurcation diagrams obtained by these analyses have been great help to explain the global and qualitative properties of the systems.

By the way, a pendulum is a simple physical model containing a sinusoidal function for an angle. The state space has a cyclic coordinate $S^1 \in \boldsymbol{R} : x + 2\pi \rightarrow x$, which is held by regarding that 0 and 2π are identical by a rotation. It is important that these mechanical rotation dynamics are re-produced equivalently as an electric circuit by using the Josephson junctions(abbr. JJ) and phase lock loops(PLL). Some combinations of these devices can be interpreted as actual pendula systems exhibiting interesting nonlinear phenomena influenced by the cyclic coordinates.

While these systems can be described as Eq.(1.1), it is worthy to investigate their qualitative properties by using the analytic or numerical methods because this analysis might be an opportunity to find or clarify unknown phenomena. Moreover, the JJ element is a superconductive device, so it can act greatly fast compared with other electric devices. Therefore if we can obtain a new knowledge or methodology for this device, it might be able to applied as the superconducting quantum interference device (SQUID), or superconducting computers in future. To this end, it is significant to not only consider new architecture of the device but also study the behavior of the solutions in the system by rigorous ways.

Many researches have analyzed the qualitative properties of JJ elements as a nonlinear system by analytical methods or computer simulations from nonlinear theoretical point of view for last two decades. Abidi and Chua[6], Odyniec and Chua[7] [8] investigated the dynamics with a single JJ element forced by d.c. and a.c. They explained global behaviors of the solution on a cylindrical phase space by neglecting the second-order derivative of the differential equation. In coupled JJ circuits with d.c. source, a strange limit cycle called "caterpillar solution" which is winding around the cylindrical space was found by Levi[9]. Doedel reported similar phenomena[10]. However only few studies have so far

been investigated as bifurcation problems, in other words, there are few studies have ever tried to clarify the qualitative properties depending on the parameter variation.

On the other hand, controlling chaos has become a keyword of the nonlinear sciences in recently years. This problem treats stabilization of an unstable fixed or periodic points, called target, embedded in a chaotic attractor. In conventional control problem, because the chaotic state is really undesirable, so the system is obeyed by using a filter, a compensator(integral or differential controller), absorber, etc. However, the whole system including such controllers is no longer the original system, i.e., controlled system is different from the original differential equation since the dimension or parameter is changed.

Otto, Grebogi and Yorke(OGY) proposed an epoch-making method to stabilize the targets of Hénon map [11]. They named their paper "*Controlling Chaos*". At present, an essential of controlling chaos is considered as a control problem using small perturbations of the state or parameter. This can be done by a property that a running chaotic orbit will approach the target eventually (ergodicity). It is interesting that we can only use a proportional-operation feedback to stabilize the target at the parameter in which the system behaves chaotically.

Stabilization methods which have been proposed for controlling chaos may be divided into three types. (1) OGY method, which uses the Poincaré mapping or a return map for the system and its derivatives. (2) Pyragas method[12], which is composed by a continuous state feedback. They are implemented many physical systems: a laser system [13], a ribbon in the magnetic field[14], a heart beat of a rabbit[15]. It is noted that the target can obtained numerically if the system can be described as a mathematical model. Controlling chaos is deeply related to bifurcations since these unstable orbit is caused by bifurcation process, so that a stabilizing method from the bifurcational point of view is required.

1.2 Purpose of the Studies

This dissertation describes on bifurcation phenomena and controlling chaos in nonlinear dynamical systems. The fundamental motivation of the studies is to understand the behavior of mechanical rotational systems; robot arms, coupled pendula, which have some cyclic coordinates in the state space due to the trigonometric characteristics of the rotation dynamics. As a simple model which exhibits rotational motions, we treated the

pendulum systems which have at least a circle S^1. We pick the several models of these pendula and obtain their bifurcation diagrams of the rotations. There is no report about the analysis for rotations containing such cyclic coordinates by a bifurcational point of view.

In Chapter 2, we summarize briefly the method to analyze the bifurcation of periodic solutions, and classify topological properties of bifurcations. Computational method to obtain a local bifurcation; parameter for period doubling, tangent, and Neimark-Sacker bifurcation are discussed.

Firstly we choose a pendulum with an elastic torsional joint. This dynamics can be interpreted as an electric circuit; an L-C-G parallel resonance circuit with a JJ element is described by a second order autonomous equation with linear and sinusoidal restoring forces. In such a system there exist many saddles and sinks caused by varying the linear restoring term. We also investigate heteroclinic bifurcations correlated with separatrices of the saddle points. The topological classification of the heteroclinic orbits is achieved by defining a linking number between the heteroclinic orbit and a suitable cross section.

Secondly, some qualitative properties of the pendula coupled by an elastic torsional joint are also investigated as the second physical model. This model is equivalent to an inductively coupled circuit containing two JJ elements with a d.c. source, which is described by a four-dimensional autonomous differential equation. The phase space can be regarded as $S^1 \times \boldsymbol{R}^3$ because the system is invariant under the action of S^1. We study the properties of periodic solutions winding around S^1 as a bifurcation problem. As a result, the bifurcation diagram of equilibria and its topological classification are obtained. The bifurcation diagram of the periodic solutions winding around S^1 are also calculated by using a suitable Poincaré mapping, and some properties of periodic solutions are discussed. From these analyses, we clarify that a periodic solution so-called "caterpillar solution"[9] is observed when the two JJ circuits are weakly coupled.

As the final example of the coupled pendula, we investigate bifurcation phenomena observed in two dumped pendula linked by a clutch exchanging frictional energy of both pendula. This model has a mechanical analog: the circuit containing two JJ coupled by a resistor. In a similar manner which is applied in previous examples, we study topological properties of the equilibria and bifurcations of the periodic solutions in the system by using Poincaré mapping. There are two types of limit cycles which distinguished by whether the motion is in $S^1 \times \boldsymbol{R}^3$ or $T^2 \times \boldsymbol{R}^2$, because two cyclic coordinates are included

in the state space. The former is a periodic solution and the latter is a quasi-periodic solution. There is a typical structure of tangent bifurcation for 2-periodic solutions with a cusp point. We found chaotic orbits via the period-doubling cascade and a long-period stepwise orbit.

In practical engineering or industrial fields, chaotic motions are frequently undesirable in the regulation or oscillation units with high-accuracy operations or rotations. We also study the method to suppress them by using bifurcation theory. In Chapter 3, we propose a stabilization method for unstable periodic orbits embedded in a chaotic attractor of continuous-time system by using discrete state feedback controller. The control technique is based on the pole assignment of the modern control theory. Although the OGY method cannot control the target which does not have any stable manifold, this method does not depend on the stability of the target. The controller is designed systematically by the Poincaré mapping and its derivatives. Although the output of the controller is applied periodically to system parameter as small perturbations discontinuously, the controlled orbit accomplishes C^0. As the stability of a specific orbit is completely determined by the design of controller, we can also use the method to destabilize a stable periodic orbit. The destabilization method may be effectively applied to escape from a local minimum in various optimization problems. As an example of the stabilization and destabilization, some numerical results of Duffing's equation are illustrated.

Finally, in order to apply the practical implementation of the control for electrical/mechanical system of the engineering fields, the pendulum equation with a periodic impulsive force is investigated. This model described by a second order differential equation is also derived from dynamics of the stepping motor. Firstly, we analyze bifurcation phenomena of periodic solutions observed in a generalized pendulum equation with a periodic impulsive force. There exist two topologically different kinds of solution which can be chaotic by changing system parameters. We try to stabilize an unstable periodic orbit embedded within the chaotic attractor by small perturbations for the parameters. Secondly, we investigate the intermittent drive characteristics of two-phase hybrid stepping motor. We suggest that the unstable operations called pull-out are caused by bifurcations. Finally, we proposed a control method to avoid the pull-out by changing the repetitive frequency and stepping rate. The method not only control the pull-out but also improve the starting characteristics of the stepping motor.

Chapter 2

Bifurcation of Nonlinear Dynamical Systems

2.1 Introduction

The term 'bifurcation' which we treated in this thesis has two senses. The first sense is *local bifurcation* that topological properties of an equilibrium or fixed/periodic point in the system are changed by varying its system parameters. In general, change of qualitative property means changing topological property, i.e., changing hyperbolic property of an equilibrium or a fixed/periodic point. This change is called bifurcation. The bifurcation frequently affects whole motions in state space of the dynamical system, so it is important to investigate the bifurcation in order to understand nonlinear phenomena. Bifurcation of equilibria or fixed/periodic points is called local bifurcation because the phenomena is caused in a point of state space. So we can analyze these phenomena sufficiently by using the linear approximation around the equilibrium point or fixed/periodic point of the Poincaré mapping.

The second sense is qualitative change of the orbit structure in a part of state space. We call it *global bifurcation*. The typical phenomenon with respect to this bifurcation is occurrence of homoclinic or heteroclinic orbits. The linear approximation is not applicable for it anymore, therefore a technique for the global analysis for the orbit structure of dynamical systems is required from various scientific fields. We propose a computational method to obtain these orbits by using the manifolds of the saddle equilibria. We consider the global bifurcation in Section 2.2.

In this section, we summarize fundamental properties of various bifurcation phenomena of equilibria or periodic solutions observed in nonlinear dynamical systems. The Poincaré section, Poincaré mapping and its derivatives are defined. Topological properties of the fixed or periodic point of the Poincaré mapping and codimension-one bifurcations of periodic solution are also discussed. Some computational methods to obtain the fixed point or bifurcation parameter are briefly noted.

2.1.1 Differential Equation and its Poincaré mapping

Let us consider an autonomous system

$$\frac{d\boldsymbol{x}}{dt} = \boldsymbol{f}(\boldsymbol{x}, \boldsymbol{\lambda}) \tag{2.1}$$

and assume that Eq.(2.1) has a solution with initial condition $\boldsymbol{x}_0 = \boldsymbol{x}(0)$, denoted by

$$\boldsymbol{x}(t) = \boldsymbol{\varphi}(t, \boldsymbol{x}_0) \quad \text{with} \quad \boldsymbol{x}(0) = \boldsymbol{\varphi}(0, \boldsymbol{x}_0) = \boldsymbol{x}_0 \tag{2.2}$$

Assume also there exists a periodic solution with a period L such that

$$\boldsymbol{\varphi}(t + L, \boldsymbol{x}_0) = \boldsymbol{\varphi}(t, \boldsymbol{x}_0). \tag{2.3}$$

We define the Poincaré section Π for the trajectory $\boldsymbol{\varphi}(t, \boldsymbol{x}_0)$ such that

$$\Pi = \{\boldsymbol{x} \in \boldsymbol{R}^n \,|\, q(\boldsymbol{x}) = 0\} \tag{2.4}$$

where $\boldsymbol{q}$ is a scalar function:

$$\begin{aligned} q &: \boldsymbol{R}^n \to \boldsymbol{R} \\ x &\mapsto q(\boldsymbol{x}) \end{aligned} \tag{2.5}$$

Suppose that the trajectory $\boldsymbol{\varphi}(t)$ is transverse to Π such that

$$\frac{\partial q}{\partial \boldsymbol{x}} \cdot \boldsymbol{f} \neq 0 \quad {}^\forall \boldsymbol{x} \in \Pi \tag{2.6}$$

Let us suppose also that $\hat{\Pi}$ is a neighborhood of $\boldsymbol{x} \in \Pi$. Then the Poincaré mapping is written as :

$$\begin{aligned} T : \hat{\Pi} &\to \Pi \\ \boldsymbol{x}_1 &\mapsto \boldsymbol{\varphi}(\tau(\boldsymbol{x}_1), \boldsymbol{x}_1). \end{aligned} \tag{2.7}$$

where $\tau(\boldsymbol{x}_1)$ is the time taken for the trajectory based at $\boldsymbol{x}_1$ to first return to Π, which is called first return time. Note that the first return time is a function of $\boldsymbol{x}$. Consequently the fixed point of the mapping is

$$T(\boldsymbol{x}_0) = \boldsymbol{x}_0 \tag{2.8}$$

and its first return time corresponds the period of the periodic solution:

$$L = \tau(\boldsymbol{x}_0) \tag{2.9}$$

To progress concrete computation, let Σ be an $(n-1)$-dimensional hyper-surface corresponding to Π:

$$\begin{aligned} h : \Pi \in \boldsymbol{R}^n &\to \Sigma \subset \boldsymbol{R}^{n-1} \\ \boldsymbol{x} &\mapsto \boldsymbol{w} = h(\boldsymbol{x}) \end{aligned} \tag{2.10}$$

where h is a non-singular and differentiable function called projection or local coordinate. While a parameterization h^{-1} is defined as follows:

$$\begin{aligned} h^{-1} : \Sigma \in \boldsymbol{R}^{n-1} &\to \Pi \subset \boldsymbol{R}^n \\ \boldsymbol{w} &\mapsto x = h^{-1}(\boldsymbol{w}) \end{aligned} \tag{2.11}$$

Let $\hat{\Sigma}$ be an open set such that $\hat{\Sigma} \subset \Sigma$. Then the Poincaré mapping in local coordinate T_ℓ is defined as

$$\begin{aligned} T_\ell : \hat{\Sigma} &\to \Sigma \\ \boldsymbol{w}_1 &\mapsto h(\boldsymbol{\varphi}(\tau(h^{-1}(\boldsymbol{w}_1)), h^{-1}(\boldsymbol{w}_1))) \end{aligned} \tag{2.12}$$

or

$$\begin{aligned} T_\ell : \hat{\Sigma} &\to \Sigma \\ \boldsymbol{w}_1 &\mapsto h \circ T \circ h^{-1}(\boldsymbol{w}_1) \end{aligned} \tag{2.13}$$

It should be noted that a fixed point $\boldsymbol{x}_0$ of T is also a fixed point $\boldsymbol{w}_0$ of T_ℓ. Thus the fixed point of T_ℓ can be obtained by solving the following equation:

$$\boldsymbol{w}_0 - T_\ell(\boldsymbol{w}_0) = \boldsymbol{0} \tag{2.14}$$

It is noted that information about the periodic solution $\boldsymbol{\varphi}(t, \boldsymbol{x}_0)$ of Eq. (2.1) has been reduced as a location of the point $\boldsymbol{w}_0 \in \boldsymbol{R}^{n-1}$ satisfying Eq. (2.14).

The difference equation obtained from (2.1) via the Poincaré mapping is rewritten as

$$\boldsymbol{w}_{k+1} = T_\ell(\boldsymbol{w}_k, \boldsymbol{\lambda}). \tag{2.15}$$

The fixed point $\boldsymbol{w} \in \boldsymbol{R}^{n-1}$ of Eq. (2.15) is defined by

$$\boldsymbol{w} = T_\ell(\boldsymbol{w}, \boldsymbol{\lambda}) \tag{2.16}$$

Similarly the p-periodic point $\boldsymbol{w}' \in \boldsymbol{R}^{n-1}$ of Eq. (2.15) is given by

$$\boldsymbol{w}' = T_\ell^p(\boldsymbol{w}', \boldsymbol{\lambda}) \tag{2.17}$$

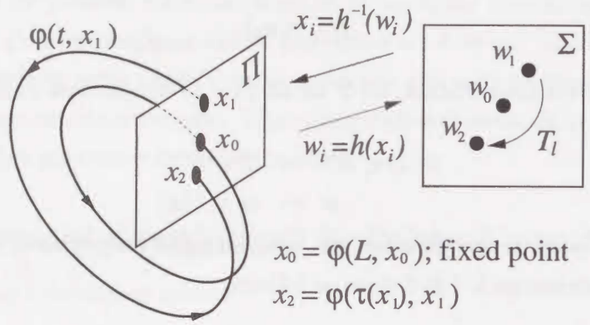

Figure 2.1: Poincaré section Π.

where T_ℓ^p is p-iterated map of T_ℓ. In this section we only treat the fixed point $\boldsymbol{w}$. Since the p-periodic point of the map T_ℓ is equivalent to the fixed point of the map T_ℓ^p, our argument is easily extend to the p-periodic point $\boldsymbol{w}'$.

The stability of the fixed point is determined by the roots of the characteristic equation:

$$|DT_\ell(\boldsymbol{w}) - \mu I_{n-1}| = 0 \tag{2.18}$$

where I_{n-1} is the $(n-1)$-size identity matrix, and $DT_\ell(\boldsymbol{w})$ is a derivative of $\boldsymbol{w}$:

$$DT_\ell(\boldsymbol{w}) = Dh \circ DT \circ Dh^{-1}. \tag{2.19}$$

where Dh, DT and Dh^{-1} are the Jacobi matrices of Eq. (2.10), (2.7) and (2.11). The fixed point $\boldsymbol{w}$ is called hyperbolic or simple if all of the roots $\mu_1, \cdots, \mu_{n-1}$ of the characteristic equation are different from unity.

Let us consider a topological classification of hyperbolic fixed points. Let $\boldsymbol{w}$ be a hyperbolic fixed point and E^u be the intersection of $\boldsymbol{R}^{n-1}$ and the direct sum of the generalized eigenspaces of $DT_\ell(\boldsymbol{w})$ corresponding to the eigenvalues μ_i such that $|\mu_i| > 1$, $i = 1, 2, \cdots, N$. Similarly, E^s be the intersection of $\boldsymbol{R}^{n-1}$ and the direct sum of the generalized eigenspaces of $DT_\ell(\boldsymbol{w})$ corresponding to the eigenvalues μ_j such that $|\mu_j| < 1$, $j = 1, 2, \cdots, M$. E^u(or E^s) is called an unstable (or stable) subspace of $DT_\ell(\boldsymbol{w})$. Then it

is known that E^u and E^s have the following properties:

$$\begin{aligned} \boldsymbol{R}^{n-1} &= E^u \oplus E^s \\ DT_\ell(E^u) &= E^u \\ DT_\ell(E^s) &= E^s \\ N &= \dim E^u = \#\{\mu_i \,|\, |\mu_i| > 1\} \\ M &= \dim E^s = \#\{\mu_j \,|\, |\mu_j| < 1\} \end{aligned} \tag{2.20}$$

where $\#\{\cdots\}$ indicates the number of elements contained in the set $\{\cdots\}$. Let $\mathcal{L}^u = DT_\ell(\boldsymbol{w})|_{E^u}$ and $\mathcal{L}^s = DT_\ell(\boldsymbol{w})|_{E^s}$. Then the topological type of a hyperbolic fixed point is determined by the $\dim E^u$ (or $\dim E^s$) and the orientation preserving or reversing property of $\mathcal{L}^u$ (or $\mathcal{L}^s$).

We define two types of hyperbolic fixed point:

Definition 2.1 *A hyperbolic fixed point $\boldsymbol{w}$ is called*

1. *a direct type (abbr. D-type), if* $\det \mathcal{L}^u > 0$
2. *an inversely type (abbr. I-type), if* $\det \mathcal{L}^u < 0$.

From Definition 2.1, at a D-type of fixed point $\boldsymbol{w}$, $\mathcal{L}^u$ is an orientation preserving mapping, whereas at an I-type of fixed point $\boldsymbol{w}$, $\mathcal{L}^u$ is an orientation reversing mapping. If E^u is an empty set, we identify $\boldsymbol{w}$ as a D-type.

The above classification is also obtained from the distribution of the eigenvalues of $DT_\ell(\boldsymbol{w})$. D-type (resp. I-type) fixed point has even (resp. odd) number of the eigenvalues on the real axis $(-\infty, -1)$. We use the notation ${}_kD_l^m$ (or ${}_kI_l^m$) which denotes a hyperbolic fixed point such that D (or I) indicates a type, k indicates the number of characteristic multiplier outside a unit circle in the complex plane, and m indicates m-periodic point, l indicates the number to distinguish the same type of fixed point. If $m = 1$, it will be omitted.

Generally, for the n-dimensional system, there are $2n$ topologically different types of hyperbolic fixed points. These types are: ${}_kD$ $(k = 0, 1, \cdots, n)$, ${}_kI (k = 0, \cdots, n-1)$. ${}_0D$ is a completely stable fixed point, ${}_nD$ is a completely unstable fixed point, and the others are saddle type fixed points.

2.1.2 Codimension-One Bifurcations

In this section we assemble the result concerning with codimension-one bifurcations [16]. There are three generic codimension-one bifurcations (tangent, period-doubling, Hopf

bifurcation) and one degenerate bifurcation (D-type of branching) for fixed points. Three generic codimension-one bifurcations correspond to eigenvalues $+1$, -1 and a pair of complex conjugate of modulus 1. D-type of branching may appear in the system which possess a symmetrical property. This type of bifurcation occurs when a real eigenvalue passes through the point $(1, 0)$ in complex plane. Hence the bifurcation condition is a degenerate case of the tangent bifurcation.

1. Tangent bifurcation
   The generation or extinction of a couple of fixed points occurs at $\lambda = \lambda_0$ under the variation of parameter λ. The types of bifurcation are

$$\begin{aligned} \phi &\leftrightarrow {}_{k-1}D + {}_kD \\ \phi &\leftrightarrow {}_{k-1}I + {}_kI \end{aligned} \tag{2.21}$$

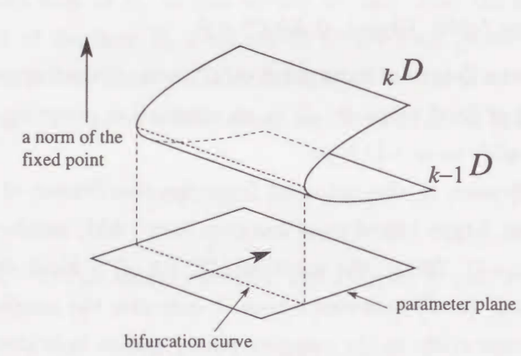

Figure 2.2: Tangent bifurcation

where the symbol $\leftrightarrow$ indicates the relation before and after the bifurcation and ϕ denotes the extinction of fixed points. We use, for convenience's sake, the notation that G denotes the tangent bifurcation parameter set in bifurcation diagram. This type of bifurcation is observed if one of the eigenvalues of Eq. (2.19) satisfies the condition $\mu = 1$.

2. Period-doubling bifurcation
   The types of bifurcations are

$$\begin{aligned} {}_kD &\leftrightarrow {}_{k+1}I + 2_kD^2 \\ {}_kD &\leftrightarrow {}_{k-1}I + 2_kD^2 \\ {}_kI &\leftrightarrow {}_{k+1}I + 2_kD^2 \\ {}_kI &\leftrightarrow {}_{k-1}I + 2_kD^2 \end{aligned} \tag{2.22}$$

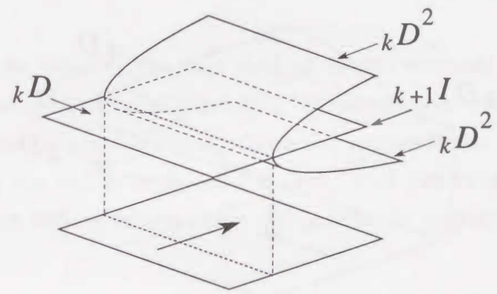

Figure 2.3: Period-doubling bifurcation

where 2_kD^2 indicates two numbers of 2-periodic point of type ${}_kD$. We use the notation that I denotes the period-doubling bifurcation parameter set. This type of bifurcation observed if $\mu = -1$.

3. The Hopf(Neimark-Sacker) bifurcation
   The types of bifurcations are

$$\begin{aligned} {}_kD &\leftrightarrow {}_{k+2}I + ICC \\ {}_kD &\leftrightarrow {}_{k-2}I + ICC \\ {}_kI &\leftrightarrow {}_{k+2}I + ICC \\ {}_kI &\leftrightarrow {}_{k-2}I + ICC \end{aligned} \tag{2.23}$$

   where ICC indicates an invariant closed curve. We use notation that H denotes the Hopf bifurcation parameter set. This type of bifurcation is observed if a simple pair of complex conjugate roots of (2.19) transverse the unit circle of the complex plane.

4. D-type of branching
   The types of bifurcation are

$$
\begin{aligned}
{}_kD &\leftrightarrow {}_{k+1}D + 2_kD \\
{}_kD &\leftrightarrow {}_{k-1}D + 2_kD \\
{}_kI &\leftrightarrow {}_{k+1}I + 2_kI \\
{}_kI &\leftrightarrow {}_{k-1}I + 2_kI
\end{aligned}
\tag{2.24}
$$

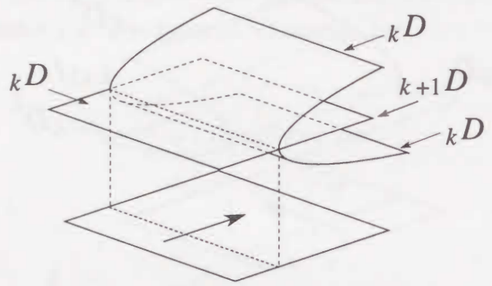

Figure 2.4: D-branching

To obtain the parameters causing above bifurcations, we should solve the following equations for $\boldsymbol{w}_0$, λ simultaneously by a suitable numerical method:

$$
\begin{aligned}
&\boldsymbol{w}_0 - T_\ell(\boldsymbol{w}_0, \lambda) = \boldsymbol{0} \\
&|DT_\ell(\boldsymbol{w}_0, \lambda) - \mu I_{n-1}| = 0
\end{aligned}
\tag{2.25}
$$

where μ is the eigenvalue causing the specified bifurcation. The derivatives of the equations are obtained from the variational equation with respect to $\boldsymbol{w}$ or λ.

2.2 Bifurcation of a Pendulum with an Elastic Torsional Joint

As stated briefly in Chapter 1, a dynamical system in which the angle is a state variable is described by a differential equation containing a trigonometric function of the state variables. Since the state space becomes a manifold constructed by a product space of the angle and its derivative (velocity), the motion might exhibit interesting nonlinear phenomena.

In this section, we consider the case that an elastic restoring force is applied to a pendulum. More precisely, let the pendulum be constrained to a vertical plane. The pivot of the pendulum is attached to a rubber rod perpendicular to the vertical plane, and the terminal of the rod is fixed, see Fig. 2.5. This pendulum system is discussed briefly by Levi[9], but little is known about the qualitative properties.

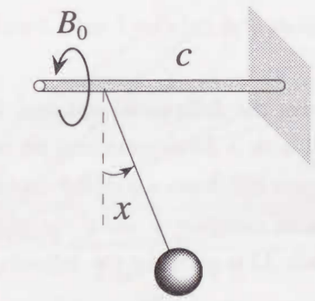

Figure 2.5: A pendulum with a restoring force.

This system is described by the two-dimensional differential equation of conventional damped pendulum with a linear restoring term of the state. As the coefficient of the linear restoring term varies, the periodicity of the solution is lost and the number of equilibria changes. This means the state space can no longer be considered as a cylindrical phase space. Topological structure of a basin of attraction for a stable equilibrium into which the orbits flow changes as the parameters vary. Between these changes there exist many heteroclinic orbits connecting between saddles. We found various types of heteroclinic orbit in case that system is weakly coupled. It is noteworthy that this model has an

equivalent electric analog: an L-C-G parallel circuit containing a JJ element.

Firstly we analyze tangent bifurcations of equilibria of the system, and clarify the periodicity of states and parameters. It suggests that the parameter range to be analyzed can be restricted. Secondly we calculate the bifurcation sets which indicate parameter value causing heteroclinic orbits. The topological classification for the basins of attractions are done by the bifurcation diagrams and linking numbers.

2.2.1 System Equation

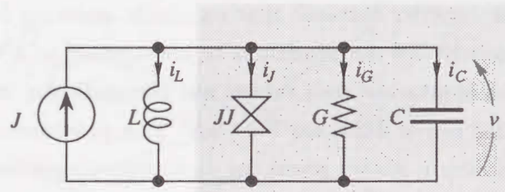

Figure 2.6: A parallel circuit of an inductor L and a Josephson junction element.

Since it is very easy to derive the differential equation from the damped pendulum, we introduce the circuit model with a JJ element and its equivalence for the pendulum with elastic torsional joint. Figure 2.6 shows a parallel circuit composed by an equivalent circuit of the JJ element, a linear inductor L and a d.c. current source J. The current and voltage characteristics of the JJ is given by the following equations[17]:

$$\begin{aligned} i_j &= I_C \sin\phi \\ \frac{d\phi}{dt} &= \frac{2e}{\hbar} v \end{aligned} \tag{2.26}$$

In an actual junction, the G is regarded as a voltage-controlled nonlinear conductor, however we assume it as a linear for the convenience sake. $\hbar$ and ϕ are Dirac's constant and the phase difference of the wave function at the center of the junction, respectively. The normalized circuit equation is as follows:

$$\begin{aligned} \frac{dx}{dt} &= y \\ \frac{dy}{dt} &= -ky - cx - \sin x + B_0. \end{aligned} \tag{2.27}$$

where

$$\begin{aligned} k &= G\sqrt{\frac{\hbar}{2eI_C C}} \\ c &= \frac{\hbar}{2eLI_C} \\ B_0 &= \frac{J}{I_C} \end{aligned} \tag{2.28}$$

2.2.2 Classification of Equilibria

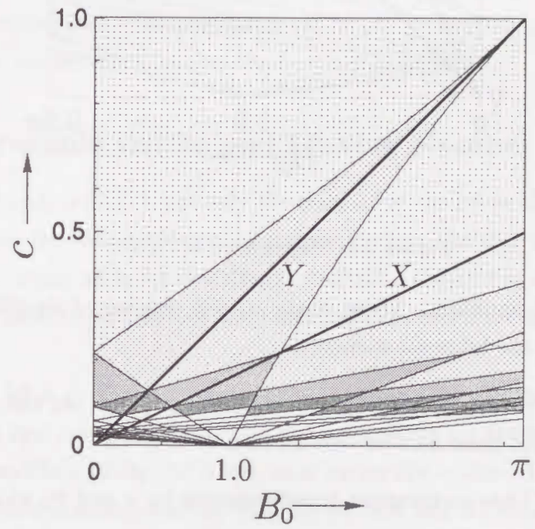

Figure 2.7: Bifurcation diagram of the equilibria with classification of the equilibrium point by number. For example, a sink is in section [ ] and 2 sinks and a saddle are in section [ ], and 3 sinks and 2 saddles are in section [ ], and so on. Number of equilibriua increases as c tends to 0.

The number of equilibria in Eq. (2.27) varies according to the values of parameter c and B_0. Figure 2.7 and 2.8 show the classification of equilibria by the numbers. The following facts are found:

1. The pieces of lines in the figures (except for the lines X and Y and dotted lines a and b) indicate tangent bifurcation for equilibria, i.e. these lines indicate alternation of

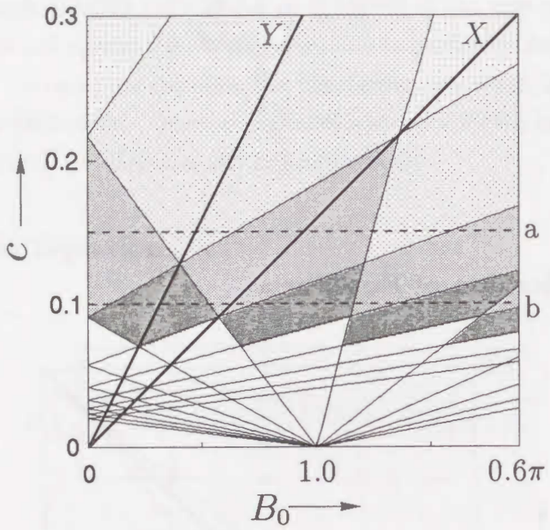

Figure 2.8: Magnification of Fig.2.7

the number of equilibria. There exists an odd number of equilibria in the region surrounded by the bifurcation curves.

2. For $c > 1$ there exists only one stable equilibrium point. As the c decreases, equilibria appear and their number reaches infinity at $c = 0$.

3. Equation (2.27) has an invariant transformation for x and B_0 when c is fixed:

$$(x, B_0) \to (x + 2n\pi, B_0 + 2nc\pi), \quad n = 0, \pm 1, \pm 2, \cdots \tag{2.29}$$

Hence,

$$B_0 = B_0^* \bmod 2c\pi \tag{2.30}$$

is held for an arbitrary B_0, where $0 \leq B_0^* < 2c\pi$. We can observe all typical phenomena around the equilibria in the parameter region surrounded by $B_0 = 0$ and $B_0 = 2c\pi$ (straight line X).

4. The following equation is also held :

$$(x, B_0) \to (2n\pi - x, 2nc\pi - B_0), \quad n = 0, \pm 1, \pm 2, \cdots \tag{2.31}$$

From Eqs.(2.30) and (2.31), two regions $0 \leq B_0^* < c\pi$ and $c\pi \leq B_0^* < 2c\pi$ are axially symmetric about $B_0 = c\pi$ (straight line Y) in Fig.2.7. The phase portrait in each region becomes identical under the following transformation:

$$(x, y) \to (2\pi - x, -y) \tag{2.32}$$

5. At fixed c, when B_0 varies, the number of equilibria increases or decreases with two as a unit. Hence the dotted line a ($c = 0.15$) in Fig.2.8 crosses two regions which have three or five equilibria only. While the dotted line b ($c = 0.1$) crosses two regions which have five or seven equilibria only.

From these investigations the parameter regions to be studied can be restricted substantially and the estimation of the results becomes possible.

2.2.3 Heteroclinic Orbits and Linking Number

In the dynamical system (2.27), not only the number of equilibria changes as the parameters vary but also the shape of basin boundary changes. In this section we define the linking number to make an index describing qualitative changes of the equilibria and orbits on the phase portrait and discuss the relationship between the index and heteroclinic orbits.

In Eq.(2.27), let $k > 0$ and $c = c_0 > 0$. Assume that the maximum numbers of $2m + 1$ equilibria that can be generated by the parameters are given by an arbitrary B_0. In general, the equilibria of Eq.(2.27) are lined up on the x axis. Thus these points are assigned with natural numbers starting with the left end and are expressed as $(x_i, 0)$. The equilibria are ether stable or saddles which are indicated by S and D. The symbols S and D are assigned independently with natural numbers from leftmost points of the same kind on the x axis:

$$\begin{gathered} S_1(x_1, 0),\ D_1(x_2, 0),\ S_2(x_3, 0),\ D_2(x_4, 0), \cdots, \\ S_m(x_{2m-1}, 0),\ D_m(x_{2m}, 0),\ S_{m+1}(x_{2m+1}, 0) \\ x_1 < x_2 < \cdots < x_{2m} < x_{2m+1}. \end{gathered} \tag{2.33}$$

The combined ensemble of the open sections:

$$]D_1, D_2[, \quad]D_2, D_3[, \cdots,]D_{m-1}, D_m[\tag{2.34}$$

is written by an interval L on x-axis as follows:

$$L = \bigcup_{k=1}^{m-1}]D_k, D_{k+1}[\tag{2.35}$$

Let two ω branches started from the saddle D_i be

$$\omega_{ij} = \{(x,y) \in \boldsymbol{R}^2 \mid \lim_{t\to\infty}(x(t), y(t)) = D_i\}, \quad j = 1, 2. \tag{2.36}$$

Definition 2.2 *Let half-line L and $\omega_{ij}, i = 1, 2, \cdots, m; j = 1, 2$ be given as above. Then a linking number of L and ω_{ij} is defined as*

$$\ell_{ij} = \#\{L \cap \omega_{ij}\} \quad i = 1, 2, \cdots, m; j = 1, 2. \tag{2.37}$$

where $\#E$ indicates the number of elements in the set E. ℓ_{ij} also indicates the number of intersections for L and the ω branch. See Fig. 2.9. The linking number is given by a matrix, which is called a crossing matrix, with $(2 \times m)$ integer elements:

$$\mathcal{C} = [\ell_{ij}] \tag{2.38}$$

For example, in case that Fig. 2.9 we have

$$\mathcal{C} = \begin{bmatrix} 0 & 2 & 0 \\ 0 & 1 & 0 \end{bmatrix} \tag{2.39}$$

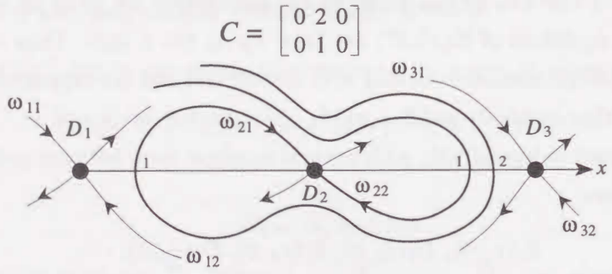

Figure 2.9: Definition of linking number.

When the linking number ℓ_{ij} either increases of decrease while the parameters (B_0, k) are varied continuously, the variation of ℓ_{ij} implies the existence of a heteroclinic orbit. This fact is clear from uniqueness of solutions since the system (2.27) is autonomous. In

planer and autonomous dynamical system, the heteroclinic orbit is structurally unstable. Therefore the parameter values which cause such orbit can be regarded as a bifurcation parameter.

In the region surrounded by the bifurcation curves, a unique crossing matrix is obtained. It is easy to reconstruct the phase portrait from factors of the matrix. Hence we obtain the qualitative index for the shape of the basin of attractions.

2.2.4 Calculation of the Heteroclinic Orbit

To calculate the heteroclinic orbit we extend the method which is designed to calculate a separatrix loop discussed in [18].

Let the solution of Eq.(2.27) starting from an initial value (x_0, y_0) at $t = 0$ be described as $x(t) = \varphi(t, x_0, y_0, \lambda_0)$ and $y(t) = \psi(t, x_0, y_0, \lambda_0)$ where λ_0 is a parameter. Let us write a heteroclinic orbit as $h(D_i, D_j)$, where D_i and D_j are the saddles, and the α and ω limit sets of the orbit become these saddles, respectively. Let a point on the α-branch away from D_i by δ_i be (x_α, y_α). Similarly (x_ω, y_ω) is also defined by the ω-branch. The existence of a heteroclinic orbit requires that, on a suitable cross section M, the location of the solution started from (x_α, y_α) after an interval τ_α in correct time coincides the location of the solution started from (x_ω, y_ω) after an interval τ_ω in reverse time:

$$M = \left\{ (x,y) \in \boldsymbol{R}^2 \;\middle|\; \begin{array}{l} \varphi(\tau_\alpha, x_\alpha, y_\alpha, \lambda) - \varphi(-\tau_\alpha, x_\omega, y_\omega, \lambda) = 0 \\ \psi(\tau_\omega, x_\alpha, y_\alpha, \lambda) - \psi(-\tau_\omega, x_\omega, y_\omega, \lambda) = 0 \end{array} \right\} \tag{2.40}$$

For more precise scheme, see Ref.[18].

2.2.5 Results

2.2.5.1 Case $c = 0.15$

This value of c corresponds to the dotted line in Fig.2.8. Figure 2.10 shows the bifurcation diagram when B_0 is varied along this line from $B_0 = 0$ to $B_0 = 2c\pi$ (the line X). Let us enumerate features of the diagram.

1. Figure 2.10 is axially symmetric with respect to $B_0 = 0.15\pi$ (vertical dotted line). This is due to the property 3, 4 in Sect. 2.3.4.

2. The intersection of the dotted line a in Fig. 2.8 and the tangent bifurcation curve corresponds to the lines G_1 and G_2 in Fig.2.10. There are five equilibria; three of

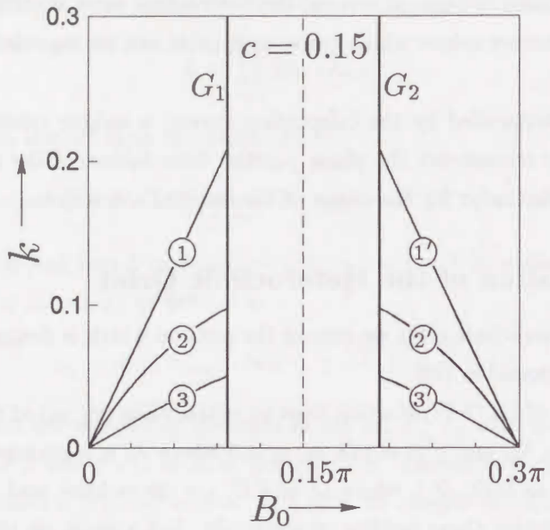

Figure 2.10: Bifurcation diagram in (B_0, k) by heteroclinic orbits at $c = 0.15$.

sinks S_1, S_2 and S_3 and two saddles D_1 and D_2 in each region $0 < B_0 < B_0(G_1)$ or $B_0(G_2) < B_0 < 0.3\pi$. In the region $B_0(G_1) < B_0 < B_0(G_2)$ we have three equilibria; two sinks and one saddle. $B(G_1) = 0.3044$ and $B_0(G_2) = 0.6381$.

3. Figures 2.11–2.13 show $h(D_1, D_2)$ orbits according to the bifurcation curve ①–③ in Fig. 2.10, respectively. The phase structures of these orbits are not homeomorphic each other. As k becomes smaller, the heteroclinic orbit wound more times around D_2. The bifurcation curves ①′ to ③′ are $h(D_2, D_1)$ and coincide with the orbits given by the bifurcation ①– ③ via transformations Eqs. (2.31) and (2.32).

4. A crosspoint of an arbitrary bifurcation curve and G_i is a codimension two bifurcation at which the tangent bifurcation of equilibria and heteroclinic orbit occurr simultaneously.

2.2.5.2 Case $c = 0.1$

This value of c corresponds to the dotted line b in Fig. 2.8. Figure 2.20 shows the bifurcation diagram when B_0 is varied along this line from $B_0 = 0$ to $B_0 = 2c\pi$ (the line

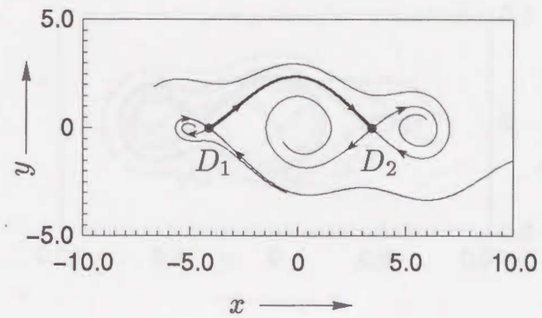

Figure 2.11: Phase portrait of $h(D_1, D_2)$ type orbit obtained on the curve ① in Fig. 2.10. $B_0 = 0.2, k = 0.1359$.

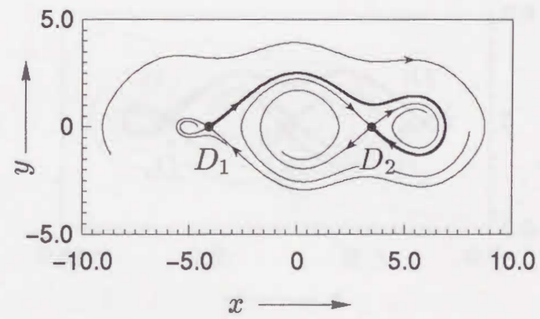

Figure 2.12: Phase portrait of $h(D_1, D_2)$ type orbit obtained on the curve ② in Fig. 2.10. $B_0 = 0.2, k = 0.07576$.

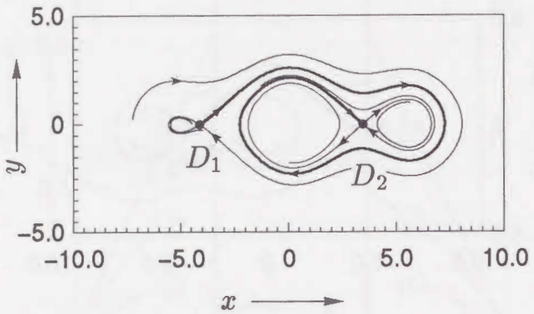

Figure 2.13: Phase portrait of $h(D_1, D_2)$ type orbit obtained on the curve ③ in Fig.2.10. $B_0 = 0.2, k = 0.03508$.

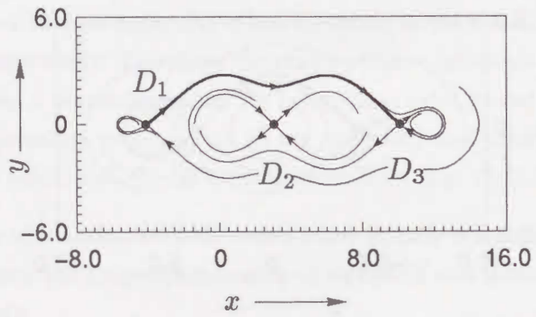

Figure 2.14: Phase portrait of $h(D_1, D_3)$ type orbit obtained on the curve ④ in Fig.2.20. $B_0 = 0.4, k = 0.04327$.

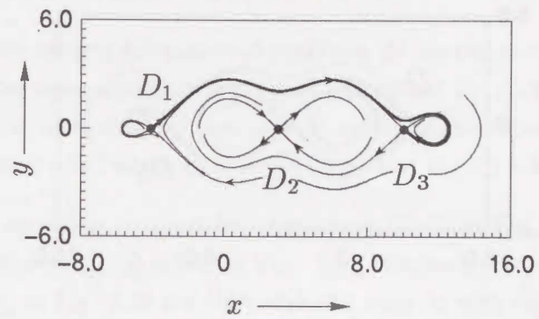

Figure 2.15: Phase portrait of $h(D_1, D_3)$ type orbit obtained on the curve ⑤ in Fig.2.20. $B_0 = 0.4, k = 0.03798$.

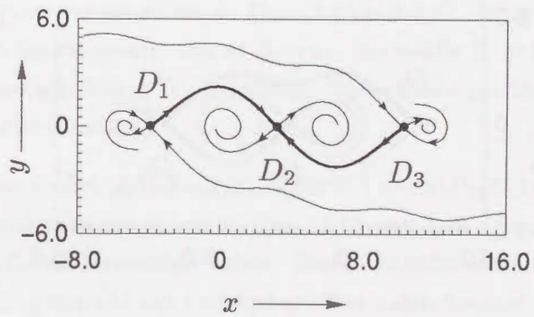

Figure 2.16: Phase portrait of $h(D_1, D_2)$ and $h(D_3, D_2)$ type orbits obtained on the point ⓐ in Fig.2.20. $B_0 = 0.3142, k = 0.2248$.

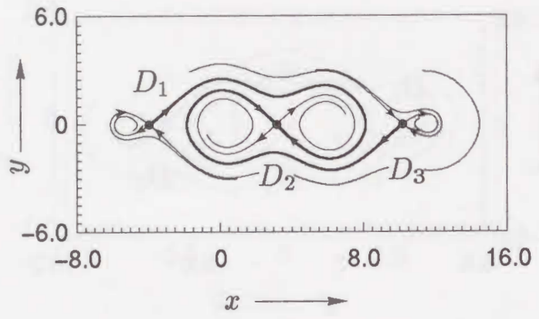

Figure 2.17: Phase portrait of $h(D_1, D_2)$ and $h(D_3, D_2)$ type orbits obtained on the point ⓒ in Fig.2.20. $B_0 = 0.3142, k = 0.07895$.

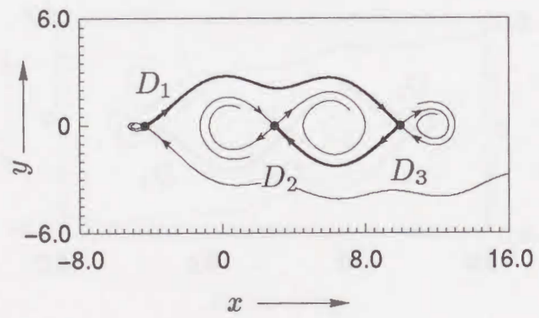

Figure 2.18: Phase portrait of $h(D_1, D_3)$ and $h(D_3, D_2)$ type orbits obtained on the point ⓑ in Fig.2.20. $B_0 = 0.4980, k = 0.09294$.

X). Let us enumerate features of the diagram.

1. Figure 2.20 is axially symmetric with respect to $B_0 = 0.1\pi$ (vertical dotted line). This is similar to the property 1 in Sect. 2.2.5.1.

2. G_1 and G_2 are tangent bifurcation of equilibria. In the region surrounded by G_1 and G_2 there exist seven equilibria (S_1, S_2, S_3 and S_4 and D_1, D_2 and D_3). There exist five equilibria (these sinks and two saddles) outside of this region ($0 < B_0 < B_0(G_2)$, $B_0(G_1) < B_0 < 0.2\pi$) where $B_0(G_2) = 0.09455$ and $B_0(G_1) = 0.5338$.

3. The orbits according to the bifurcation curve ①–③ in Fig. 2.20 are $h(D_1, D_2)$ and equivalent to ①–③ orbits in Fig. 2.10. Similarly the orbits on bifurcation curves ①'–③' in Fig. 2.10 are $h(D_2, D_1)$ and coincide with the orbits given by the bifurcation ①'– ③' in Fig.2.20.

4. The orbits $h(D_2, D_3)$ and $h(D_2, D_1)$ could not for $k > 0$.

5. In contrast to the case of $c = 0.15$, there exists a new type of heteroclinic orbit $h(D_1, D_3)$, see Figs. 2.14 and 2.15. Their bifurcation curves are marked by ④ and ⑤ in Fig. 2.20. There also exist bifurcation curves ④' and ⑤' of $h(D_3, D_1)$ which can be regarded as symmetry to ④ and ⑤ via relationship (2.31) and (2.32).

6. At the points ⓐ and ⓒ in Fig. 2.20, $h(D_1, D_2)$ and $h(D_3, D_2)$ exist simultaneously. The phase portraits are shown in Figs. 2.16 and 2.17. Since the parameter takes the value on the symmetric axis of $B_0 = c\pi$, the saddle $D_2 = (\pi, 0)$ is a fixed point of transformations Eqs.(2.31) and (2.32). These phase portraits are also invariant for these transformations.

7. At the points ⓑ and ⓓ in Fig.2.20, $h(D_1, D_3)$ and $h(D_3, D_2)$ exist simultaneously. The phase portraits are shown in Figs. 2.18 and 2.19. D_3 is both the α and ω limits for different heteroclinic orbits. Hence the bifurcation curves ② and ③ for $h(D_1, D_2)$ are generated and vanished at these points because a part of the orbit of $h(D_1, D_2)$ are coalesced to D_3 due to the change of the parameters (B_0, k).

2.2.5.3 Details of the linking number and bifurcations

Figure 2.21 shows a magnification of Fig. 2.20. The crossing matrices are also indicated in every region.

1. There exist $h(D_1, D_3)$ orbit indicated by ⑤. Since this orbit is similar to ④, any $h(D_1, D_2)$ curves, e.g., ②', ③' etc., are terminated by this bifurcation.

2. It is possible to determine the crossing matrix $\mathcal{C}$ in each region surrounded by the bifurcation curves. When the parameter (B_0, k) moves from one region to an adjacent region, one of the elements in the crossing matrix or the linking number varies by one. The exception is the region surrounded by the bifurcation curves ④ and ⑤.

3. There exists the region surrounded by the bifurcation curves ④ and ⑤. The interior of this region is subdivided into smaller regions by the traversing bifurcation curves of $h(D_3, D_2)$. For the change of the parameter exceeding the adjacent subdivided small region, the linking number in a crossing matrix changes by two. This is considered to be the phenomenon that the traversing bifurcation curve of $h(D_3, D_2)$ preserves the property of codimension two bifurcation at the intersection between the bifurcation curves ④ and ⑤. (such as ⓑ, ⓑ', ⓓ and ⓓ')

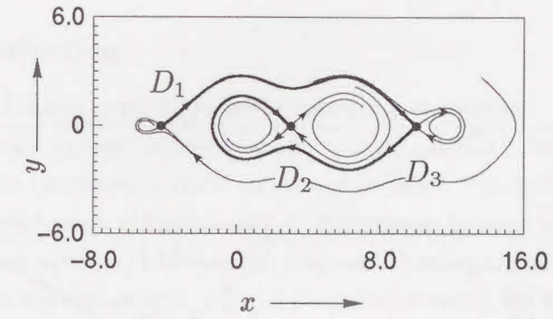

Figure 2.19: Phase portrait of $h(D_1, D_3)$ and $h(D_3, D_2)$ type orbits obtained on the point ⓓ in Fig.2.20. $B_0 = 0.4310, k = 0.05992$.

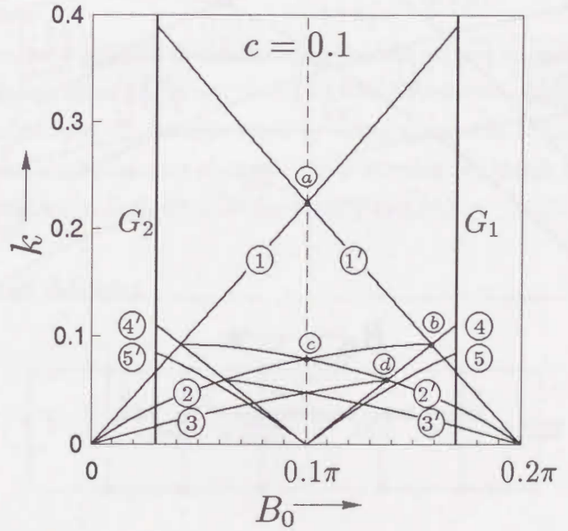

Figure 2.20: Bifurcation diagram in (B_0, k) by heteroclinic orbits at $c = 0.1$.

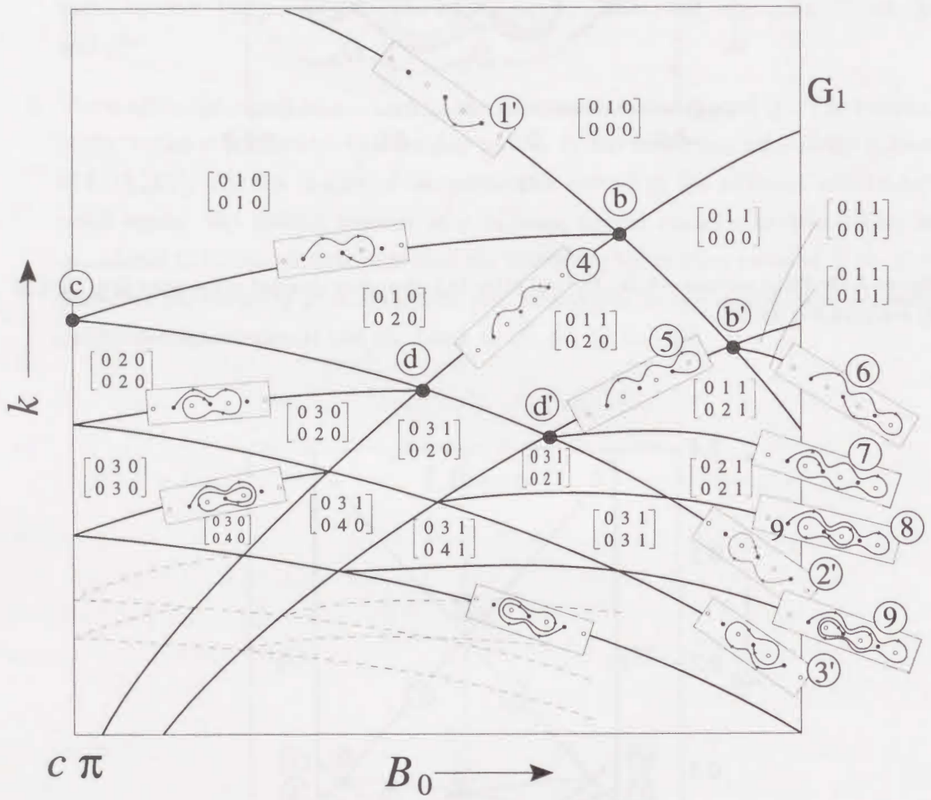

Figure 2.21: Magnification of Fig. 2.20.

2.3 Bifurcation of Pendula Coupled by Elastic Torsional Joint

2.3.1 Introduction

In Ref. [9], the JJ circuit coupled by a linear inductor is investigated. The circuit equation is four-dimensional autonomous system and the coupled pendula is derived as a mechanical interpretation. An interesting periodic solution or so-called "caterpillar solution" and the explanation for mechanism of the solution are briefly done by some qualitative properties in the planer phase portraits. However, the diagram of beating mode domains is explained heuristically, thus the approximate value of parameters causing the caterpillar solution is not specified.

In this section, we treat the coupled pendula. The rod connected between both pendula is made of rubber same as the previous section. The equation of motion is interpreted as an inductively coupled circuit containing two JJ elements with a d.c. source. The phase space can be regarded as $S^1 \times \boldsymbol{R}^3$ because the system has a periodicity for the invariant transformation. We study the properties of periodic solutions winding around S^1 as a bifurcation problem.

Firstly, we analyze equilibria in this system. The bifurcation diagram of equilibria and its topological classification are given. Secondly, the bifurcation diagram of the periodic solutions winding around S^1 are calculated by using a suitable Poincaré mapping, and properties of periodic solutions are discussed. In particular, we clarify that the caterpillar solution is observed when both pendula are weakly coupled.

2.3.2 Circuit Model

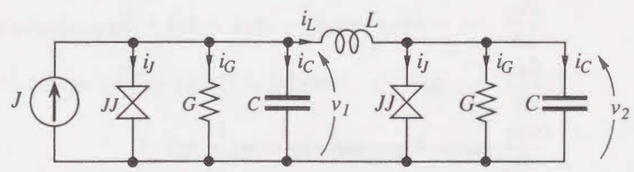

Figure 2.22: The circuit with two Josephson junction elements coupled by inductance L.

Figure 2.22 shows an inductively coupled circuit containing two JJ elements with the

same characteristics. This circuit is equivalent to a SQUID(superconducting quantum interference device) containing two junctions. The characteristics of a JJ element are assumed as:

$$i_J = I_c \sin\phi_i, \quad \frac{d\phi_i}{dt} = \frac{2e}{\hbar} v_i \quad i = 1, 2. \tag{2.41}$$

where, I_c, e, $\hbar$ are the critical current of a JJ element, the charge of electron, and Dirac's constant, respectively. ϕ is the phase difference of the wave function at the center of the junction plane.

To normalize circuit equations, we introduce the following new parameters and variables:

$$\begin{aligned} k &= \sqrt{\frac{\hbar}{2eI_cC}}G \\ c &= \frac{\hbar}{2eI_cL} \\ B_0 &= \frac{J}{I_c} \\ \tau &= \sqrt{\frac{2eI_c}{\hbar C}}t \\ x_i &= \phi_i \\ y_i &= \sqrt{\frac{2eC}{\hbar I_c}}v_i, \end{aligned} \tag{2.42}$$

where, $i = 1, 2$. For simplicity, we assume that G is a linear conductance. If we rewrite τ as t, we obtain the following four-dimensional autonomous differential equations:

$$\begin{aligned} \frac{dx_1}{dt} &= y_1 \\ \frac{dy_1}{dt} &= -ky_1 - \sin x_1 - c(x_1 - x_2) + B_0 \\ \frac{dx_2}{dt} &= y_2 \\ \frac{dy_2}{dt} &= -ky_2 - \sin x_2 - c(x_2 - x_1). \end{aligned} \tag{2.43}$$

The system (2.43) is equivalent to a parallel pendula connected by an elastic torsional joint with the gravity force. Therefore, k is interpreted as the coefficient of damping, c as an elasticity constant, and B_0 as an external torque. See Fig. 2.23.

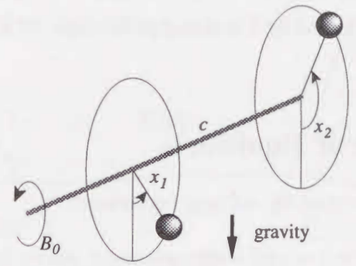

Figure 2.23: Physical interpretation of the system (2.43). Both terminals of the joint are free(not fixed).

2.3.3 Properties of the System

2.3.3.1 Invariance

Equations (2.43) are invariant for the transformation:

$$(x_1, y_1, x_2, y_2) \to (x_1 + 2n\pi, y_1, x_2 + 2n\pi, y_2), \tag{2.44}$$

where, n is an integer. Note that x_1, and x_2 cannot be taken modulo 2π individually, but $x_1 + x_2$ can be. Hence state space of this system can be considered as $S^1 \times \boldsymbol{R}^3$. To visualize a circle S^1 in x_1-x_2 plane, a new coordinate (u, v) is introduced as follows:

$$u = \frac{1}{2}(x_1 + x_2), \quad v = \frac{1}{2}(x_1 - x_2). \tag{2.45}$$

From Eq. (2.44) and (2.45), we can find S^1 as the semi-open interval $[0, 2\pi)$ on u without information of y_1 and y_2. This transformation is useful to analyze periodic solutions discussed in Sec. 2.3.5

2.3.3.2 Boundedness

The mechanical energy of Eqs.(2.43) is follows:

$$\begin{aligned} E &= \frac{1}{2}(y_1^2 + y_2^2) - \cos x_1 - \cos x_2 \\ &\quad -B_0 x_1 + \frac{1}{2}c(x_1 - x_2)^2. \end{aligned} \tag{2.46}$$

Any solution of Eqs.(2.43) is bounded because dE/dt is negative for $k > 0$. This also shows that there is no periodic solution homotopic to an equilibrium[19]. Thus, there

exists a finite set M in the $\boldsymbol{R}^4$, and any orbit started from arbitrary initial condition enters to M eventually, and it is captured by a stable equilibrium, or a limit cycle winding around the cylindrical space.

2.3.4 Classification of Equilibria

Equilibria of (2.43) are calculated by solving equations:

$$f(x_2) = \sin(\frac{1}{c}\sin x_2 + x_2) + \sin x_2 = B_0 \tag{2.47}$$

$$x_1 = x_2 + \frac{1}{c}\sin x_2. \tag{2.48}$$

Note that $f(x_2)$ is a periodic function with period 2π. Thus tangent(saddle-node) bifurcations for equilibria can be calculated at $df(x_2)/dx_2 = 0$ in $0 \le x < 2\pi$. Figure 2.24 shows the the bifurcation diagram of equilibria.

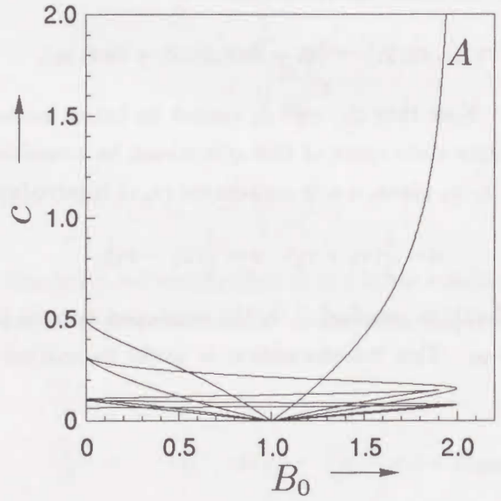

Figure 2.24: The bifurcation diagram of equilibria of Eqs.(2.43).

Topological properties of an equilibrium is determined by roots of the characteristic equation corresponding to the Jacobi matrix of Eqs.(2.43). Using Routh-like criterion of stabilities, the topological classification of equilibria is achieved in B_0-c plane. Figure 2.25 shows the enlargement of Fig. 2.24 for $c < 0.5$ with topological classification of equilibria.

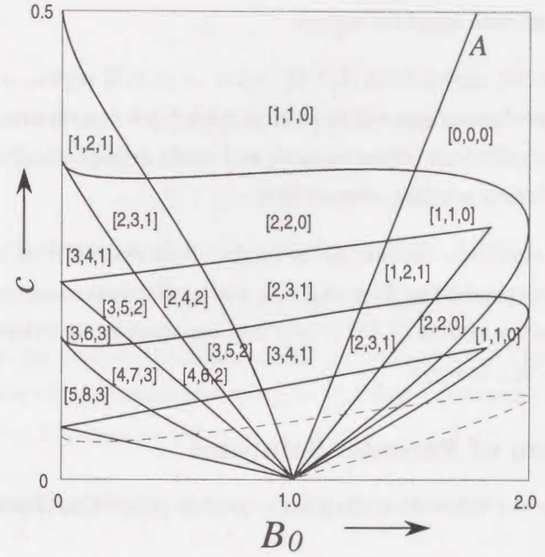

Figure 2.25: Schematic diagram of Fig.2.24. Any sequence means $[\#\{{}_0O\}, \#\{{}_1O\}, \#\{{}_2O\}]$.

The following properties are found in Figs.2.24 and 2.25:

1. In each region surrounded by bifurcation curves, the number of equilibria is invariant.

2. For $k > 0$, we have only three types of equilibria: ${}_0O$(completely stable), ${}_1O$(1-dimensionally unstable), ${}_2O$(2-dimensionally unstable). Other types which are possible combinations; ${}_3O$(3-dimensionally unstable) and ${}_4O$(completely unstable), can not exist in the system. ${}_1O$ means that either of the pendula is in an unstable equilibrium. In Fig.2.25, we indicate the number of each type of equilibria by $[\#\{{}_0O\}, \#\{{}_1O\}, \#\{{}_2O\}]$. $\#\{\}$ indicates the number of elements contained in the set $\{\}$.

3. When parameters vary across any bifurcation curves, $\#\{{}_1O\}$ changes by 1, and either of $\#\{{}_2O\}$ and $\#\{{}_0O\}$ changes by 1.

4. $B_0 = 2.0$ is an asymptotic line for bifurcation curve labeled by A, because Eq. (2.47) tends to $2\sin x_2 = B_0$ as $c \to \infty$. In the circuit model, $c \to \infty$ means $L \to 0$. Then

this is reduced to the circuit containing a single JJ element with d.c. source or the damped pendulum with constant torque.

5. When any parameter moves from $[1,1,0]$ region to $[0,0,0]$ region, equilibria disappear. From boundedness discussed in section 2.3.3.2, we can observe that the orbit captured by the equilibrium begins to move and tends asymptotically toward a limit cycle(periodic solution winding around S^1).

6. As $c \to 0$, many equilibria appear. Accordingly, orbits started from any initial state tend to behave independently. Just at $c = 0$, the equilibrium converges to $(x_1, x_2) = (\mathrm{Sin}^{-1} B_0, 0)$, then the system (2.43) is split into two completely independent second-order system (x_1, y_1), (x_2, y_2).

2.3.5 Bifurcation of Periodic Solutions

In this section, we show the bifurcation diagram to explain properties of periodic solutions of Eqs.(2.43).

2.3.5.1 Poincaré Mapping

In order to discuss the properties of periodic solutions and their bifurcations, we define the following Poincaré mapping.

For simplicity, let Eqs. (2.43) be rewritten as:

$$\frac{d\boldsymbol{x}}{dt} = \boldsymbol{f}(\boldsymbol{x}, \boldsymbol{\lambda}) \tag{2.49}$$

where, $\boldsymbol{x} = \{x_1, y_1, x_2, y_2\}$, $\boldsymbol{\lambda} = \{k, c, B_0\}$. We denoted also the solution of Eq.(2.49) with the initial value $\boldsymbol{x}_0$ at $t = 0$ as:

$$\boldsymbol{x}(t) = \boldsymbol{\varphi}(t, \boldsymbol{x}_0), \quad \boldsymbol{x}(0) = \boldsymbol{\varphi}(0, \boldsymbol{x}_0) = \boldsymbol{x}_0. \tag{2.50}$$

Suppose that we have a periodic solution as:

$$\boldsymbol{x}(t) = \boldsymbol{\varphi}(t, \hat{\boldsymbol{x}}). \tag{2.51}$$

We can choose a hyperplane Π through $\hat{\boldsymbol{x}} \in \boldsymbol{R}^4$ transverse to the solution of Eq. (2.49). For each point $\boldsymbol{x} \in U$, a small neighborhood of $\hat{\boldsymbol{x}}$ in Π, the solution $\boldsymbol{\varphi}(t, \boldsymbol{x})$ will intersect Π after a finite time τ, i.e.,

$$\boldsymbol{\varphi}(\tau, \boldsymbol{x}) = \boldsymbol{x}_\tau \in \Pi \tag{2.52}$$

Hence we define a mapping T_λ called a Poincaré mapping from U into Π as:

$$\begin{aligned} T_\lambda : \Pi \supset U &\to \Pi \\ \boldsymbol{x} &\mapsto \boldsymbol{x}_\tau = \boldsymbol{\varphi}(\tau, \boldsymbol{x}) \end{aligned} \tag{2.53}$$

Note that the return time τ depends on the initial value $\boldsymbol{x} \in U$. For Eqs. (2.43), we can consider Π as:

$$\Pi = \{\boldsymbol{x} \in \boldsymbol{R}^4 : x_1 + x_2 = 0\} \tag{2.54}$$

from the property of the transformation (2.44), however,

$$\Pi = \{\boldsymbol{x} \in \boldsymbol{R}^4 : x_1 = 0\} \tag{2.55}$$

is chosen for the convenience of taking modulo 2π for x_1 and x_2. Thus, we can calculate the bifurcation values of the parameters using by T_λ and its derivative DT_λ. In the following, system parameter k is fixed at 0.2.

2.3.5.2 Bifurcation Diagram

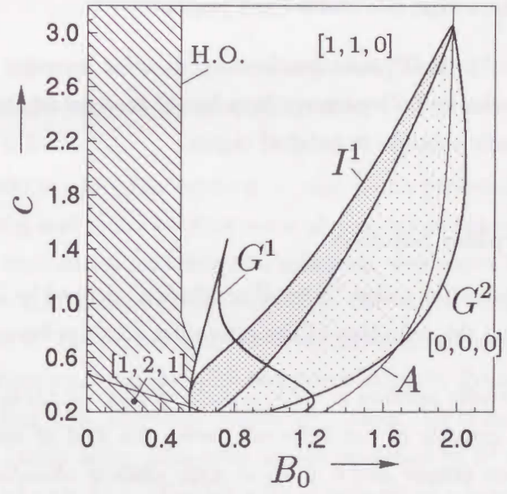

Figure 2.26: Bifurcation diagram of periodic solutions. $k = 0.2$.

Figure 2.26 shows a bifurcation diagram of periodic solutions. For simplicity, we studied $c > 0.2$ mainly because this plane is almost covered by $[1,1,0]$ region containing two equilibria; a sink and a saddle.

We observed two types of bifurcation in this system; local bifurcations and global bifurcations. The former is tangent bifurcation and period doubling bifurcation for periodic solutions, and the latter is the homoclinic bifurcation for the trajectory.

The following properties are found in Fig. 2.26.

1. In the white region, there exists a periodic solution corresponding to a fixed point of T_λ. This synchronous solution has constant and positive velocities with a small phase shift. See Figure 2.28(b).

2. I^1 shaping the dark shaded island is a period doubling bifurcation curve for the fixed point.

3. G^2 indicating the tangent bifurcation curve for the 2-periodic point is connected to I^1 curve. See Fig.2.27. The 2-periodic point bifurcated from the upper portion of I^1 disappears by the lower portion of G^2.

4. G^1 is the tangent bifurcation curve for the fixed points. In the region surrounded by this curve, there exist two stable fixed points.

5. The line labeled by 'H.O.' indicates homoclinic orbit meaning global bifurcation, i.e., a periodic orbit and a separatrix loop for ${}_1O$ coalesce at this parameter. Thus there is no periodic solution in hatched region.

2.3.5.3 The Caterpillar Solution

We observe a periodic solution called "caterpillar solution" defined by Levi[9] as a periodic points for T_λ. We recall the definition of the caterpillar solution from Ref.[9]:

Definition 2.3 *A periodic solution $\boldsymbol{\varphi} = (\varphi, \dot{\varphi}, \psi, \dot{\psi})$ of Eqs. (2.43) is called a caterpillar solution if its period consists of two intervals during the first of which φ increases by $2m\pi + R_1$, m being an integer and $0 < R_1 < \pi/2$, while ψ changes by less than $\pi/2$; during the second time interval φ and ψ exchange roles: ψ increases by $2m\pi + R_2$ and φ changes by less than $\pi/2$.*

This definition gives only the quantity corresponding to its wave form, however, to calculate accurate region satisfying the definition is not our goal. We assert that bifurcations for the periodic solutions are the essential reason why the caterpillar solution is involved.

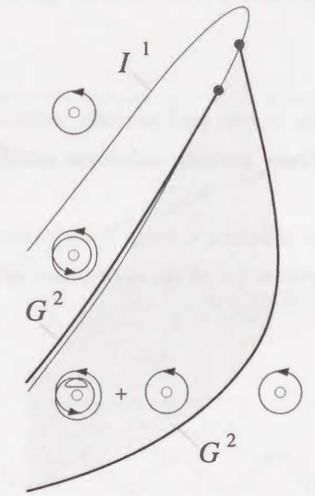

Figure 2.27: Magnification of Fig.2.26.

In practical, if the distance between upper and lower G^2 curves is separated sufficiently, then the wave form of 2-periodic points bifurcated by I^1 is distorted as c tends to 0. See property 6 in Sec. 2.3.4

Figure 2.29 shows a caterpillar solution. τ_1 and τ_2 are periods for Poincaré mapping. Note that velocities y_1 and y_2 can be observed as almost out-of-phase synchronous motions. To obtain another explanation for caterpillar solutions, we observe the motion of orbits in x_1-x_2 plane. Figure 2.30 illustrates the coordinate introduced by Eq.(2.45) containing a circular space S^1 on u. The period of the orbit corresponds to the number of black circles indicating intersection points of the orbit and v-axis using by Poincaré section (2.54). In this figure, two orbits with 2-periodic points are drawn. ⓐ is an orbit whose periodic points are located nearly on v. This orbit is just branched by I^1 in Fig. 2.26 and runs almost parallel to coordinate u. The orbit ⓑ considered as a caterpillar solution whose parameters are equal to the solution drawn in Fig. 2.29 and which is distorted from ⓐ as c decreases. It is clear that the caterpillar solution moves like a step function for the coordinate x_1 or x_2.

In Fig. 2.27, the periodic solution bifurcated by G^1 also can be regarded as a caterpillar solution. See Fig.2.31. In $c < 0.5$, therefore, we conclude that bifurcations for a periodic

solution and small value of c are closely related to the generation of caterpillar solutions.

2.3.5.4 Other Solutions

There are so many bifurcation curves and periodic solutions in the region surrounded by I^1, G^1 and G^2. Some of these periodic solutions satisfy the condition of caterpillar solution.

Fig. 2.32 shows a chaotic solution caused by a period doubling cascade, but this solution does not satisfy Definition 2.3 of the caterpillar solution.

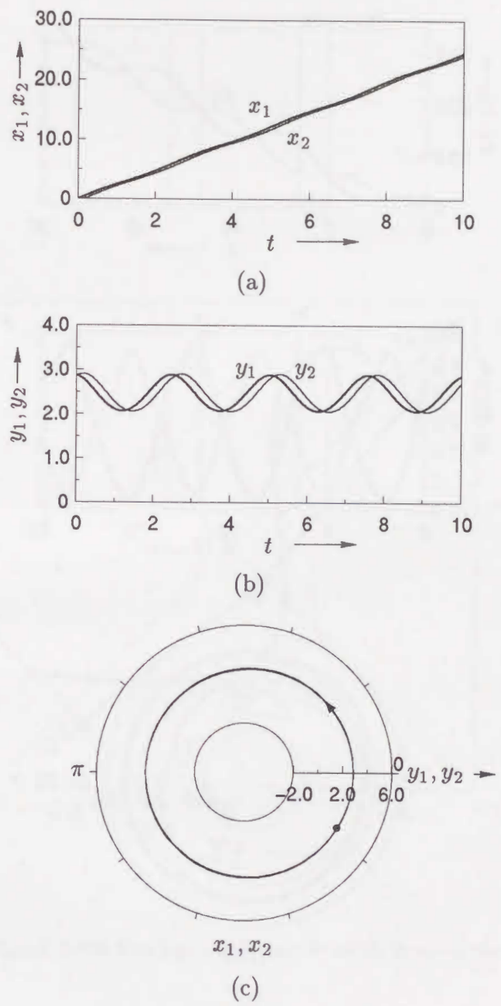

Figure 2.28: Time response of periodic solution with fixed point for T_λ. (a) States, (b) Velocities, (c) Cylindrical phase portrait. A circled point indicate a periodic point. $c = 1.2, B_0 = 1.0\ \tau = 2.503$.

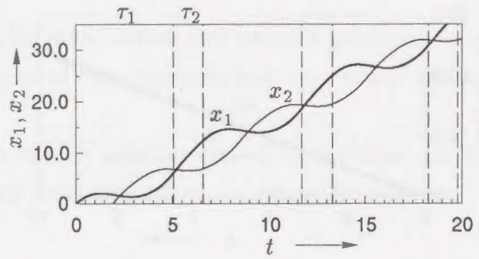

(a)

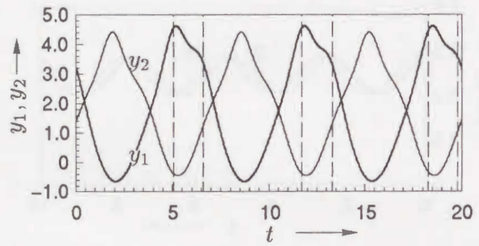

(b)

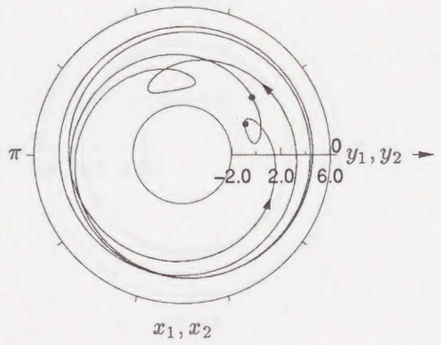

(c)

Figure 2.29: Time response of 2-periodic caterpillar solution. (a) States, (b) Velocities, (c) Cylindrical phase portrait. A circled point indicate a periodic point. $c = 0.48, B_0 = 1.36\ \tau_1 = 5.056, \tau_2 = 1.5217$.

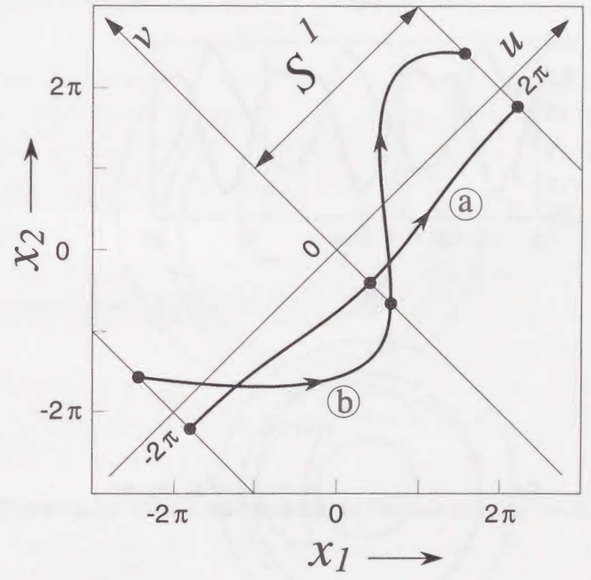

Figure 2.30: Two types of 2-periodic orbits in x_1-x_2 plane.

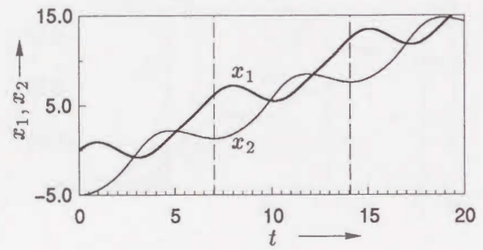

(a)

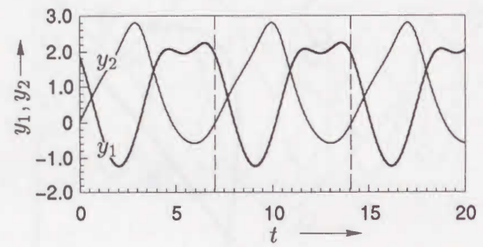

(b)

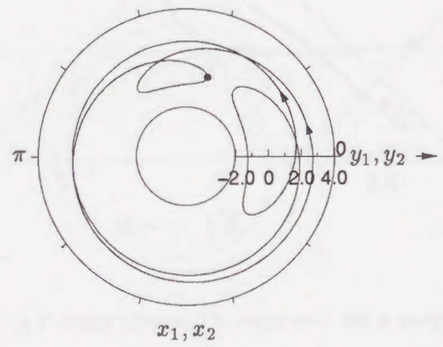

(c)

Figure 2.31: Time response of periodic solutions with fixed point, $c = 0.4, B_0 = 1.0, \tau = 7.0195$,

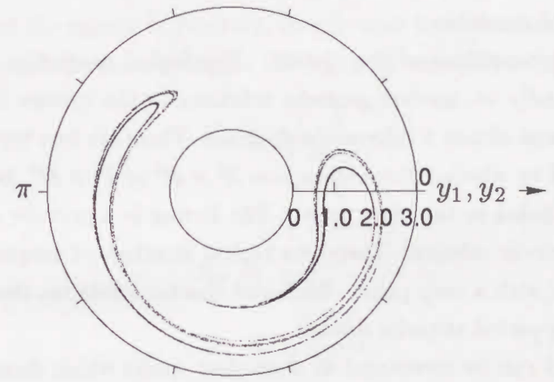

Figure 2.32: Chaotic solution with the Poincaré mapping. $c = 0.48, B_0 = 0.86$.

2.4 Bifurcation of Pendula Coupled by a Frictional Clutch

2.4.1 Introduction

In the preceding section, we have treated the running-periodic solutions which keep to wind around the cylindrical phase space, and investigate their bifurcations. It is essential that there was no oscillatory behavior for each pendulum in the system. In this section, bifurcation phenomena observed in two dumped pendula linked by a clutch exchanging kinetic energy of both pendula, say, two pendula connected by a friction clutch, are investigated. This model also has an electrical analog: the circuit containing two Josephson junctions coupled by a resistor.

Firstly we study equilibria of the system. Topological properties of the equilibria are clarified. Secondly we analyze periodic solutions in the system by using suitable Poincaré mapping and obtain a bifurcation diagram. There are two types of limit cycles which distinguished by whether the motion is in $S^1 \times \boldsymbol{R}^3$ or $T^2 \times \boldsymbol{R}^2$, because two cyclic coordinates are included in the state space. The former is a periodic solution and the latter is a quasi-periodic solution. There is a typical structure of tangent bifurcation for 2-periodic solutions with a cusp point. We found chaotic orbits via the period-doubling cascade. and a long-period stepwise orbit.

Since this model can be considered as a simplest model which demonstrates the interactions between a rotational-energy supply and a load in mechanical systems, it is important to clarify the principal bifurcation structures of the periodic solutions observed in the model. It is interesting that the chaotic vibration is observed when the pendula are not perfectly in the clutch.

2.4.2 The JJ Circuit Coupled by a Resistor

We investigate a circuit shown in Fig.2.33. This is obtained from the circuit discussed in Sect. 2.3 by using R instead of L as a coupling device. Assume that the current-voltage characteristics of a JJ element is described as :

$$i_J = I_C \sin\phi_i, \quad \frac{d\phi_i}{dt} = \frac{2e}{\hbar} v_i \quad i = 1, 2. \tag{2.56}$$

where, I_C, e, $\hbar$ are maximum current of JJ element, charge of electron, Dirac's constant, respectively. ϕ is the phase difference of the wave function at the center of the junction

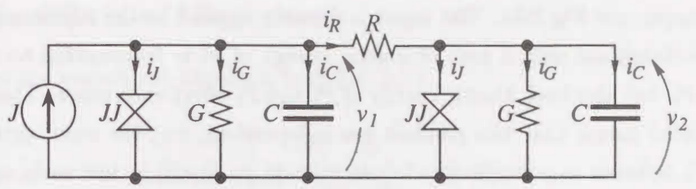

Figure 2.33: The JJ circuit coupled by a resistor

plane. If ϕ is considered as magnetic flux, then the JJ element behaves as a nonlinear inductor which is controllable by the magnetic flux. Usually a nonlinear conductance is supposed for G. We treat it as a linear one for the sake of mechanical interpretation, global behavior of the system is, however, not changed by this assumption.

To normalize the equation, we define the following variables and parameters:

$$\begin{aligned} k &= \sqrt{\frac{\hbar}{2eI_C C}} G \\ c &= \sqrt{\frac{\hbar}{2eI_C C}} \frac{1}{R} \\ B_0 &= \frac{J}{I_C} \\ \tau &= \sqrt{\frac{2eI_C}{\hbar C}} t \\ x_i &= \phi_i \\ y_i &= \sqrt{\frac{2eC}{\hbar I_C}} v_i \end{aligned} \tag{2.57}$$

where $i = 1, 2$. By rewriting τ as t, we have a four-dimensional autonomous differential equation:

$$\begin{aligned} \frac{dx_1}{dt} &= y_1 \\ \frac{dy_1}{dt} &= -ky_1 - \sin x_1 - c(y_1 - y_2) + B_0 \\ \frac{dx_2}{dt} &= y_2 \\ \frac{dy_2}{dt} &= -ky_2 - \sin x_2 - c(y_2 - y_1). \end{aligned} \tag{2.58}$$

System (2.43) can be regarded as parallel pendula connected by a friction clutch. k is interpreted as the coefficient of damping, c as frictional transmission constant, and B_0 as

an input torque, see Fig.2.34. The input is directly applied to the a primary pendulum P_1. By the clutch not only a part of kinetic energy of P_1 is transmitted to a secondary pendulum P_2, but also both kinetic energy of P_1 and P_2 affect each other. Thus $c \to 0$ (let out the clutch) means that two pendula are independent, i.e., the input drives only P_1, and then P_2 behaves as a simple pendulum without an input, at last rests in the origin. Otherwise, $c \to \infty$ (let in the clutch) means that the P_1 and P_2 can be regarded as a single pendulum because both pendula are connected equivalently by a rigid rod.

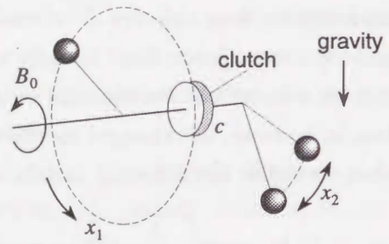

Figure 2.34: Frictionally coupled pendula model.

There exists an invariant transformation in system (2.58):

$$\mathcal{T} : (x_1, y_1, x_2, y_2) \mapsto (x_1 \pm 2n\pi, y_1, x_2 \pm 2m\pi, y_2) \tag{2.59}$$

where, n, m are integers. Equation (2.59) means that x_1 and x_2 can be added integral multiples of 2π independently, i.e., there exist two cyclic coordinates $S^1 \times S^1 = T^2$ in the system. It should be noted that the system is very different from the case discussed in Section 2.3 upon two points: 1) the state space can include T^2, say, a coupling inductor constructs $S^1 \times \boldsymbol{R}^3$, and a coupling resistor can construct not only $S^1 \times \boldsymbol{R}^3$ but also $T^2 \times \boldsymbol{R}^2$. 2) there are very few equilibria in this system at all values of the parameters. We consider the latter point in the following section.

2.4.3 Equilibria of the System

Equilibria of the system are obtained from Eq.(2.58):

$$\begin{aligned} x_1 &= \begin{cases} \mathrm{Sin}^{-1} B_0 & y_1 = 0 \\ \pi - \mathrm{Sin}^{-1} B_0, & \end{cases} \\ x_2 &= \begin{cases} 0 & y_2 = 0 \\ \pi, & \end{cases} \end{aligned} \tag{2.60}$$

where, x_1, x_2 are in $[0, 2\pi)$. So we obtain a schematic diagram of the torus phase space for equilibria in (x_1, x_2) plane at $0 < B_0 < 1$. See Fig.2.35.

In the system, there exist only three types of equilibria and at most four equilibria in the fixed parameters. Figure 2.35 also shows directions of solution flow with respect to each the equilibria on x_1-x_2 plane and Table 2.1 indicates the classification for stability of the equilibria. In Fig.2.35, it is noted that ${}_2O$ is regarded that each of the pendula is on an unstable equilibrium (saddle point) simultaneously. Note also that ${}_3O$ does not exist in this system.

The condition of the parameter region in which there exist equilibria is $|B_0| < 1$. $B_0 = 1$ is tangent bifurcation value of equilibria. In the other value of B_0, there exists no equilibrium and at least one limit cycle since the system is dissipative.

Table 2.1: Classification of equilibria in Eq.(2.58).

symbol	notation	topological property
●	${}_0O$	completely stable
⊗	${}_1O$	1-dimensionally unstable
⊗	${}_1O$	1-dimensionally unstable
○	${}_2O$	2-dimensionally unstable

2.4.4 Bifurcation of Periodic Solutions

Equations (2.58) are rewritten as:

$$\frac{d\boldsymbol{x}}{dt} = f(\boldsymbol{x}, \lambda) \tag{2.61}$$

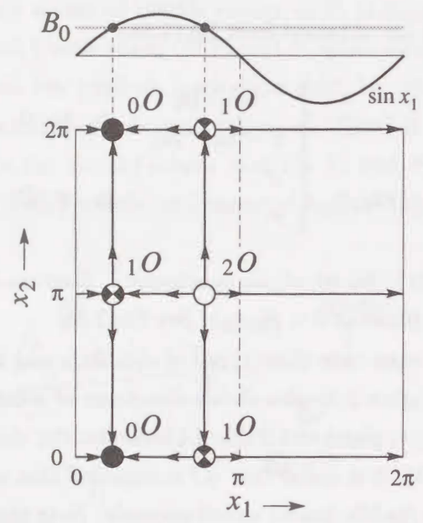

Figure 2.35: Phase portrait of the system (2.58) in torus.

where, $\boldsymbol{x} = (x_1, y_1, x_2, y_2)$, $\lambda \in \boldsymbol{R}$ are parameters. Suppose that the solution of Eq.(2.61) is denoted by:

$$\boldsymbol{x}(t) = \boldsymbol{\varphi}(t, \boldsymbol{x}_0), \quad \boldsymbol{x}_0 = \boldsymbol{x}(0). \tag{2.62}$$

We should notice that there is no periodic solution in $\boldsymbol{R}^4$ if $k \neq 0$. The periodic solution we called in this section is a modified periodic solution defined in Ref.[9]:

$$\begin{aligned} x_1(t_0) &= x_1(0) + 2\pi\ell \\ y_1(t_0) &= y_1(0) \\ x_2(t_0) &= x_2(0) + 2\pi m \\ y_2(t_0) &= y_2(0) \end{aligned} \tag{2.63}$$

where $t_0 > 0$ is a period and $\ell \geq 1, m \geq 0$ are integers. This definition means that P_1 must rotate to generate a periodic solution. We classify periodic solutions with respect to their behavior of the motions as follows:

1. **(Type-I)**: P_1 is winding around the circle $S^1 = \{0 \leq x_1 < 2\pi\}$, but P_2 is rolling about a constant angular. Thus the motion is in $S^1 \times \boldsymbol{R}^3$.

2. **(Type-II)**: Both P_1 and P_2 are winding around the circles $S^1 \times S^1 = T^2$. They behave quasi-periodic motion in $T^2 \times \boldsymbol{R}^2$.

Type-I solution evolves to chaos by changing the system parameters. In this section, we mainly treat the bifurcation of this type of solutions. In the following we fix the system parameter k as 0.2.

To calculate bifurcation parameter we define the Poincaré mapping T and its section Π as:

$$\begin{aligned} T : \Pi &\to \Pi \\ \boldsymbol{x}_0 &\mapsto \left\{ \varphi(t_0, \boldsymbol{x}_0) \mid x_1 - 2\pi, \begin{array}{ll} \text{if} & x_2 \geq 2\pi \quad \text{then} \quad x_2 - 2\pi \\ \text{if} & x_2 \leq 2\pi \quad \text{then} \quad x_2 \end{array} \right\} \end{aligned} \tag{2.64}$$

where t_0 is the time of first return of the initial state $\boldsymbol{x}_0$ to Π. Because all types of periodic solutions have at least an S^1 for x_1, we choose the Poincaré section as:

$$\Pi = \{\boldsymbol{x} \in S^1 \times \boldsymbol{R}^3 \subset \boldsymbol{R}^4 : x_1 = 0\} \tag{2.65}$$

Thereby we can calculate the bifurcation values of the parameters by Newton's method using T and its derivatives.

Figure 2.36 shows bifurcation diagram of the system (2.58) in B_0-c plane. The following properties are found:

1. I^i, G^i, $i = 1, 2$ indicate period-doubling and tangent bifurcation of the Type-I i-periodic solution, respectively. In the shaded region edged by I^1 and G^1, there exists stable periodic solution with the fixed point, x_1 winds around S^1 and x_2 tumbles around a constant angle, see Figs.2.37(a-1), (a-2). One of 2-periodic orbits bifurcated by I^1 is shown in Figs.2.37(b-1),(b-2).

2. Every solution bifurcated by I^2 evolves to chaos via period-doubling cascade. Figures 2.38(a-1), (a-2) show the a chaotic orbit and the Poincaré mapping of a chaotic attractor.

3. In whole parameters, there exist quasi-periodic (Type-II) solutions. Figures 2.38(b-1) and (b-2) show the orbit and an invariant closed curve of the Poincaré mapping on the cylindrical phase space. As c increases, the solution bind to a synchronized orbit.

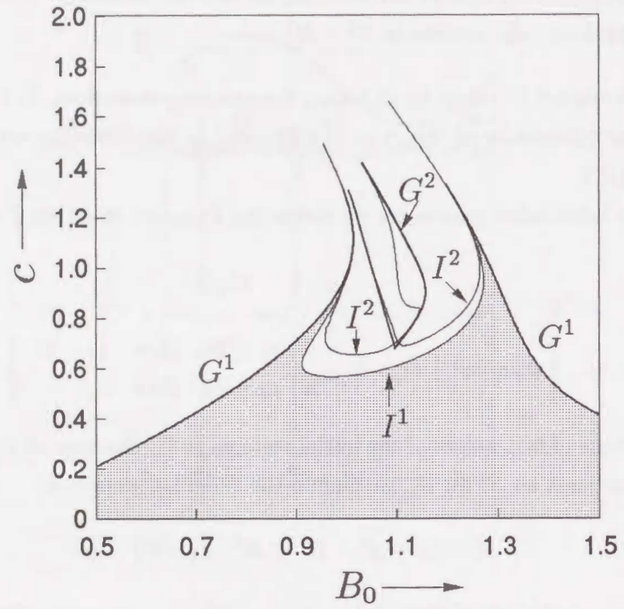

Figure 2.36: Bifurcation diagram for periodic solutions.

4. I^2 curves are overhung each other by G^2 with a cusp point. In this region, we can observe coexistent 2-periodic and higher-periodic solutions. This is a typical structure of the higher-periodic bifurcation set.

5. The end points of all bifurcation curves are caused by touching homoclinic orbits. Also the chaotic orbits are frequently disappeared by meeting this global bifurcation and attracted into Type-II orbits.

6. The equilibrium disappears in $B_0 = 1.0$. Just at this parameter, the orbit stopped at a stable equilibrium begins to start and approaches the neighborhood of the point in which the equilibrium exists originally. This orbit shown in Fig. 2.39 resembles Shil'nikov type homoclinic orbit, but this orbit is only a periodic solution because the manifolds of saddle-type equilibrium also disappears. It is interesting that the solution has a long period and a stepwise response.

7. Figure 2.40 illustrates the schematic bifurcation diagram. There exist chaotic orbits

in the dark shaded region, however all of them are disappeared by homoclinic orbits by changing the parameter toward the center of the island edged by I^2. It is emphasized that a simple mechanical transmission can behave chaotically by controlling the clutch.

2.5 Conclusions of Chapter 2

In this chapter, an *L-C-G* parallel circuit containing a JJ element is investigated as an example of above rotational dynamical systems. Firstly we analyze equilibria of the system with its tangent bifurcations and clarify the periodicity with respect to the relationship between solutions and parameters. It suggests that the parameter range to be analyzed can be restricted. Secondly we calculate the bifurcation sets which indicate parameter value causing heteroclinic orbits. The topological classification for the basins of attractions are done by the bifurcation diagrams and linking numbers. Future topics to be studied as follows:

1. Analysis of the bifurcation phenomena of the periodic solution when an external force is applied in (2.58), i.e., B_0 is changed to $B_0 + B\sin\nu t$.

2. Studies for more higher dimensional coupled system.

Furthermore, properties for equilibria and periodic solutions observed in the inductively coupled JJ circuit are investigated and their bifurcation diagram are obtained. Firstly, the parameter region in which equilibria exist is given. We clarify that the topological properties of equilibria using by the bifurcation diagram and suitable classifications. Secondly, the bifurcation diagram of periodic solutions winding around S^1 are obtained. This explains some properties of periodic solutions. Particularly, it is clear that the caterpillar solution are caused by a small parameter c and bifurcations.

Further research is needed to obtain a detailed bifurcation diagram for $c < 0.2$. Moreover, investigations of the properties of the circuit in non-autonomous system and a circuit with JJ elements coupled by a resistor are future objectives of research.

Some properties of system (2.58) are investigated. This result compared with the results discussed in Sect.2.3 suggests that the coupling element governs the structure of phase space without changing its order of the circuit equations. An inductor constructs $S^1 \times \boldsymbol{R}^3$, and R can construct $T^2 \times \boldsymbol{R}^2$ phase space. Our future researches are as follows:

- to investigate the bifurcation diagram for higher-periodic solutions in detail. In case that k is small, it might have more complex phenomena.
- to obtain the homoclinic orbits in this system. Particularly the relationship with disappearance of chaotic attractor is interesting.

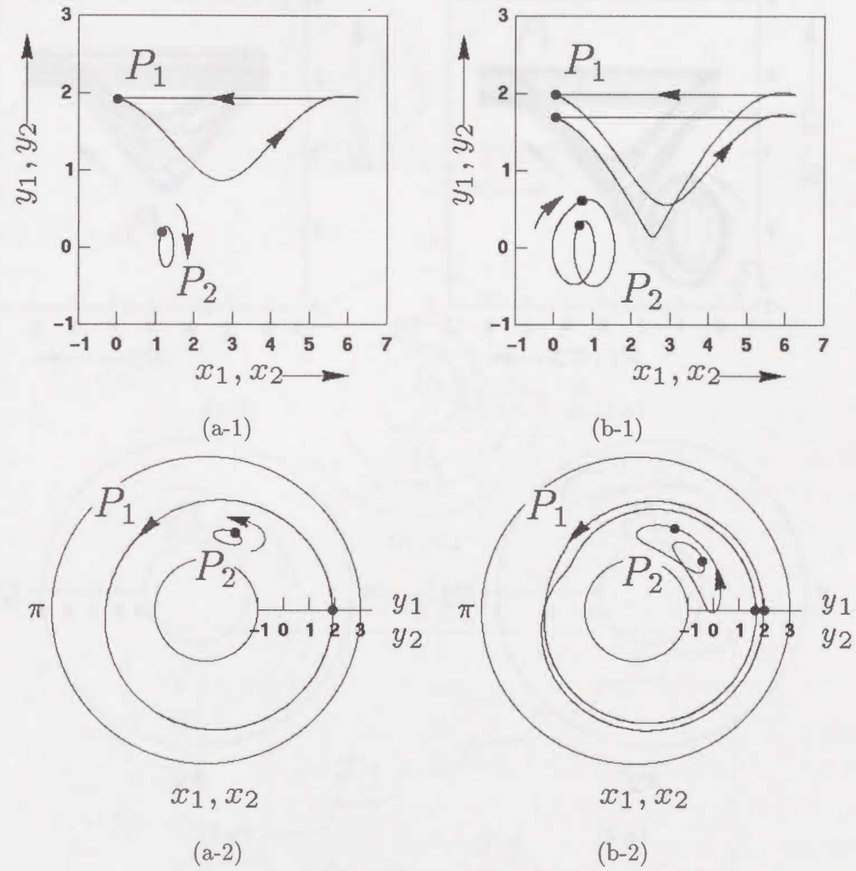

Figure 2.37: Phase portraits. (a-1),(a-2): periodic orbit (Type I) with a fixed point. $B_0 = 1.3$, $c = 0.7$. (b-1),(b-2): 2-periodic orbit bifurcated by I^1, $B_0 = 0.97$, $c = 0.66$.

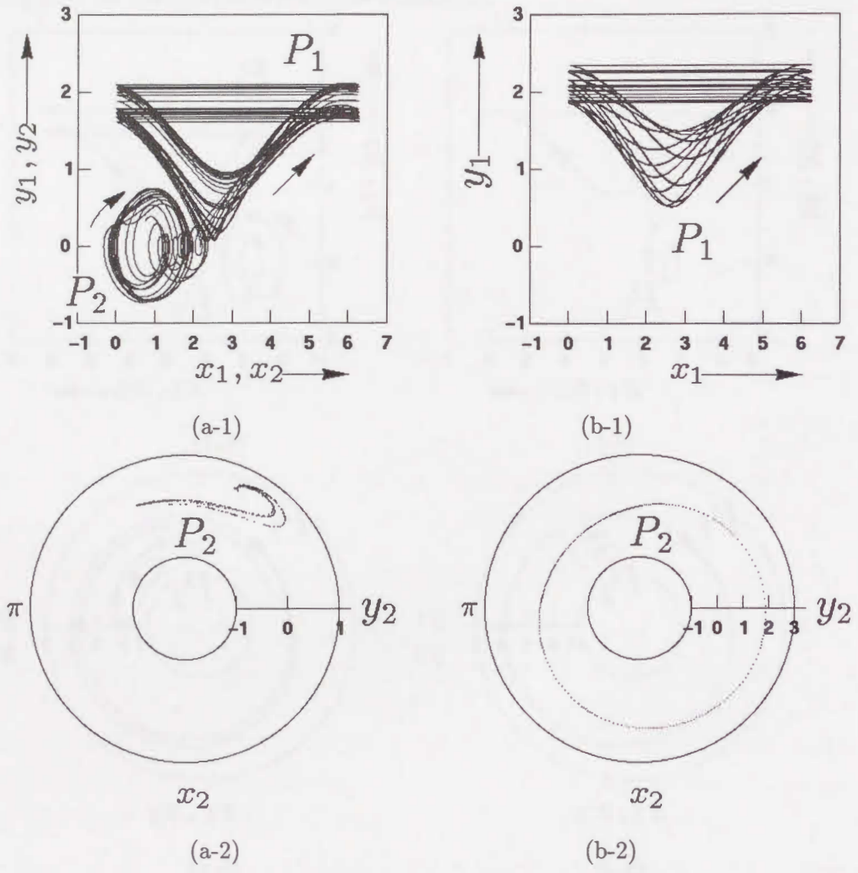

Figure 2.38: Phase portraits. (a-1),(a-2): Chaotic orbit via a period-doubling cascade and its Poincaré mapping $B_0 = 1.12$, $c = 0.73$. (b-1),(b-2): Quasi-periodic (Type II) orbit, (d-2) shows the Poincaré mapping of x_2, $B_0 = 0.7$, $c = 0.7$.

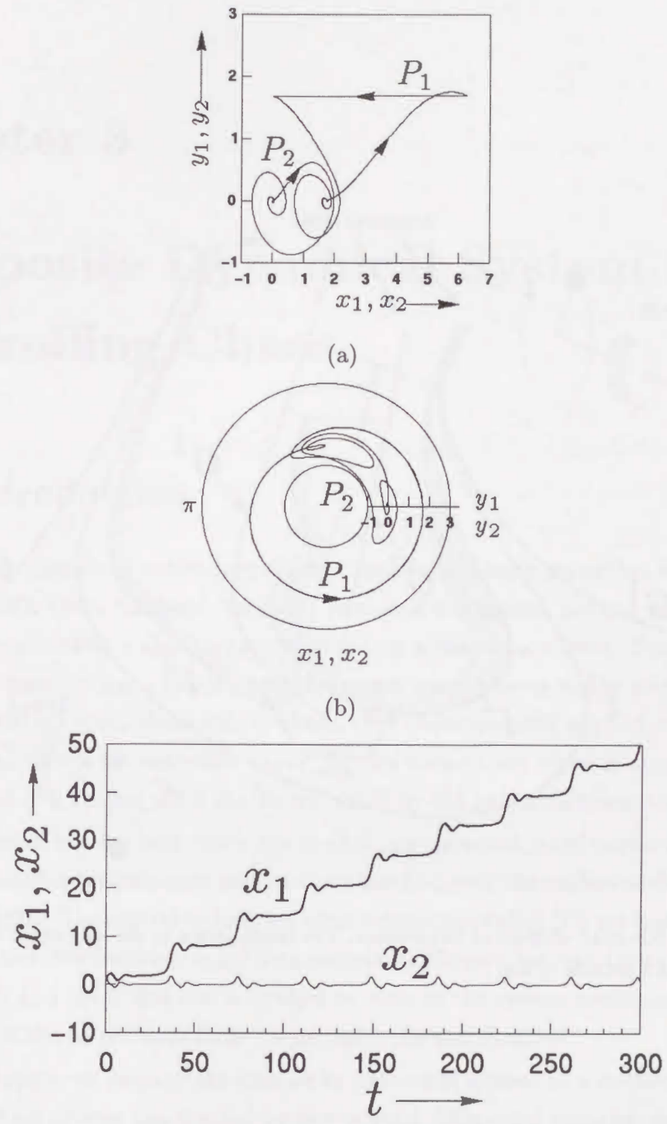

Figure 2.39: Periodic orbit with a fixed point near the disappearance of the equilibria, $B_0 = c = 1.0$.

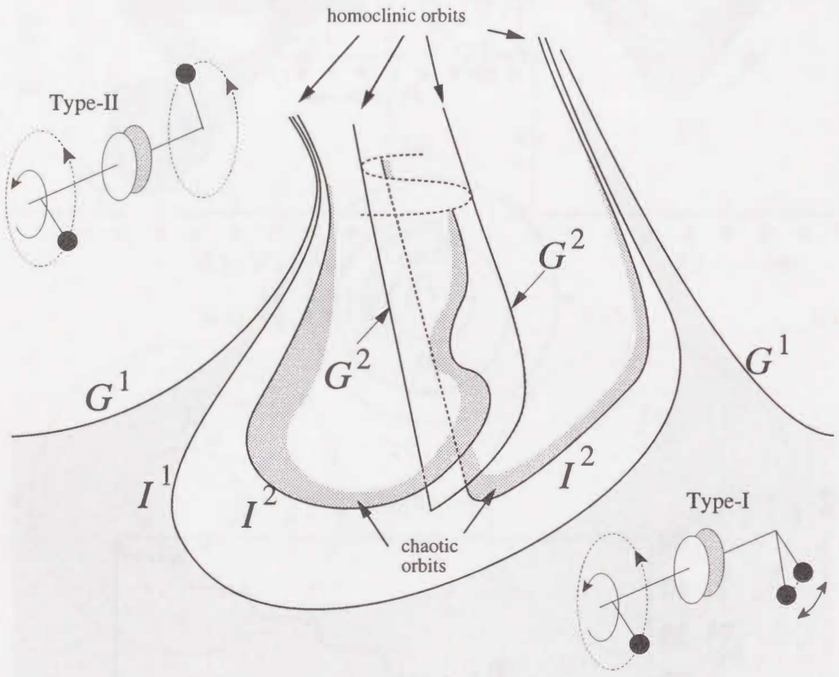

Figure 2.40: Schematic diagram of bifurcations. The sheets shown in the area edged by G^2 indicate the manifolds of 2-periodic orbits.

Chapter 3

Composite Dynamical System for Controlling Chaos

3.1 Introduction

Recently, the topic about controlling chaos is one of remarkable researches in engineering fields. In 1990, Otto, Grebogi, Yorke[11] proposed a standard method to stabilize an unstable periodic orbit, called target embedded, in a chaotic attractor. But this method requires the target being a saddle, i.e., the target must possess stable manifolds to determine a feedback gain. Romeiras, Grebogi, Ott, Dayawansa[20] applied a conventional state feedback theory to controlling chaos. By this method any types of unstable fixed or periodic point in a chaotic state can be stabilized by the pole assignment technique.

On the other hand, many other approaches are proposed, e.g., parameter variation technique, absorber, entrainment and feedback method, etc., the outline of them are given by Ogorzalek[21]. The central techniques using control theory[22] [12] are traditional state feedback control: the feedback signal determined by difference between the target unstable periodic orbit and controlled one is applied to state of the system continuously, thus all information of the target wave form are necessary for stabilization.

In this chapter, we propose the composite dynamical system as a method for controlling chaos. This system constructed by the original differential equation and difference equation derived from linearization in the neighborhood of the target by the Poincaré mapping. We have only to design a controller stabilizing unstable characteristics of the target on the discrete system described by the difference equation. Some significant fea-

tures must be pointed out compared with Ref.[20]:

- How to embed the control value to the parameter, which is implicit in many articles, is clarified. Although the parameter varies discontinuously by the control, a controlled orbit can be C^0 since the state space is never manipulated.
- To calculate the controller, we can obtain derivatives of the Poincaré mapping numerically without using analytic or embedding methods.

Consequently, we develop the systematic design method for controlling chaos in case that the mathematical model is given. Moreover the method is applied to destabilize a stable orbit to escape from an undesirable stable state. We show some illustrations of stabilizing or destabilizing the target of the Duffing's equation and the modified BVP equation.

3.2 Composite Dynamical System

3.2.1 System Equation and its Poincaré Mapping

For simplicity, let us consider an n-dimensional ordinary differential equation(ODE):

$$\frac{d\boldsymbol{x}}{dt} = \boldsymbol{f}(\boldsymbol{x}, \boldsymbol{\lambda}) \tag{3.1}$$

where, $\boldsymbol{x} \in \boldsymbol{R}^n$ is the state vector and $\boldsymbol{\lambda} \in \boldsymbol{R}^r$ is the system parameter. We assume that $\boldsymbol{f}$ is periodic in t with period 2π:

$$\boldsymbol{f}(t + 2\pi, \boldsymbol{x}, \boldsymbol{\lambda}) = \boldsymbol{f}(t, \boldsymbol{x}, \boldsymbol{\lambda}) \tag{3.2}$$

and sufficiently differentiable for all variables. Suppose also that Eq.(3.1) have a unique solution for the initial value problem. We denote the solution $\boldsymbol{x}(t)$ with initial value $\boldsymbol{x}_0$ at $t = 0$ as:

$$\boldsymbol{x}(t) = \boldsymbol{\varphi}(t, \boldsymbol{x}_0, \boldsymbol{\lambda}) \tag{3.3}$$

Thus the relation

$$\boldsymbol{x}(0) = \boldsymbol{\varphi}(0, \boldsymbol{x}_0, \boldsymbol{\lambda}) = \boldsymbol{x}_0 \tag{3.4}$$

holds. Let us define a differentiable map:

$$\begin{aligned} T : \boldsymbol{R}^n \times \boldsymbol{R}^r &\rightarrow \boldsymbol{R}^n \\ (\boldsymbol{x}_0, \boldsymbol{\lambda}) &\mapsto \boldsymbol{x}_1 = T(\boldsymbol{x}_0, \boldsymbol{\lambda}) \\ &\qquad\quad = \boldsymbol{\varphi}(2\pi, \boldsymbol{x}_0, \boldsymbol{\lambda}). \end{aligned} \tag{3.5}$$

For a fixed $\boldsymbol{\lambda}$ the mapping T becomes the ordinary Poincaré mapping. For the latter use we call the sampling interval 2π the Poincaré sampling period or simply Poincaré period, which is equal to the period of the original system (3.1), see Eq.(3.2). A fixed or m-periodic point corresponds to a periodic solution of Eq.(3.1) with period 2π or $2m\pi$, respectively. Moreover all topological properties of the solution of Eq.(3.1) can be reduced to that of the discrete dynamical system (3.5). We consider following two problems:

1. Assuming that Eq.(3.1) has a chaotic attractor, design a controller stabilizing a specific periodic orbit, also called a target orbit, embedded in the chaotic attractor.
2. Assuming that Eq.(3.1) has a stable periodic orbit, destabilize it by a suitable controller.

Note that these two problems are the same if the pole assignment technique is used. Stabilization and destabilization correspond to the stable and unstable pole assignment, respectively. Note also that in the following we shall discuss the stabilization or destabilization method for Eq.(3.1), but this method can be easily applied to an autonomous ODE by changing the definition of the Poincaré mapping.

3.2.2 Stabilizing Unstable Periodic Orbit with a Fixed Point

Let us consider an unstable periodic solution $\boldsymbol{x}^*(t)$ of Eq.(3.1) with period 2π, which is our target orbit embedded in a chaotic attractor. Suppose that $\boldsymbol{x}^*$ is a fixed point of T, which corresponds to the target orbit $\boldsymbol{x}^*(t)$:

$$\boldsymbol{x}^* = T(\boldsymbol{x}^*, \boldsymbol{\lambda}^*) = \boldsymbol{\varphi}(2\pi, \boldsymbol{x}^*, \boldsymbol{\lambda}^*) \tag{3.6}$$

where we denote $\boldsymbol{\lambda}^*$ as the nominal value of the parameter. For any integer k, let us consider the perturbations:

$$\boldsymbol{x}(2\pi k) = \boldsymbol{x}_k = \boldsymbol{x}^* + \boldsymbol{\xi}(k), \quad \boldsymbol{\lambda}_k = \boldsymbol{\lambda}^* + \boldsymbol{u}(k). \tag{3.7}$$

After one iteration of T we have

$$\begin{aligned} &\boldsymbol{x}(2\pi(k+1)) = \boldsymbol{x}_{k+1} = \boldsymbol{x}^* + \boldsymbol{\xi}(k+1) = T\left(\boldsymbol{x}^* + \boldsymbol{\xi}(k), \boldsymbol{\lambda}^* + \boldsymbol{u}(k)\right) \\ &= T(\boldsymbol{x}^*, \boldsymbol{\lambda}^*) + \left.\frac{\partial T}{\partial \boldsymbol{x}}\right|_{\substack{\boldsymbol{x}=\boldsymbol{x}^* \\ \boldsymbol{\lambda}=\boldsymbol{\lambda}^*}} \boldsymbol{\xi}(k) + \left.\frac{\partial T}{\partial \boldsymbol{\lambda}}\right|_{\substack{\boldsymbol{x}=\boldsymbol{x}^* \\ \boldsymbol{\lambda}=\boldsymbol{\lambda}^*}} \boldsymbol{u}(k) + \cdots \end{aligned} \tag{3.8}$$

Therefore we obtain the difference equation defined by the derivative of T:

$$\boldsymbol{\xi}(k+1) = \boldsymbol{A}\boldsymbol{\xi}(k) + \boldsymbol{B}\boldsymbol{u}(k). \tag{3.9}$$

where we put

$$\boldsymbol{A} = \left.\frac{\partial T}{\partial \boldsymbol{x}}\right|_{\substack{\boldsymbol{x}=\boldsymbol{x}^* \\ \boldsymbol{\lambda}=\boldsymbol{\lambda}^*}} \text{ and } \boldsymbol{B} = \left.\frac{\partial T}{\partial \boldsymbol{\lambda}}\right|_{\substack{\boldsymbol{x}=\boldsymbol{x}^* \\ \boldsymbol{\lambda}=\boldsymbol{\lambda}^*}} \tag{3.10}$$

Note that if $\boldsymbol{u}(k) = 0$, the origin is the unstable fixed point of Eq.(3.9) provided that $\boldsymbol{x}^*$ is embedded in a chaotic attractor.

Now we construct a state feedback control to stabilize the origin:

$$\boldsymbol{u}(k) = \boldsymbol{C}^\top \boldsymbol{\xi}(k), \tag{3.11}$$

where $\boldsymbol{C}$ is an $r \times n$ matrix must be designed. Substituting Eq.(3.11) into Eq.(3.9) we have

$$\boldsymbol{\xi}(k+1) = [\boldsymbol{A} + \boldsymbol{B}\boldsymbol{C}^\top]\boldsymbol{\xi}(k). \tag{3.12}$$

By the linear control theory, especially by the pole assignment technique, we can choose an appropriate matrix $\boldsymbol{C}$ to stabilize the origin, equivalently say the fixed point $\boldsymbol{x}^*$, provided that the controllability condition is satisfied[23]:

$$\text{rank}[\boldsymbol{B}|\boldsymbol{A}\boldsymbol{B}|\cdots|\boldsymbol{A}^{n-1}\boldsymbol{B}] = n \tag{3.13}$$

Hence we obtain the following theorem:

Theorem 3.1 *Let $\boldsymbol{x}^*$ be an unstable fixed point of the mapping T, which corresponds to an unstable periodic solution $\boldsymbol{x}^*(t)$ of Eq.(3.1) with the period 2π. Assume that the controllability condition (3.13) is satisfied. Then we can choose a matrix $\boldsymbol{C}$ such that Eq.(3.9) becomes stable, i.e., the matrix*

$$\boldsymbol{A} + \boldsymbol{B}\boldsymbol{C}^\top \tag{3.14}$$

is stable. Moreover by applying piecewise constant control $\boldsymbol{u}(k) = \boldsymbol{C}^\top \boldsymbol{\xi}(k)$ to the parameter $\boldsymbol{\lambda}$:

$$\boldsymbol{\lambda} = \boldsymbol{\lambda}^* + \boldsymbol{u}(k) = \boldsymbol{\lambda}^* + \boldsymbol{C}^\top \boldsymbol{\xi}(k) = \boldsymbol{\lambda}^* + \boldsymbol{C}^\top \{\boldsymbol{x}(2\pi k) - \boldsymbol{x}^*\} \quad \textit{with} \quad 2\pi k \le t < 2\pi(k+1) \tag{3.15}$$

the periodic solution $\boldsymbol{x}^*(t)$ becomes stable.

Remark 1 $\boldsymbol{A}$ and $\boldsymbol{B}$ in Eq.(3.10) are obtained numerically by solving the following linear ODEs from $t = 0$ to $t = 2\pi$:

$$\begin{aligned} \frac{d}{dt}\boldsymbol{A} &= \left.\frac{\partial \boldsymbol{f}}{\partial \boldsymbol{x}}\right|_{\substack{\boldsymbol{x}=\boldsymbol{x}^* \\ \boldsymbol{\lambda}=\boldsymbol{\lambda}^*}} \boldsymbol{A} \\ \frac{d}{dt}\boldsymbol{B} &= \left.\frac{\partial \boldsymbol{f}}{\partial \boldsymbol{x}}\right|_{\substack{\boldsymbol{x}=\boldsymbol{x}^* \\ \boldsymbol{\lambda}=\boldsymbol{\lambda}^*}} \boldsymbol{B} + \left.\frac{\partial \boldsymbol{f}}{\partial \boldsymbol{\lambda}}\right|_{\substack{\boldsymbol{x}=\boldsymbol{x}^* \\ \boldsymbol{\lambda}=\boldsymbol{\lambda}^*}} \end{aligned} \tag{3.16}$$

with initial condition

$$\boldsymbol{A}|_{t=0} = I, \quad \boldsymbol{B}|_{t=0} = 0, \tag{3.17}$$

where I is an identity matrix. Therefore, any analytic or estimating method to obtain $\boldsymbol{A}$ and $\boldsymbol{B}$ is not necessary.

Remark 2 A schematic block diagram of this control is illustrated in Fig. 3.1.

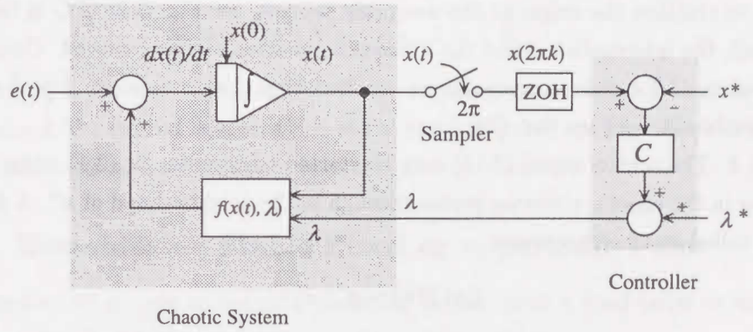

Figure 3.1: Composite dynamical system

In this figure the sampler operates at every instant $2\pi k$, say the Poincaré sampling instant. At every instant $2\pi k$, the sampled signal $x(2\pi k)$ is clamped during the Poincaré period or until next sampling is achieved. Therefore the parameter $\boldsymbol{\lambda}$ is changed discontinuously at every instant $2\pi k$. Such a sampled data system with zero-order hold(clamper; ZOH) is the most commonly known sampled data system. Note that, however, for the sampled data control system sampled interval is chosen as much shorter than our Poincaré period.

Remark 3 Eq.(3.9) is used only for designing the control matrix $\boldsymbol{C}$. Therefore it does not explicitly appear in the diagram shown in Fig. 3.1. We use the linear difference

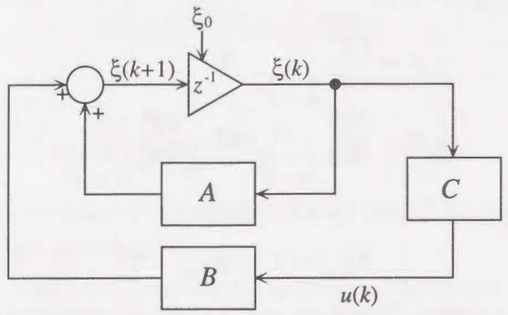

Figure 3.2: State feedback control described by Eq.(3.9) and (3.11).

equation to stabilize the origin at the designing process, see Fig. 3.2. If $\boldsymbol{C}$ is calculated once for all, the information about the difference equation can be removed. Design steps of the matrix $\boldsymbol{C}$ for pole assignment are omitted here, but it is easily found in linear control textbooks, e.g., see Ref. [24].

Remark 4 The control signal (3.15) may be started to apply to Eq.(3.1) when an orbit wandering in the chaotic attractor passes through in the neighborhood of $\boldsymbol{x}^*$. A detecting element, called watcher, measures

$$||\boldsymbol{x}(2\pi k) - \boldsymbol{x}^*|| < \epsilon \tag{3.18}$$

at every Poincaré sampling instant, and switches the control signal.

The controlled system is then totally described by

$$\begin{aligned} &\frac{d\boldsymbol{x}(t)}{dt} = \boldsymbol{f}\left(t, \boldsymbol{x}(t), \boldsymbol{\lambda}^* + \boldsymbol{C}^\top \boldsymbol{\xi}(k)\right), \\ &\qquad \text{for} \quad 2\pi k \le t < 2\pi(k+1) \\ &\boldsymbol{\xi}(k) = [\boldsymbol{A} + \boldsymbol{B}\boldsymbol{C}^\top]\boldsymbol{\xi}(k-1), \\ &\qquad \text{at} \quad t = 2\pi k \end{aligned} \tag{3.19}$$

with $\boldsymbol{\xi}(k) = \boldsymbol{x}(2\pi k) - \boldsymbol{x}^*$ for every integer k. This is a mixed continuous and discrete dynamical system, which we call a composite dynamical system(CDS). The most significant property of Eq.(3.19) is that the stability of the solutions $\boldsymbol{x}^*(t)$ and $\boldsymbol{\xi}(k) = \boldsymbol{0}$ is determined by the discrete part:

$$\boldsymbol{\xi}(k) = [\boldsymbol{A} + \boldsymbol{B}\boldsymbol{C}^\top]\boldsymbol{\xi}(k-1) \tag{3.20}$$

Hence if $\boldsymbol{A} + \boldsymbol{B}\boldsymbol{C}^\top$ is designed to be stable, then $(\boldsymbol{\xi}(k), \boldsymbol{u}(k))$ tends to $(0,0)$ as $k \to \infty$. This means at the steady state the parameter $\boldsymbol{\lambda}$ seems to be invariant as $\boldsymbol{\lambda}^*$ so that $\boldsymbol{x}^*$ is exactly the same trajectory as the uncontrolled original system, see Fig. 3.3(a). Note that the solution $\boldsymbol{x}(t)$ is unstable if we consider only the first equation of (3.19), but it becomes stable in the CDS.

3.2.3 Stabilizing Unstable m-Periodic Orbit

Similar result can be easily obtained for m-periodic point of T. Let the following m points:

$$\begin{cases} \boldsymbol{x}^*(2\pi) = \boldsymbol{x}_1^* = T(\boldsymbol{x}_m^*, \boldsymbol{\lambda}^*), \\ \boldsymbol{x}^*(2\pi k) = \boldsymbol{x}_k^* = T(\boldsymbol{x}_{k-1}^*, \boldsymbol{\lambda}^*), \\ \qquad \text{for} \quad k = 2, 3, \cdots, m. \end{cases} \tag{3.21}$$

be m-periodic points of T. This means that

$$\boldsymbol{x}_k^* = T^m(\boldsymbol{x}_k^*, \boldsymbol{\lambda}^*), \quad \text{for} \quad k = 1, 2, \cdots, m. \tag{3.22}$$

holds, i.e., $\boldsymbol{x}_k^*$ is the fixed point of T^m. Hence choosing the Poincaré period as $2m\pi$, we can construct the control matrix $\boldsymbol{C}$ at every $2\pi mk$ instant, see Fig. 3.3(b). For more detailed information, see Ref.[23].

3.2.4 Destabilizing Stable Fixed or m-periodic Point

In this section we discuss to design a controller destabilizing a fixed point or m-periodic of the mapping T. We have the following destabilizing theorem.

Theorem 3.2 *Let $\boldsymbol{x}^*$ be a stable fixed point of the mapping T, which corresponds to a stable periodic solution $\boldsymbol{x}(t)$ of Eq.(3.1) with the period 2π. Assume that the controllability condition (3.13) is satisfied. Then we can choose a matrix $\boldsymbol{C}$ such that Eq.(3.9) becomes unstable, i.e., the matrix*

$$\boldsymbol{A} + \boldsymbol{B}\boldsymbol{C}^\top \tag{3.23}$$

is unstable. Moreover by applying piecewise constant control $\boldsymbol{u}(k) = \boldsymbol{C}^\top \boldsymbol{\xi}(k)$ to the parameter $\boldsymbol{\lambda}$:

$$\begin{aligned} &\boldsymbol{\lambda} = \boldsymbol{\lambda}^* + \boldsymbol{u}(k) = \boldsymbol{\lambda}^* + \boldsymbol{C}^\top \boldsymbol{\xi}(k) \\ &= \boldsymbol{\lambda}^* + \boldsymbol{C}^\top \left\{\boldsymbol{x}(2\pi k) - \boldsymbol{x}^*\right\}, \\ &\qquad \textit{for} \quad 2\pi k \le t < 2\pi(k+1) \end{aligned} \tag{3.24}$$

the periodic solution $\boldsymbol{x}^*(t)$ becomes unstable.

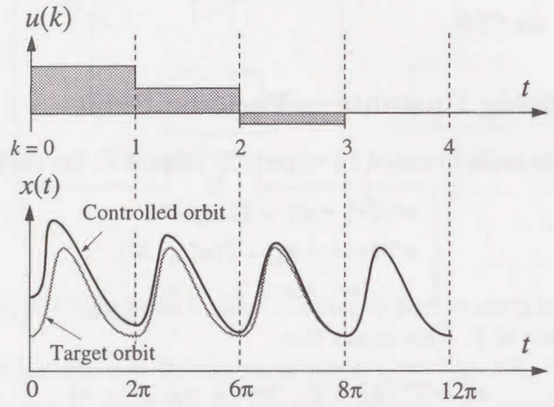

(a)

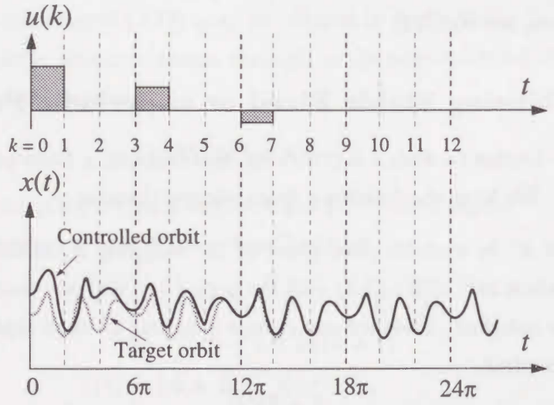

(b)

Figure 3.3: Response of the control signal and state $\boldsymbol{x}(t)$. (a):fixed point, (b):3-periodic point.

Remark 5 After the destabilization the orbit of CDS (3.19) may be chaotic, periodic, or convergent to another stable attractor.

3.2.5 In Case of Autonomous System

We can design the controller in the same way mentioned above except for the Poincaré mapping and its derivatives. Suppose that the system is described by Eq.(2.1) in Chapter 2. In the same way the initial conditions are defined by Eq.(2.2)–(2.12). The fixed point $\boldsymbol{w}^* \in \boldsymbol{R}^{n-1}$ of the map T_ℓ is written as:

$$\boldsymbol{w}^* = T_\ell(\boldsymbol{w}^*, \boldsymbol{\lambda}^*) = h(\boldsymbol{\varphi}(\tau(h^{-1}(\boldsymbol{w}^*)), h^{-1}(\boldsymbol{w}^*), \boldsymbol{\lambda}^*) \tag{3.25}$$

where $\boldsymbol{\lambda}^*$ is a nominal value of the parameter. Small perturbations of the state and parameter are defined by:

$$\begin{aligned} &\boldsymbol{w}(k+1) = \boldsymbol{w}^* + \boldsymbol{\xi}'(k) = h(\boldsymbol{\varphi}(\tau(h^{-1}(\boldsymbol{w}^* + \boldsymbol{\xi}'(k))), \boldsymbol{w}^* + \boldsymbol{\xi}'(k)) \\ &\boldsymbol{\lambda}(k) = \boldsymbol{\lambda}^* + \boldsymbol{u}'(k). \end{aligned} \tag{3.26}$$

By Substituting Eqs.(3.26) to Eq.(3.25) we have

$$\boldsymbol{w}(k+1) = T_\ell(\boldsymbol{w}^*) + DT_\ell(\boldsymbol{w}^*)\boldsymbol{\xi}'(k) + DT_\ell(\boldsymbol{\lambda}^*)\boldsymbol{u}'(k) + \cdots \tag{3.27}$$

Therefore, the linearized system of Poincaré mapping can be described as:

$$\boldsymbol{\xi}'(k+1) = \boldsymbol{A}'\boldsymbol{\xi}'(k) + \boldsymbol{B}'\boldsymbol{u}'(k). \tag{3.28}$$

where

$$\begin{aligned} \boldsymbol{A}' &= DT_\ell(\boldsymbol{w}^*) = Dh \cdot DT(\boldsymbol{x}^*) \cdot Dh^{-1} \\ \boldsymbol{B}' &= DT_\ell(\boldsymbol{\lambda}^*) = Dh \cdot DT(\boldsymbol{\lambda}^*) \end{aligned} \tag{3.29}$$

$$\begin{aligned} DT(\boldsymbol{x}) &= \left[I_n - \frac{1}{\dfrac{\partial q}{\partial \boldsymbol{x}} \cdot \boldsymbol{f}} \boldsymbol{f} \cdot \frac{\partial q}{\partial \boldsymbol{x}} \right] \frac{\partial \boldsymbol{\varphi}}{\partial \boldsymbol{x}_0} \\ DT(\boldsymbol{\lambda}) &= \left[I_n - \frac{1}{\dfrac{\partial q}{\partial \boldsymbol{x}} \cdot \boldsymbol{f}} \boldsymbol{f} \cdot \frac{\partial q}{\partial \boldsymbol{x}} \right] \frac{\partial \boldsymbol{\varphi}}{\partial \boldsymbol{\lambda}} \end{aligned} \tag{3.30}$$

Variations of Eq.(3.30) are obtained by solving the following equation from $t = 0$ to $t = L$(period of the target):

$$\begin{aligned}\frac{d}{dt}\left(\frac{\partial\boldsymbol{\varphi}}{\partial\boldsymbol{x}_0}\right) &= \frac{d\boldsymbol{f}}{d\boldsymbol{x}_0}(t,\boldsymbol{\varphi}(t,\boldsymbol{x}_0))\frac{\partial\boldsymbol{\varphi}}{\partial\boldsymbol{x}_0}\\ \frac{d}{dt}\left(\frac{\partial\boldsymbol{\varphi}}{\partial\boldsymbol{\lambda}}\right) &= \frac{d\boldsymbol{f}}{d\boldsymbol{x}_0}(t,\boldsymbol{\varphi}(t,\boldsymbol{x}_0))\frac{\partial\boldsymbol{\varphi}}{\partial\boldsymbol{x}_0}+\frac{\partial\boldsymbol{\varphi}}{\partial\boldsymbol{\lambda}}\end{aligned} \tag{3.31}$$

$$\text{with}\quad \left.\frac{\partial\boldsymbol{\varphi}}{\partial\boldsymbol{x}_0}\right|_{t=0} = I_n,\quad \left.\frac{\partial\boldsymbol{\varphi}}{\partial\boldsymbol{\lambda}}\right|_{t=0} = \mathbf{0}$$

Now we determine the $((n-1)\times r)$ control vector $\boldsymbol{C}'$ to stabilize $\boldsymbol{\xi}'(k)$ into $\mathbf{0}$ by suitable pole assignment provided the controllability is satisfied:

$$\det[\boldsymbol{B}'|\boldsymbol{A}'\boldsymbol{B}'|\cdots|\boldsymbol{A}'^{n-2}\boldsymbol{B}'] \neq 0 \tag{3.32}$$

Finally, the controlled input is given by:

$$\boldsymbol{u}'(k) = \boldsymbol{C}'^{\top}\boldsymbol{\xi}'(k) \tag{3.33}$$

It should be noted that this procedure to design the controller is achieved at an $(n-1)$-dimensional local coordinate. The controlled input $\boldsymbol{u}'$ can be added to the parameter of the original system. It is interesting that the dimensional reduction which is one of concepts for the Poincaré mapping is utilized real control problems.

3.2.6 Target Generating and Noise Effect

To calculate a target(fixed or periodic point), the Newton's method using the Jacobian matrix $\boldsymbol{A}$(or $\boldsymbol{A}'$) is available. Any precision of the target location can be obtained by this method unless that the Jacobian matrix $\boldsymbol{A}$ is singular. When a deterministic differential equation is given, the local properties of the orbit is completely described by $\boldsymbol{A}$, which is the solution of the first equation of Eqs.(3.16). Therefore, if the target can be calculated by $\boldsymbol{A}$ and the condition (3.13) is held, control can be succeed by suitable choice of ϵ.

The width of ϵ giving the control available region called basin of attraction depends on stability of the target, control parameters, and assigned poles. especially, the basin tends to reduce as the period of the target becomes higher. This disadvantage causes that the transient chaotic response is too long. If the basin of attraction can be wide, not only suppressing for transient responses but also the robustness of the control against disturbances or noise is earned. We must investigate to enlarge the basin in future for physical implementations.

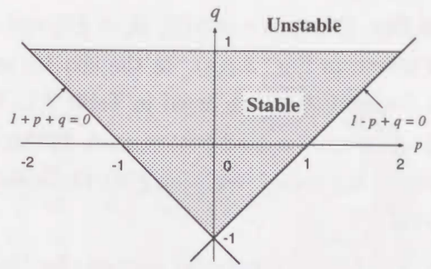

Figure 3.4: Stability in p-q plane for Eq.(3.35).

3.2.7 Illustrated Examples

3.2.7.1 Duffing's Equation

We choose Duffing's equation:

$$\begin{aligned}\frac{dx}{dt} &= y\\ \frac{dy}{dt} &= -\kappa y - x^3 + B_0 + B\cos t\end{aligned} \tag{3.34}$$

to demonstrate our method of control. For simplicity in this section we assume that we know the system, i.e., we can obtain all information for constructing the control matrix $\boldsymbol{C}$. Hence unstable fixed or periodic point embedded in some chaotic attractor is calculated in advance by using Newton's method.

Now we choose B_0 as the control parameter and calculate control vector $\boldsymbol{C}(2\times 1)$. Any other parameter can be chosen if the condition Eq.(3.13) is held. To determine the control vector $\boldsymbol{C}$ we consider the characteristic equation from Eq.(3.14):

$$|\boldsymbol{A}+\boldsymbol{B}\boldsymbol{C}^{\top}-\mu I| = \mu^2 - p\mu + q = 0. \tag{3.35}$$

Thus the modulus of the root of Eq.(3.35) is less than unity if p and q are placed in the triangle such that:

$$q < 1,\quad 1+p+q > 0,\quad 1-p+q > 0. \tag{3.36}$$

Figure 3.4 shows the stable region in p-q plane. Note that when B is chosen as the control parameter and controllability is also held, the external force $B_0+(B+u(2\pi)k)\cos t$ can be smooth.

Example 1 — Stabilization —

We fix the parameters in Eqs. (3.34) as $\kappa = 0.02$, $B_0 = 2.0$, and $B = 2.2$. The equations have a chaotic attractor shown in Fig. 3.5(a). In the chaotic attractor we see unstable fixed or periodic points. Some of them are listed in Table 3.1. We calculate the control vector $\boldsymbol{C}$ so as $p = q = 0$ which gives a dead beat control. In this case $\boldsymbol{A} + \boldsymbol{B}\boldsymbol{C}^\top$ becomes a nilpotent matrix. Hence for any initial condition $\boldsymbol{\xi}(0)$, the state $\boldsymbol{\xi}(k)$ falls into 0 at most twice iteration of $\boldsymbol{A} + \boldsymbol{B}\boldsymbol{C}^\top$.

Figure 3.5–3.10 show the stabilized periodic solutions by the controlling (3.15). For the fixed point of Fig. 3.6, this is given by:

$$B_0 = 2.0 + 2.3071(x(2\pi k) - 2.3891) + 0.3784(y(2\pi k) - 0.0256). \tag{3.37}$$

Table 3.1: Fixed or periodic points and the values of control vectors.

figure	period	fixed/periodic point	eigenvalues	control vector $\boldsymbol{C}$
Fig.3.6	1	$(2.3891, 0.0256)$	$(-0.1776, -4.9633)$	$[2.3071 \quad 0.3784]$
Fig.3.7	3	$(2.1868, -1.2681)$	$(-0.2681, -2.5579)$	$[2.4317 \quad 0.0140]$
Fig.3.8	5	$(2.4427, -0.8255)$	$(-0.01366, -39.0295)$	$[2.3561 \quad 0.0673]$
Fig.3.9	7	$(1.9857, 3.6287)$	$(-0.02167, -19.1425)$	$[4.1572 \quad 4.1529]$
Fig.3.10	9	$(1.9391, 0.7922)$	$(0.005869, 54.9848)$	$[0.9811 \quad -0.8679]$

Example 2 — Destabilization —

Now we consider the case where $\kappa = 0.1$, $B_0 = 0.0$, and $B = 0.3$. In this case we have two stable fixed points ${}^1S$ and ${}^2S$ as shown in Fig. 3.11(a). Let us try the destabilization of the fixed point ${}^2S$ in Fig. 3.11(a) by placing the poles of Eq.(3.35) out of the triangle Eq.(3.36) so that solution enters in the basin of the stable fixed point ${}^1S$ and finally tends to ${}^1S$. The transient process is shown in Fig. 3.11(b). This example suggests that the destabilization method may be efficiently applied to escape from a local minimum in various optimization problems.

Example 3 — Making Chaos —

As the final example of this section, we consider the case where Eq.(3.34) have only one stable fixed point. In this case we may observe a chaotic attractor by choosing $\boldsymbol{C}$ appropriately. Two examples are shown in Fig.3.12(a) and (b). Both attractors have positive Lyapunov exponents, see Fig.3.12.

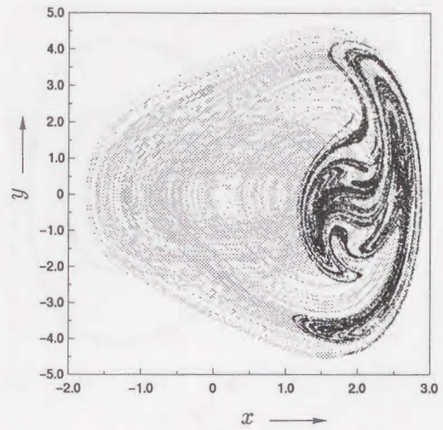

Figure 3.5: Chaotic attractor (the orbit with the Poincaré mapping), $\kappa = 0.02$, $B_0 = 2.0$, $B = 2.2$.

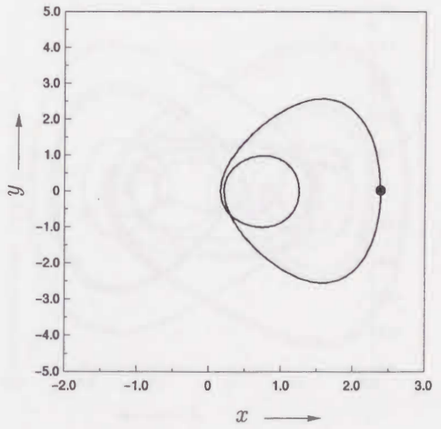

Figure 3.6: Stabilized unstable periodic orbit with a fixed point

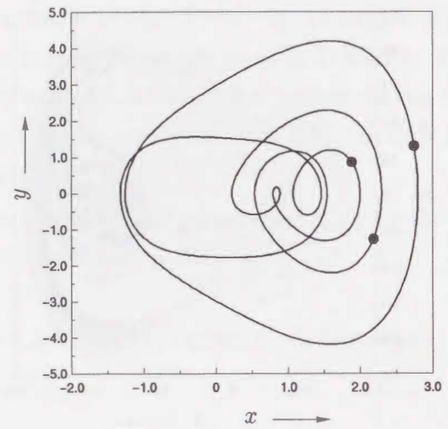

Figure 3.7: Stabilized unstable 3-periodic orbit.

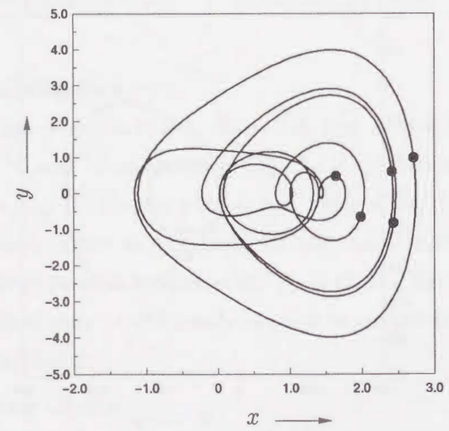

Figure 3.8: Stabilized unstable 5-periodic orbit.

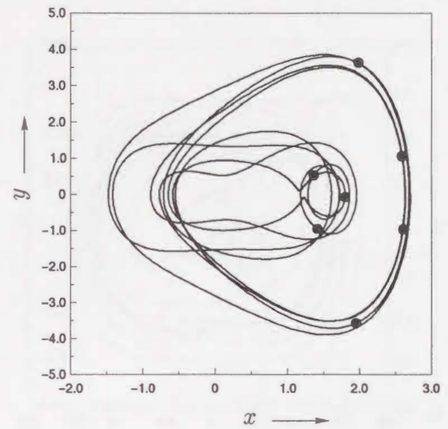

Figure 3.9: Stabilized unstable 7-periodic orbit.

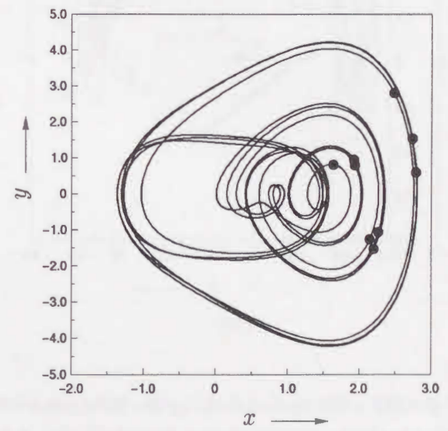

Figure 3.10: Stabilized unstable 9-periodic orbit.

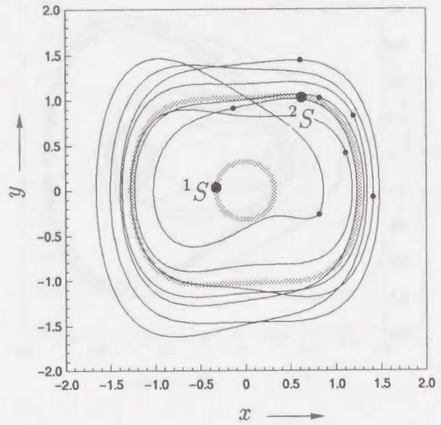

(a)

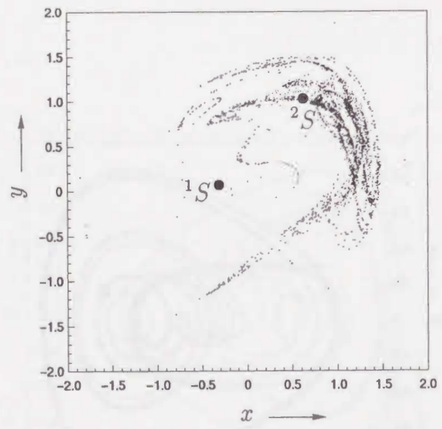

(b)

Figure 3.11: (a):Created 7-periodic orbit by destabilizing the fixed point ^2S. Poles are -4.0 and 4.0, $\epsilon = 0.3$. (b):Created chaotic transient eventually falling into the basin of ^1S. Poles are 6.6 and 0.0, $\epsilon = 0.3$

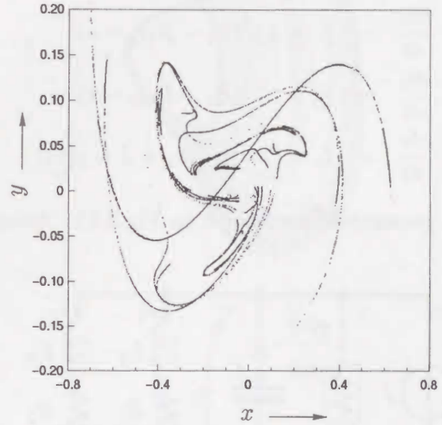

(a)

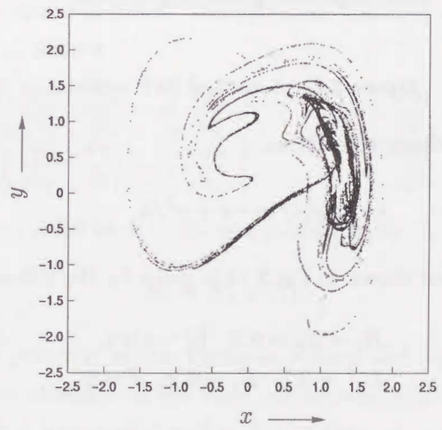

(b)

Figure 3.12: Created chaotic attractor. (a): $B = 0.1$, Poles are -9.0 and 0.0, $\epsilon = 0.1$. (b): $B = 0.5$. Poles are -12.0 and 6.0, $\epsilon = 0.3$. The maximum Lyapunov exponents of these examples are 0.3471, 0.1303, respectively.

3.2.7.2 Modified BVP Equation

As an example for autonomous system, we choose the modified BVP equation[25]:

$$\begin{aligned} \frac{di_1}{dt} &= f_1 = L_1^{-1}(E_1 - R_1 i_1 - v) \\ \frac{di_2}{dt} &= f_2 = L_2^{-1}(E_2 - R_2 i_2 - v) \\ \frac{dv}{dt} &= f_3 = C^{-1}(i_1 + i_2 + J - g(v)) \end{aligned} \tag{3.38}$$

where the variables and parameters are shown in Fig.3.13. Assume that the nonlinear

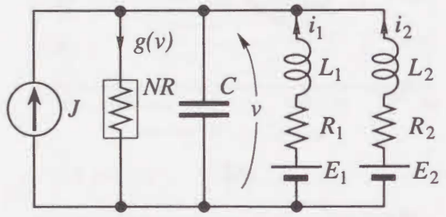

Figure 3.13: A modified BVP oscillator

resistor NR has a cubic characteristics as:

$$g(v) = -v + v^3/3 \tag{3.39}$$

A typical chaotic attractor shown in Fig.3.14 is given by the following parameters.

$$\begin{aligned} &R_1 = R_2 = 0.5, \;\; L_1^{-1} = 0.4, \\ &L_2^{-1} = 0.1, \;\; E_1 = 0.2, \;\; J = 0 \end{aligned} \tag{3.40}$$

We choose the Poincaré section Π as

$$\Pi = \{\boldsymbol{x}_0 = (i_1, i_2, v) \in \boldsymbol{R}^3 \,|\, v = v_0, i_1 + i_2 > i_{10} + i_{20}\} \tag{3.41}$$

where (v_0, i_{10}, i_{20}) is the unstable equilibrium point surrounded by the chaotic attractor on the plane spanned by eigenvectors. Consequently, the local coordinate is given by $(i_1, i_2) \in \boldsymbol{R}^2$. Let us consider an example that the voltage E is chosen as the control parameter. Since the controllability Eq.(3.32) is held, we can obtain the control vector

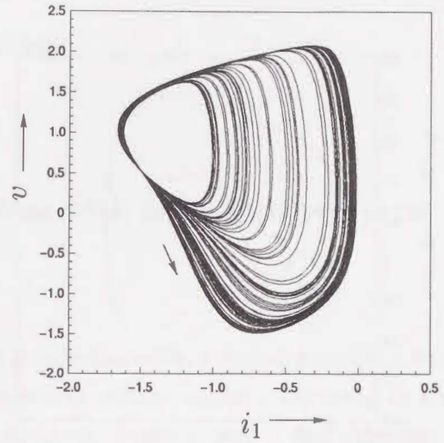

Figure 3.14: Chaotic attractor observed in Eq.(3.38).

Eq.(3.33) with suitable specified poles. The Jacobian matrices $\boldsymbol{A}'$ and $\boldsymbol{B}'$ in Eq. (3.28) are described in detail as follows.

$$\boldsymbol{A}' = \begin{bmatrix} \frac{\partial \varphi_1}{\partial i_1} - \frac{f_1}{f_3}\frac{\partial \varphi_3}{\partial i_1} & \frac{\partial \varphi_1}{\partial i_2} - \frac{f_1}{f_3}\frac{\partial \varphi_3}{\partial i_2} \\ \frac{\partial \varphi_2}{\partial i_1} - \frac{f_2}{f_3}\frac{\partial \varphi_3}{\partial i_1} & \frac{\partial \varphi_2}{\partial i_2} - \frac{f_2}{f_3}\frac{\partial \varphi_3}{\partial i_2} \end{bmatrix} \qquad \boldsymbol{B}' = \begin{bmatrix} \frac{\partial \varphi_1}{\partial E_2} - \frac{f_1}{f_3}\frac{\partial \varphi_3}{\partial E_2} \\ \frac{\partial \varphi_2}{\partial E_2} - \frac{f_2}{f_3}\frac{\partial \varphi_3}{\partial E_2} \end{bmatrix} \tag{3.42}$$

Finally the control input is fed back to E_2 as a perturbation:

$$E_2 \to E_2 + u(k) \tag{3.43}$$

We show the phase portraits of this example, a fixed and 3-periodic unstable points embedded in the chaotic attractor at the fixed parameters indicated in Eq.(3.40). These data and designed control vector are listed in Tab. 3.2.

Table 3.2: Fixed point/periodic points, eigenvalues at the local coordinate, and control vectors

Figure	period	fixed/periodic point	eigenvalues	control vector
Fig. 3.15	1	$(-0.1900, 1.2883, 0.9118)$	$(0.0002, -5.9191)$	$[0.1099, -0.5481]$
Fig. 3.16	3	$(-0.7623, 1.1129, 0.9118)$	$(0.0000, -2.7397)$	$[0.1805, -0.8324]$

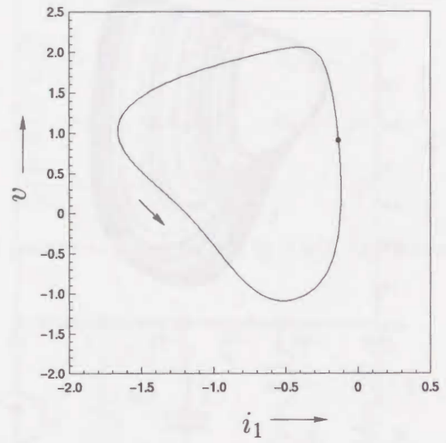

Figure 3.15: Stabilized fixed point(black circle). The arrow indicates the direction of the orbit.

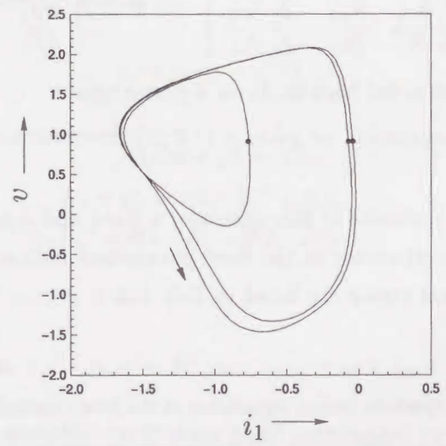

Figure 3.16: Stabilized 3-periodic point.

3.3 Bifurcation and Control for Pendulum Forced by Impulses

3.3.1 A Pendulum with an Impulsive Force

The equation of motion for a kicked rotor, a stepping motor, a circuit containing a Josephson junction with an impulsive voltage source is described as a second order differential equation containing a sinusoidal function with a discontinuous external force. In such systems, two topologically different kinds of periodic solutions are found; revolving and oscillatory solutions. The former winds around a cylindrical phase space, and latter does not, see Fig.3.17. We observed higher periodic orbits or chaotic states for both these solutions.

In this section, we investigate some properties of the pendulum equation with a periodic impulsive force. First of all, we analyze periodic orbits by using the bifurcation theory. Although this equation has an impulsive force, i.e., the orbit changes discontinuously we can calculate bifurcation parameters since its Poincaré mapping is constructed as a differentiable map[26]. As the result, some properties of the periodic solutions are explained from bifurcation diagrams. In Sec.3.3.5 we propose a method to stabilize the unstable periodic orbit embedded in a chaotic attractor by small perturbations of the system parameter.

The equation is also described the behavior of a stepping motor on the velocity error plane. Especially if the orbit converges to any revolving orbit the motor cannot be controlled to generate the desirable velocity. In Sec.3.3.6.2, we study the bifurcation phenomena of periodic orbit in the case that the motor is driven by an intermittent sequence [27], and obtain the bifurcation diagram. Moreover in Sec.3.3.6, we propose a method to avoid the pull-out and to improve the transient responses by changing the repetitive frequency and stepping rate of the intermittent drive sequence.

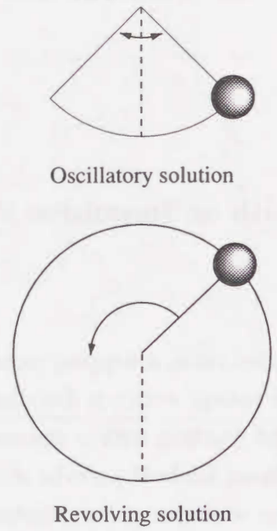

Figure 3.17: Oscillatory solution and revolving solution.

3.3.2 Mathematical Model

The motion of a pendulum with damping is described by the following autonomous equation:

$$\begin{aligned} \frac{dx}{dt} &= y &&= f(x,y) \\ \frac{dy}{dt} &= -\kappa y - \sin x &&= g(x,y) \end{aligned} \tag{3.44}$$

where, $(x,y) \in \boldsymbol{R}^2$ is state, $\kappa > 0$ is damping coefficient. Note that the state space is regarded as $S^1 \times \boldsymbol{R}$, where $S^1 = \{x \in \boldsymbol{R} \bmod 2\pi\}$. Since the system (3.44) is dissipative, there is no periodic solution except for $k = 0$. Now we assume an input which achieves the periodic discontinuity of initial state by using the sequence of impulses. Then the equation (3.44) is rewritten as follows:

$$\begin{aligned} \frac{dx}{dt} &= f(x,y) + \frac{\pi}{2} h \sum_{k=0}^{\infty} \delta(t - k\tau) \\ \frac{dy}{dt} &= g(x,y). \end{aligned} \tag{3.45}$$

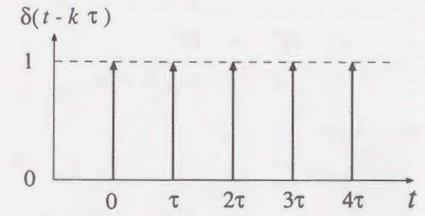

Figure 3.18: Sequence of implusive waves $\sum_{k=0}^{\infty} \delta(t - k\tau)$

where, $\delta(t)$ is the Dirac's delta function, and h, τ are height and interval of the impulse, respectively. See Fig.3.18. $\pi/2$ is added for the convenience sake.

Adding the periodic impulsive force to $f(x,y)$ is frequently assumed to simulate the response of the periodically stimulated neuron model by a BVP oscillator[28].

3.3.3 Poincaré Mapping

We construct the Poincaré mapping to analyze periodic solutions observed in Eq.(3.45) in $h > 0$. The impulsive external force affects the orbit of Eq.(3.45) as an instantaneous translation. The computational method to obtain periodic points and bifurcation parameters of the periodic solution driven by a discontinuous input are already proposed[26], hence the bifurcational analysis for oscillations observed in this system is possible. In the following, we summarize this scheme briefly.

We rewrite the Eq.(3.45) as the following form:

$$\frac{d\boldsymbol{x}}{dt} = \boldsymbol{f}(t, \boldsymbol{x}, \lambda) + \boldsymbol{h} \sum_{k=0}^{\infty} \delta(t, \tau) \tag{3.46}$$

where, $\boldsymbol{x} \in \boldsymbol{R}^n$ and $\lambda \in \boldsymbol{R}$ are the state and the system parameter, respectively. Suppose $\boldsymbol{f} : \boldsymbol{R} \times \boldsymbol{R}^n \times \boldsymbol{R} \to \boldsymbol{R}^n$ is C^∞. Let a solution of Eq.(3.45) be

$$\boldsymbol{x}(t) = \boldsymbol{\varphi}(t, \boldsymbol{x}_0, \lambda) \tag{3.47}$$

where,

$$\boldsymbol{x}(0) = \boldsymbol{\varphi}(0, \boldsymbol{x}_0, \lambda) = \boldsymbol{x}_0. \tag{3.48}$$

We choose the interval of the Poincaré mapping as a period τ of the impulse sequence. In the moment at which the impulse is added to the system, a composition of the following

two maps is considered as the Poincaré mapping. P_1 is a map which translates $\boldsymbol{x}$ to $\boldsymbol{x}+\boldsymbol{h}$:

$$\begin{aligned} P_1 : \boldsymbol{R}^n &\rightarrow \boldsymbol{R}^n \\ \boldsymbol{x} &\mapsto \boldsymbol{x}+\boldsymbol{h}=\boldsymbol{x}_1 \end{aligned} \tag{3.49}$$

P_2 is an ordinary time τ mapping:

$$\begin{aligned} P_2 : \boldsymbol{R}^n &\rightarrow \boldsymbol{R}^n \\ \boldsymbol{x}_1 &\mapsto \boldsymbol{\varphi}((k+1)\tau, \boldsymbol{x}(k\tau), \lambda) \end{aligned} \tag{3.50}$$

Hence the Poincaré mapping P is described by:

$$\begin{aligned} P : \boldsymbol{R}^n &\rightarrow \boldsymbol{R}^n \\ \boldsymbol{x} &\mapsto P(\tau, \boldsymbol{x}, \lambda) = P_2 \circ P_1(\tau, \boldsymbol{x}, \lambda). \end{aligned} \tag{3.51}$$

We use this composite mapping and its derivatives to calculate not only fixed or periodic points and bifurcation parameters, but also the gain of controller stabilizing chaotic state.

3.3.4 Bifurcation Diagrams

For simplicity, we fix the parameter B_0 as 0. In this case, there exist a sink$(0,0)$ and a saddle$(\pi,0)$ in $S^1 \times \boldsymbol{R}$ with $h=0$. Figures 3.19 and 3.20 show bifurcation diagrams in the τ-h and τ-k plane. In the following we fix $h=2.0, \kappa=0.2$. G_i^1 and I_i^1 $i=1,2$ indicate tangent and period doubling bifurcations for the fixed point, respectively. Almost regions of these diagrams there exist revolving solutions, see Fig.3.21. The oscillatory solutions exist in the shaded region. There also exit two kinds of oscillatory solutions in the dark-shaded region, see Figs.3.22 and 3.23. In each of the regions encircled by I_1^1 or I_2^1, there are many higher periodic and chaotic orbits. Figures 3.24–3.26 show the orbits bifurcated by the cascade of period doubling in $h=2.0$. Figure 3.27 is a chaotic orbit winding around S^1.

3.3.5 Controlling the Unstable Orbit

In this section, we consider a control strategy of any periodic orbit included in Eq.(3.45) by applying the control discussed in Sect. 3.2. As the preliminary, We modify the notations and definitions of maps and variables used in Sect. 3.2.

Suppose that the system (3.45) has a fixed point, i.e., there exist $\boldsymbol{x}^* \in \boldsymbol{R}^n$ and $\lambda^* \in \boldsymbol{R}$ such that

$$\boldsymbol{x}^* = P(\tau, \boldsymbol{x}^*, \lambda^*). \tag{3.52}$$

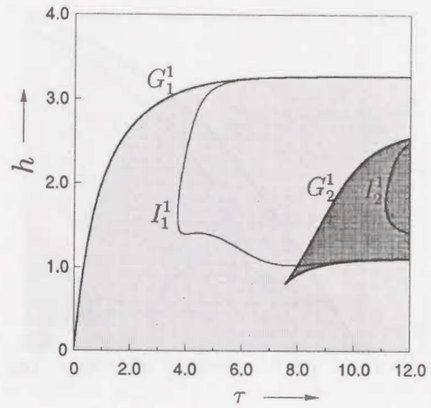

Figure 3.19: Bifurcation diagram of periodic solutions in (τ-k) plane. $h=2.0$.

We call this point target.

The variational equation in the neighborhood of the target $\boldsymbol{x}^*$ is described as follows:

$$\boldsymbol{x}(k\tau) = \boldsymbol{x}^* + \boldsymbol{\xi}(k), \;\; \lambda = \lambda^* + u(k). \tag{3.53}$$

where, k is an integer, $u(k)$ is the perturbation of λ^*. From Eq.(3.52), we have

$$\begin{aligned} \boldsymbol{x}^* + \boldsymbol{\xi}(k+1) &= P\left(\tau, \boldsymbol{x}^* + \boldsymbol{\xi}(k), \lambda^* + u(k)\right) \\ &= P(\tau, \boldsymbol{x}^*, \lambda^*) + \boldsymbol{A}\boldsymbol{\xi}(k) + \boldsymbol{b}u(k) + \cdots \end{aligned} \tag{3.54}$$

where,

$$\boldsymbol{A} = \left.\frac{\partial P}{\partial \boldsymbol{x}}\right|_{\boldsymbol{x}=\boldsymbol{x}^*,\ \lambda=\lambda^*} \qquad \boldsymbol{b} = \left.\frac{\partial P}{\partial \lambda}\right|_{\boldsymbol{x}=\boldsymbol{x}^*,\ \lambda=\lambda^*} \tag{3.55}$$

Thus, we obtain a linearized difference equation in the neighborhood of the target as follows:

$$\boldsymbol{\xi}(k+1) = \boldsymbol{A}\boldsymbol{\xi}(k) + \boldsymbol{b}u(k). \tag{3.56}$$

Note that the matrix $\boldsymbol{A}$ and vector $\boldsymbol{b}$ are obtained numerically by solving the following differential equations from $t=0$ to $t=\tau$:

$$\begin{aligned} \frac{d}{dt}\frac{\partial P}{\partial \boldsymbol{x}} &= \frac{\partial \boldsymbol{f}}{\partial \boldsymbol{x}}\frac{\partial P}{\partial \boldsymbol{x}} \quad \text{with} \quad \left.\frac{\partial P}{\partial \boldsymbol{x}}\right|_{t=0} = I \\ \frac{d}{dt}\frac{\partial P}{\partial \lambda} &= \frac{\partial \boldsymbol{f}}{\partial \boldsymbol{x}}\frac{\partial P}{\partial \lambda} + \frac{\partial \boldsymbol{f}}{\partial \lambda} \quad \text{with} \quad \left.\frac{\partial P}{\partial \lambda}\right|_{t=0} = 0 \end{aligned} \tag{3.57}$$

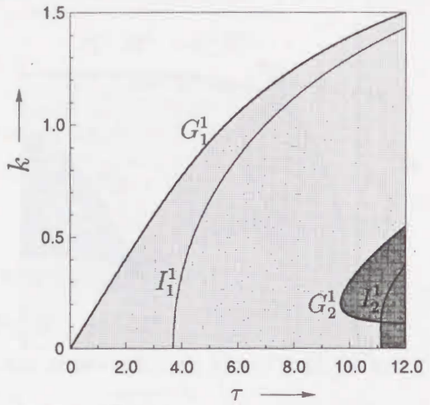

Figure 3.20: Bifurcation diagram of periodic solutions in (τ-k) plane. $\kappa = 0.2$.

These equations are already calculated to obtain the fixed point or bifurcation set by using the Poincaré mapping (3.52). We construct the state feedback to control Eq.(3.56):

$$u(k) = \boldsymbol{c}^{\top}\boldsymbol{\xi}(k) \tag{3.58}$$

where, $\boldsymbol{c}$ is a control vector $(1 \times n)$, and $\top$ indicates a transposition. As is well known, if

$$\det[\boldsymbol{b}|\boldsymbol{A}\boldsymbol{b}|\cdots|\boldsymbol{A}^{n-1}\boldsymbol{b}] \neq 0, \tag{3.59}$$

then Eq.(3.56) is controllable by Eq.(3.58). Consequently, we can choose a control vector determined by the solution of the pole assignment problem for characteristic equation:

$$\det[\boldsymbol{A} + \boldsymbol{b}\boldsymbol{c}^{\top} - \mu I] = 0. \tag{3.60}$$

where, I is the identity matrix. Finally, the composite dynamical system defined in Chapter 3 for Eq.(3.45) is described as follows:

$$\begin{aligned} \frac{d\boldsymbol{x}}{dt} &= \boldsymbol{f}\left(t, \boldsymbol{x}(t), \lambda^* + \boldsymbol{c}^{\top}\left(\boldsymbol{x}(k\tau) - \boldsymbol{x}^*\right)\right) \\ &\quad \text{with} \quad k\tau \leq t < (k+1)\tau \\ \boldsymbol{x}(k\tau) - \boldsymbol{x}^* &= [\boldsymbol{A} + \boldsymbol{b}\boldsymbol{c}^{\top}]\left(\boldsymbol{x}((k-1)\tau) - \boldsymbol{x}^*\right) \end{aligned} \tag{3.61}$$

Note that the control input calculated by (3.58) is applied constantly to the system parameter λ during the period τ, see Fig.3.29.

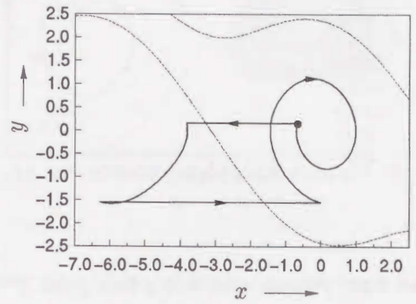

Figure 3.21: Periodic orbit with a fixed point(black circle) winding around a cylindrical phase space. $\kappa = 0.2$, $h = 2.0$, $\tau = 11.8$. The right oriented arrow shows taking modulo 2π and broken line shows separatrix.

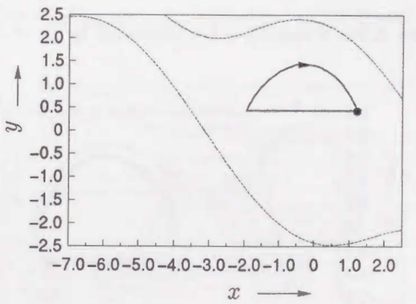

Figure 3.22: Periodic orbit with a fixed point. $\tau = 3.0$

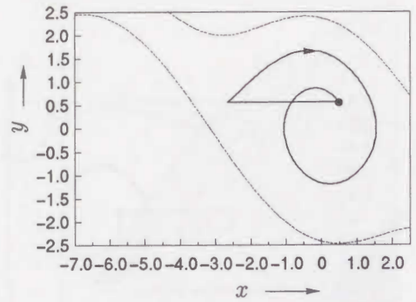

Figure 3.23: Periodic orbit with a fixed point. $\tau = 10.0$

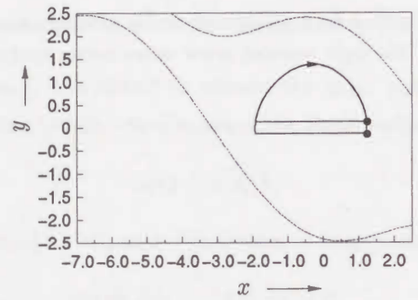

Figure 3.24: 2-periodic orbit bifurcated by I_1^1. $\tau = 3.32$

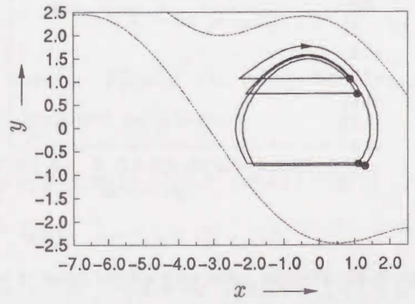

Figure 3.25: 4-periodic orbit. $\tau = 4.16$

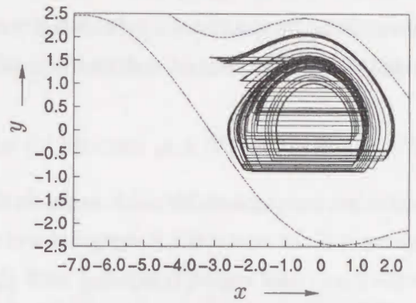

Figure 3.26: Chaotic orbit bifurcated by the cascade of period doubling. $\tau = 4.24$.

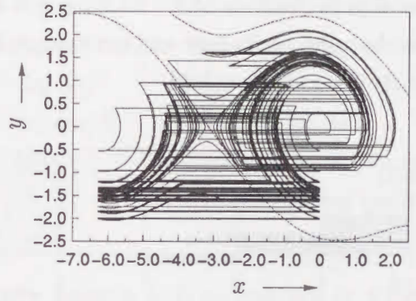

Figure 3.27: A chaotic orbit winding around a cylindrical phase space. $\kappa = 0.2$, $h = 2.0$, $\tau = 4.32$.

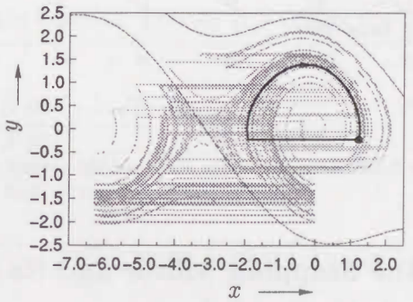

Figure 3.28: Stabilized periodic orbit(thick curve). $\tau = 4.32$, $\epsilon = 0.01$. The original eigenvalues for the fixed point are $\mu_1 = -0.2868$, $\mu_2 = -1.4697$.

In general, some methods for controlling chaos uses a property that the neighborhood of target will be visited before long by the chaotic orbit while wandering in the attractor. Equation (3.61) is also designed that the control is done if the orbit satisfies the following condition:

$$||\boldsymbol{x}(k\tau) - \boldsymbol{x}^*|| < \epsilon, \quad \epsilon > 0. \tag{3.62}$$

In case that the system parameter having a stable orbit varies to the destabilizing direction (bifurcation), we can suppress it if the controller is designed instantly. Therefore a robust operation is achieved in wide parameter region compared with the non-controlled system. Note that the control available region called basin of attraction depends on $\boldsymbol{f}$, ϵ and assigned poles[23].

Figure 3.28 shows a stabilized unstable periodic orbit with fixed point embedded in a chaotic attractor by small perturbations of h. Its poles are assigned to 0 (dead beat control). We also confirm that any oscillatory and revolving solution with a fixed point can be controlled by h or B_0 if Eq.(3.59) is held.

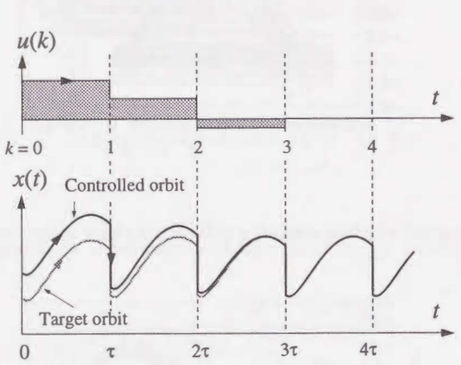

Figure 3.29: Response of the state and the control input.

3.3.6 Failure of the Stepping Motor and its Control

Stepping motors have been used in many position and speed control systems. However, there are failure operations called pull-out depending on the motor parameters. An analysis for the failure model of the stepping motor is studied in Ref.[29]. In this section, we

derive the equation of motions for the stepping motor, and show that the equation on the velocity error plane is identical to Eq.(3.45). Moreover, we investigate the characteristics of the motor driven by the intermittent sequence shown in Fig. 3.30.

3.3.6.1 The Equation of Motion and Velocity Error Plane

The torque equation of two-phase hybrid stepping motor is described by the following differential equation:

$$J\frac{d^2\theta}{dt^2} + D\frac{d\theta}{dt} + T_L = \sqrt{2}KI_m \sin\{N(U(t) - \theta)\} \tag{3.63}$$

where,

J	[kg·cm·s^2]	the moment of inertia
D	[kg·cm/rad/s]	viscous friction coefficient
T_L	[kg·cm]	load torque
K	[kg·cm/A]	torque constant
I_m	[A]	maximum motor current
N		number of rotor teeth
U	[rad]	mechanical angle

In Eq.(3.63) the stepwise function $U(t)$ corresponds to a stepping input signal which is given by:

$$U(t) = \frac{\pi h}{2N}\sum_{k=0}^{\infty} u(t - kT) \tag{3.64}$$

where, $u(t)$ is the unit step function. Putting $\Theta = N\theta$ we try to rewrite Eq.(3.64) into a normalized form as:

$$\frac{d^2\Theta}{dt^2} + \frac{D}{J}\frac{d\Theta}{dt} + \frac{N\sqrt{2}KI_m}{J}\sin\{\Theta - NU(t)\} + \frac{N}{J}T_L = 0 \tag{3.65}$$

By scaling the time axis as $t' = \omega t$, Eq.(3.65) becomes

$$\frac{d^2\Theta}{dt'^2} + \kappa\frac{d\Theta}{dt'} + \sin\{\Theta - NU\left(\frac{t'}{\omega}\right)\} + B_0 = 0 \tag{3.66}$$

where

$$\omega = \sqrt{\frac{N\sqrt{2}KI_m}{J}} \quad \kappa = \frac{D}{\sqrt{N\sqrt{2}KI_mJ}} \quad B_0 = \frac{T_L}{\sqrt{2}KI_m}. \tag{3.67}$$

Finally, by changing the variables in Eq.(3.66) such that

$$t = t', \;\; x = \Theta - NU\left(\frac{t'}{\omega}\right), \;\; y = \frac{d\Theta}{dt} \tag{3.68}$$

Eq.(3.65) is normalized as

$$\begin{cases} \dfrac{dx}{dt} = y - \dfrac{\pi}{2}\displaystyle\sum_{k=0}^{\infty}\delta(t - k\omega T) \\ \dfrac{dy}{dt} = -\kappa y - \sin x - B_0 \\ x(0) = y(0) = 0. \end{cases} \tag{3.69}$$

This equation is equivalent to Eq.(3.45) with $h = \omega = 1$ and its phase space (x, y) is called velocity error plane[29].

After the transient state, if the orbit of Eq.(3.69) stays at $0 \le x < 2\pi$ as $t \to \infty$ without taking modulo 2π, the normal operation is almost achieved. If the orbit is jumped across left separatrix one by one then the system behaves the asynchronous oscillation called pull-out operation. Figure 3.21 is also classified to this operation. One of our objectives of this study is to clarify this phenomenon depending on system parameters by using bifurcation theory.

3.3.6.2 Characteristics of Intermittent Drive

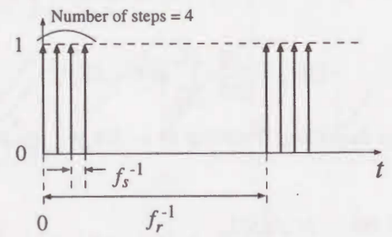

Figure 3.30: Intermittent drive sequence.f_s is the stepping rate, f_r is the repetitive frequency.

In the industrial fields, there exist many demands of the mechanism which accomplishes the synchronized operation for other intermittent motions, e.g., paper feeder, sawing machine, etc. The stepping motor driven by the intermittent sequence as shown in Fig. 3.30 is suitable to realize such motions. Ref.[27] suggests that some choices of the stepping rate f_s and repetitive frequency f_r involve pull-out. In this section, we investigate

these phenomena by the bifurcation theory, and control them by the method discussed in Sec.3.3.5.

We fix the parameters as follows:

$$J = 1.12 \times 10^{-3}, \;\; D = 0.2, \;\; T_L = 0, \;\; \sqrt{2}KI_m = 22.$$

and the number of steps on a period is 4. Thus the natural frequency and damping are as follows:

$$f_n = \omega/2\pi \approx 158[\text{Hz}]$$
$$\kappa \approx 0.18$$

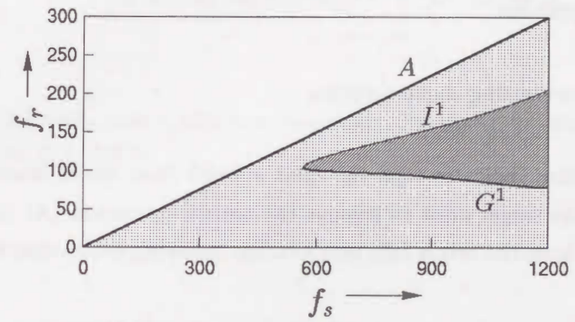

Figure 3.31: Bifurcation diagram of periodic orbit driven by intermittent drive sequence.

Figure 3.31 shows the bifurcation diagram of periodic solutions driven by intermittent sequences in f_s-f_r plane. In this figure, the line A indicates

$$f_r = \text{number of steps} \times f_s. \tag{3.70}$$

The drive sequence on A is identical to Fig.3.18, i.e., the impulses are arranged in equally interval. Therefore, the intermittent driving is achieved under this line. In light-shaded region under A there exist stable oscillatory or revolving orbits with a fixed point. In dark-shaded region enclosed G^1 and I^1 these orbit are bifurcated and progressed to chaotic revolving orbits. Figure 3.32 shows a 2-period orbit bifurcated by I^1. The neighborhood of the point crossing G^1 and I^1 we cannot trace the both bifurcation curves anymore because many higher periodic revolving and oscillatory solutions are found around there by changing slight parameter perturbations.

Note that Fig. 3.31 is not considered the starting characteristics. The orbit started from $(x_0, y_0) = (0, 0)$ is not always falls into the stable oscillatory orbit at last; in other words, it may not realize the normal operation.

3.3.6.3 Controlling Pull-Out

In Sec.3.3.5 a control method suppressing bifurcations for original stable target is proposed. We can also apply this method to the intermittent drive stepping motor. In this section, we propose a controller satisfying the following specifications:

- Avoid the pull-out.
- Consider the starting characteristics.

The latter condition indicates that the orbit started from initial state $(x_0, y_0) = (0, 0)$ should fall into the target orbit to achieve the normal operation. At the steady state, if the orbit started from the origin falls into a stable revolving orbit, then it can be regarded as pull-out.

Figure 3.33 shows pull-out started from the origin. In the same system parameters there also exists a basin falling into the stable oscillatory target. To avoid this starting failure we manipulate the basin of attraction for stable target by developing a compensator.

The compensator designed by same method discussed in Sec.3.3.5 gives an opportunity to change the attractor into which the orbit falls and improves the transient response by manipulating poles of the characteristic equation for the stable target. We choose $1/f_r$ which allows large scale perturbations, as the control parameter to enlarge the control area ϵ because the control value is proportional to the deviation $\boldsymbol{\xi}$. Thus the compensator changing timings of adding input sequences. Note that we assume the ratio f_s/f_r is constant. Figure 3.34 shows the case that both poles of the compensator assigned to 0, but several times the orbit winding around S^1. On the other hand, Figure 3.35 shows a satisfactory example which poles are assigned to 0 and -0.5. The control value is perturbed within 16.5% for $1/f_r$. For practical use, we should investigate a compensator using the fixed stepping rate.

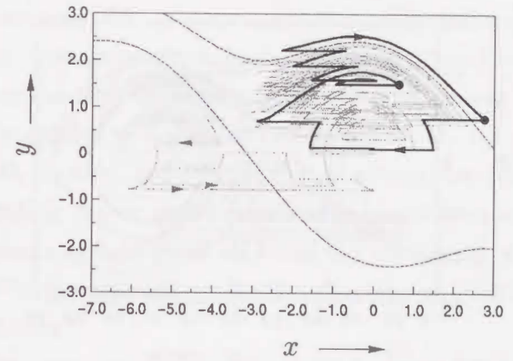

Figure 3.32: 2-period stable orbit started from the origin. The shaded line shows transient state. $\kappa = 0.18$, $f_r = 198.2$Hz, $f_s = 1982$Hz.

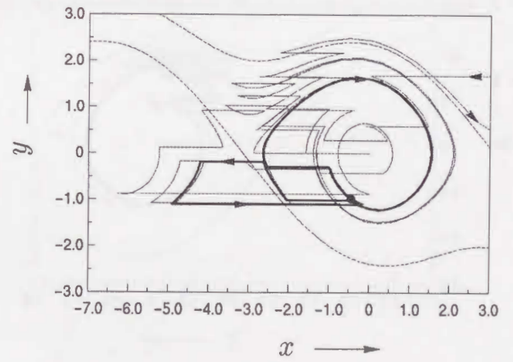

Figure 3.33: Pull-out orbit(thick curve) and the fixed point. $\kappa = 0.18$, $f_r = 90$Hz, $f_s = 900$Hz.

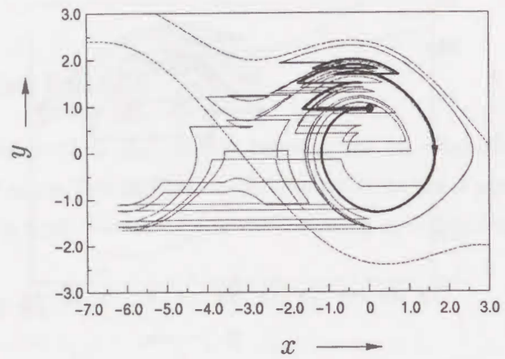

Figure 3.34: Stabilized orbit. Both poles are assigned to 0. $\epsilon = 2.0$

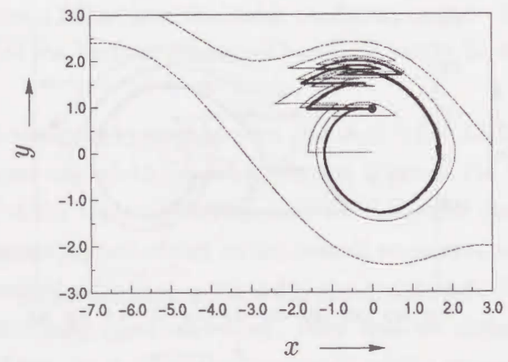

Figure 3.35: Improved transient state. The poles are assigned to 0 and -0.5. $\epsilon = 1.0$

3.4 Conclusions of Chapter 3

We propose the stabilization and destabilization method of periodic orbits for continuous dynamical system described ODE. In our stabilization method all trajectories are remain to be continuous and converge to a specific unstable orbits. Dead beat control design is one of the conventional method for this purpose. Many techniques known in the linear control theory can be applied to design the control matrix $\boldsymbol{C}$. For examples an output feedback method with observer, and optimal control method are directly applied to our problems. For controlling chaotic signal generated from unknown system we must construct target(the location of fixed point etc.) and the matrices $\boldsymbol{A}$ and $\boldsymbol{B}$ only by using the chaotic signal. For the practical application this type of question is an interesting problem left to the future.

Also we investigate some properties of Eq.(3.45) by using bifurcation diagrams. In this system,there exist the revolving and oscillatory solutions, and chaotic solutions are caused by their bifurcation. We also propose a method to control the target orbit by small perturbations of the system parameter, and show an example of controlling. Further, we study the properties of the stepping motor by using velocity error plane. In the case that the motor driven by intermittent impulse sequences, there exist failure operations called pull-out operations. Then we construct a compensator to avoid them by changing the intermittent driving frequency and stepping rate, and illustrate some examples applied the pole assign technique. To develop the actual implementations is a future problem.

Chapter 4

Conclusions

Bifurcation phenomena and controlling chaos in nonlinear dynamical systems, especially the pendulum systems, have been investigated.

In Chapter 2 we have summarized the bifurcation theory and classified topological properties of bifurcations. Bifurcation of equilibrium, periodic solution for local bifurcations, and stabilities of these points have been also discussed. Computational method to obtain a local bifurcation; parameter for period doubling, tangent, and Neimark-Sacker bifurcation has been discussed.

Firstly we have been studied a pendulum with an elastic torsional joint, and its equivalent electric circuit; an L-C-G parallel circuit with a JJ element. We have investigated heteroclinic bifurcations correlated with separatrices of the saddle points and classified the topological properties of the heteroclinic orbit with a linking number between the heteroclinic orbit and a suitable cross section. The results of the study will be important as a fundamental analysis for higher-dimensional autonomous systems.

Secondly, we study some qualitative properties of the two pendula linked by a elastic torsional rod. This model also regarded as an inductively coupled circuit containing two JJ elements with a d.c. source. The system is described by a four-dimensional autonomous differential equation. However, the phase space can be regarded as $S^1 \times \boldsymbol{R}^3$ because the system is invariant under the transformation. We studied the properties of periodic solutions winding around S^1 as a bifurcation problem. The bifurcation diagram of equilibria and its topological classification have been given. The bifurcation diagram of the periodic solutions winding around S^1 have been also calculated by using a suitable Poincaré mapping, and some properties of periodic solutions have been discussed. From these analyses, we clarify that a periodic solution so-called "caterpillar solution"[9] is

observed when the two JJ circuits are weakly coupled.

Thirdly we investigate two pendula linked by a frictional clutch. This model has also a circuit analog; a resistively coupled JJ circuit. The equilibria of the system are few than the foregoing model, but the solution can behaves in $S^1 \times \boldsymbol{R}^3$ or $T^2 \times \boldsymbol{R}^2$. We found the chaotic oscillation when the pendula are not perfectly in the clutch. We clarify the bifurcation structure of the $S^1 \times \boldsymbol{R}^2$ solutions.

In Chapter 3, a stabilization method for an unstable periodic orbits embedded in a chaotic attractor of continuous time system has been proposed. The control technique is based on the pole assignment of the modern control theory. It has been also suggested that the stability of a specific orbit is completely determined by the design of controller. Although the OGY method cannot control the target which does not have any stable manifold, this method does not depend on the stability of the target. The availability of the method to destabilize a stable periodic orbit has been confirmed. The destabilization method would be effectively applied to escape from a local minimum in various optimization problems. As an example of the stabilization and destabilization, some numerical results of Duffing's equation have been illustrated.

Finally, the pendulum equation with a periodic impulsive force, which is equivalent to the model derived from dynamics of the stepping motor has been investigated. Bifurcation phenomena of periodic solutions observed in a generalized pendulum equation with a periodic impulsive force and their topologically classifications have been investigated. As an example of control for a physical system, the intermittent drive characteristics of two-phase hybrid stepping motor has been controlled. A novel control method to avoid the pull-out phenomena by changing the repetitive frequency and stepping rate has been proposed and confirmed its performances.

Bibliography

[1] T. Kohda and K. Aihara. "Chaos in Discrete Systems and Diagnosis of Experimental Chaos". *Trans. IEICE*, Vol. E73, No. 6, pp. 772–783, 1990.

[2] T. Endo and T. Saito. "Chaos in Electrical and Electronic Circuits and Systems". *Trans. IEICE*, Vol. E73, No. 6, pp. 763–771, 1990.

[3] R. J. Field and M. Burger. *Oscillations and Traveling Waves in Chemical Systems.* John Wiley & Sons, 1985.

[4] T. Nagashima, J. Kawashima, and Y. Takahashi. *Towards the Harnessing of Chaos.* Elsevier, 1994.

[5] S. Oishi and T. Koga. "Chaos as Challenging Area in Engineering Science — A Brief Introduction to Engineering Chaos —". *Trans. IEICE*, Vol. E73, No. 6, pp. 759–762, 1990.

[6] A. A. Abidi and L. O. Chua. "On the Dynamics of Josephson-Junction Circuits". *Elect. Circuits and Systs.*, Vol. 3, No. 7, 1979.

[7] M. Odyniec and L. O. Chua. "Josephson-Junction Circuit Analysis Via Integral Manifolds". *IEEE Trans.*, Vol. CAS-30, No. 1, pp. 34–45, 1983.

[8] M. Odyniec and L. O. Chua. "Josephson-Junction Circuit Analysis Via Integral Manifolds: Part II". *IEEE Trans.*, Vol. CAS-32, No. 1, pp. 784–796, 1985.

[9] M. Levi. "Beating Modes in the Josephson Junction". In *Chaos in Nonlinear Dynamical Systems*, pp. 56–73. US Army Research Office, SIAM, 1984.

[10] E. J. Doedel, D. G. Aronson, and H. G. Othmer. "The Dynamics of Coupled Current-Baiased Josephson Junctions: Part I". *IEEE Trans.*, Vol. CAS-35, No. 7, pp. 810–817, 1988.

[11] E. Ott, C. Grebogi, and J. Yorke. "Controlling Chaos". *Phys. Rev. Lett.*, Vol. 64, No. 11, pp. 1196–1199, 1990.

[12] K. Pyragas. "Continuous Control of Chaos by Self-Controlling Feedback". *Phys. Lett.*, Vol. A, No. 170, pp. 421–428, 1992.

[13] R. Roy, T. W. Murphy, T. D. Maier, Z. Gills, and E. R. Hunt. "Dynamical control of chaotic laser: Experimental stabilization of a globally coupled system". *Phys. Rev. Lett.*, Vol. 65, No. 26, pp. 3215–3218, 1990.

[14] W. L. Ditto, S. N. Rauseo, and M. L. Spanoa. "Experimental Control of Chaos". *Phys. Rev. Lett.*, Vol. 65, No. 26, pp. 3211–3214, 1990.

[15] A. Garfinkel, M. L. Spano, W. L. Ditto, and J. N. Weiss. "Controlling Cardiac Chaos". *Science*, Vol. 257, No. 8, pp. 1230–1235, 1992.

[16] H. Kawakami. "Bifurcation of Periodic Responses in Forced Dynamic Nonlinear Circuits: Computation of Bifurcation Values of the System Parameters". *IEEE Trans. Circuits & Systs.*, Vol. CAS–31, pp. 248–260, 1984.

[17] T. van Duzer and C. Turner. *Principles of Superconductive Devices and Circuits.* Elsevier North Holland, Inc., 1981.

[18] H. Kawakami and Y. Katsuta. "Computation of Separatrix Loop of a Saddle Point". *Trans. IECE*, Vol. J64-A, No. 10, pp. 860–861, 1981 (in Japanese).

[19] H. Kawakami. "Qualitative Properties of Forced Oscillations on the Cylindrical Phase Surface". *Trans. IECE*, Vol. J64–A, No. 11, pp. 916–923, 1981 (in Japanese).

[20] F. Romeiras, C. Grebogi, E. Ott, and W. Dayawansa. "Controlling Chaotic Dynamical Systems". *Physica*, Vol. D, No. 58, 1992.

[21] M. Ogorzalek. "Taming Chaos: Part II—Control". *IEEE Trans.*, Vol. CAS-40, No. 10, pp. 700–706, 1993.

[22] G. Chen and X. Dong. "On Feedback Control of Chaotic Continuous-Time Systems". *IEEE Trans.*, Vol. CAS-40, No. 9, pp. 591–601, 1993.

[23] H. Kawakami and T. Ueta. "Controlling Theory as Applied to Controlling Chaotic Dynamical Systems". *IEICE Tec. Rep.*, Vol. NLP94-63, pp. 175–182, 1994.

[24] K. Ogata. *Modern Control Engineering.* Prentice-Hall International, 2nd edition, 1990.

[25] T. Yoshinaga and H. Kawakami. "A Circuit Metaphor for Nonlinear Oscillation in a Chemical System at a Water-Oil Interface". *IEICE Trans.*, Vol. J71-A, No. 10, pp. 1843–1851, 1988.

[26] O. Morimoto and H. Kawakami. "Bifurcation Diagram of a BVP Equation with Impulsive External Force". In *Proc. 1994 Symposium on Nonlinear Theory and its Applications NOLTA '94*, pp. 205–208, 1994.

[27] I. Morita and T. Hojo. "Intermittent Drive Characteristics of Hybrid Stepping Motor ". In *Proc. Small Motor International Conference (SMIC '93)*, pp. 113–118, 1993.

[28] S. Doi and S. Sato. "The Global Bifurcation Structure of BVP Neural Model Driven by Periodic Pulse Trains". *IEICE Tec. Rep.*, Vol. CAS92-91, pp. 107–114, 1993.

[29] C. Taft and R. Guthier. "Stepping Motor Failure Model". *IEEE Trans. Ind. Electron. Contr. Instrum*, Vol. AC-13, No. 3, pp. 464–474, 1969.

Appendix A

A List of the Related Papers by the Author

Main Papers

1. T. Ueta and H. Kawakami, "Heteroclinic Orbits in a Circuit containing a Josephson Junction Element". *Transactions of IEICE*, **J76-A**, No. 10, pp. 1450–1456, 1993 (in Japanese).

2. T. Ueta and H. Kawakami. "Bifurcation of an Inductively Coupled Josephson Junction Circuit". *IEICE Transactions on Fundamentals*, **E77-A**, No. 11, pp. 1758–1763, 1994.

3. T. Ueta and H. Kawakami. "Composite Dynamical System for Controlling Chaos". *IEICE Transactions on Fundamentals*, **E78-A**, No. 6, pp. 708–714, 1995.

4. T. Ueta, H. Kawakami, and I. Morita. "A Study of the Pendulum Equation with a Periodic Impulsive Force — Bifurcation and Control —". *IEICE Transactions on Fundamentals*, **E78-A**, No. 10, pp. 1269–1275, 1995.

International Conferences

1. T. Ueta and H. Kawakami. "Bifurcation of an Inductively Coupled Josephson Junction Circuit". In *Proc. of International Symposium on Nonlinear Theory and its Applications NOLTA '93*, Vol. 3, pp. 1019–1022, Hawaii, USA, 1993.

2. T. Ueta, H. Kawakami, and Ikuro Morita. "Bifurcation of the Pendulum Equation with a Periodic Implusive Force". In *Proc. of Symposium on Nonlinear Theory and its Applications NOLTA '94*, pp. 201–204, Ibusuki, Kagoshima, Japan, 1994.

3. H. Kawakami and T. Ueta. "Stabilization and Destabilization of Chaotic Systems". In *Proc. of International Congress on Industrial and Applied Mathematics ICIAM '95*, Hamburg, Germany, 1995.

4. T. Ueta and H. Kawakami. "Bifurcation Phenomena in the Josephson Junction Circuit Coupled by a Resistor". In *Proc. of International Symposium on Nonlinear Theory and its Applications NOLTA '95*, Vol. 1, pp. 343–346, Las Vegas, Nevada, USA, 1995.

5. M. Tsueike, T. Ueta, and H. Kawakami. "Basin of Attractions in Controlled Chaotic System". In *Proc. of International Symposium on Nonlinear Theory and its Applications NOLTA '95*, Vol. 2, pp. 985–988, Las Vegas, Nevada, USA, 1995.

6. T. Kousaka, T. Ueta, and H. Kawakami. "Destabilizing Control of Stable Orbits". In *Proc. of International Symposium on Nonlinear Theory and its Applications NOLTA '95*, Vol. 2, pp. 997–1000, Las Vegas, USA, Nevada, 1995.

7. T. Ueta and H. Kawakami. "Unstable Saddle-Node Connecting Orbits in the Averaged Duffing-Rayleigh Equation". *IEEE International Symposium on Circuits and Systems ISCAS '96*, Atlanta, Georgia, USA, 1996 (to appear).

National Conferences

1. T. Ueta and H. Kawakami, "Heteroclinic Orbits in Quasi-Rotative System". *1993 Spring National Convention Records of IEICE*, p. A-85, 1993 (in Japanese).

2. T. Ueta and H. Kawakami. "Heteroclinic Orbits in a Circuit containing a Josephson Junction Element". *Technical Report of IEICE*, **NLP92-105**, pp. 43–48, 1993 (in Japanese).

3. T. Ueta and H. Kawakami. "Bifurcation Phenomena in a Josephson Junction Circuit Coupled by a Resistor". *1994 Spring National Convention Records of IEICE*, p. A-75, 1994.

4. T. Ueta and H. Kawakami. "Bifurcation Phenomena in a Josephson Junction Circuit Coupled by a Resistor". *Technical Report of IEICE*, **NLP93-91**, pp. 47–54, 1994.

5. T. Ueta and H. Kawakami. "Stabilization Method of Controlling Chaotic Systems". *Technical Report of IEICE*, **NLP94-62**, pp. 167–174, 1994.

6. O. Morimoto, T. Ueta and H. Kawakami. "Computation of Bifurcation Sets for Nonlinear Differential Equation with a Discontinuous External Force and its Application to BVP Equation" *Technical Report of IEICE*, **NLP94-2**, pp. 9–14, 1994 (in Japanese).

7. H. Kawakami and T. Ueta. "Control Theory as Applied to Controlling Discrete Chaotic Dynamical Systems". *Technical Report of IEICE*, **NLP94-63**, pp. 175–182, 1994.

8. T. Ueta and H. Kawakami. "Controlling Chaos of High Order Autonomous Systems ". *Technical Report of IEICE*, **NLP94-79**, pp. 71–78, 1994 (in Japanese).

9. T. Kousaka, T. Ueta and H. Kawakami. "Destabilization of Stable Orbits by Controlling Chaos". *Technical Report of IEICE*, **NLP94-102**, pp. 51–58, 1995 (in Japanese).

10. T. Ueta and H. Kawakami. "Controlling Chaos of an Inverted Pendulum Driven by a Periodic Force". *Proc. of 1995 General Conference of IEICE*, p. 72, 1995 (in Japanese).

11. M. Tsueike, T. Kousaka, N. Sone, T. Ueta, Y. Nishio and M. Morii. "An Implementation of a Chaotic Cryptsystem for MIME". *Technical Report of IEICE*, **OSF95-10**, pp. 11–16, 1995 (in Japanese).

12. T. Ueta and H. Kawakami. "A Computational Method to Obtain Bifurcation Parameters of Limit Cycles". *Technical Report of IEICE*, **NLP95-43**, pp. 47–52, 1995 (in Japanese).

13. T. Ueta and H. Kawakami. "Controlling Chaos of Coupled Systems". *Technical Report of IEICE*, **NLP95-81**, pp. 133–139, 1995 (in Japanese).

14. T. Ueta and H. Kawakami. "On Saddle-Node Connecting Orbits in Nonlinear Dynamical Systems", *Proc. of 1996 General Conference of IEICE*, pp. 435–436, 1996.

Other Works

1. Y. Tanaka, T. Ueta, H. Kawakami. "Efficient Dynamic Simulation Method of Cranes with a Spherical Pendulum". *Trans. of Japan Society of Mechanical Engineers*, Vol. 59, **559-C**, pp. 186–190, 1993 (in Japanese).

2. Y. Tanaka, Y. Yoshida, T. Ueta, and H. Kawakami. "Vibration Suppressing Control of Flexible Rotary Crane Using Tip Position Sensor". *Journal of Robotics and Mechatronics*, 4, No. **6**, pp. 520–525, 1993.

3. H. Kawakami and T. Ueta. Chaos CG by Language C. Science-sha, 1994.

4. Y. Tanaka, T. Ueta, and H. Kawakami. "A Robotic Truck Crane with Vibration Sensors". In *Proc. of Japan-France Congress on Mechatronics JFCM*, pp. 731–734, Takamatsu, Kagawa, 1994.

5. Y. Tanaka, T. Ueta, H. Kawakami, and T. Sumitomo. "A Robotic Truck Crane with Vibration Sensors". *Journal of Robotics and Mechatronics*, 7, No. **3**, pp. 213–217, 1995.

6. T. Kousaka, T. Ueta, H. Kawakami. "A Method to Generate a Chaotic Attractor by Destabilization", *IEICE Trans.*, **J79-A**, 1996(in press).

様式9

論文審査の結果の要旨

報告番号	甲　工 乙　工　第 22 号 工　修	氏　名	上　田　　哲　史
審査委員	主　査　　川　上　　博 副　査　　高　橋　義　造 副　査　　大　恵　俊一郎		

学位論文題目

Bifurcation and Controlling Chaos in Nonlinear Dynamical Systems

審査結果の要旨

本論文は非線形力学系における分岐現象の解析と系に生じるカオス現象を制御し安定な周期状態を実現する一般的手法について研究したものである．主な内容は次のとおりである：強制外力を加えた振り子結合系，ジョセフソン接合素子の結合系（超電導量子干渉計）などの力学系は，常微分方程式に三角関数を含んでいる．そのため，状態空間とパラメータ空間との積空間において周期性を有し，観測される現象もその周期性を反映して複雑になっている．これら力学系にみられる平衡点，周期解の分岐現象を解析し，解の振舞いの定性的性質を検討した．

第2章では，回転方向に弾性復元力をもつ振り子を取り上げ，パラメータの変化に伴い発生するヘテロクリニック軌道の分岐構造を解明した．また，2個の振り子を，弾性復元力のある梁で接続した場合と，クラッチを有する剛体で接続した場合について，定トルクを加えたとき発生する平衡点，周期解の分岐の詳細を検討した．これらの解析により，従来知られていなかった，高次元回転系の大域的な解の振舞いを定性的に説明することができた．

連続時間系においてカオス応答がみられるとき，そのカオスアトラクタ中に埋め込まれている不安定な周期軌道を安定化する問題をカオス制御という．第3章では，カオス制御理論についての新手法，およびその応用を述べた．従来のカオス制御系の手法の多くは，離散系に対してのみ制御器を構成していたが，本手法では，ポアンカレ写像から導かれる離散系の周期点を安定化する制御器を設計し，状態フィードバックを極配置法で構成する．その制御入力を元の微分方程式系のパラメータへ摂動として加える．すなわち，差分方程式系と微分方程式との組合せによる合成力学系での制御系設計を新しく提案した．

応用例としてステッピングモータにみられる脱調現象の制御問題を取り上げた．この脱調現象は周期倍分岐連鎖によって引き起こされるカオスであり，実用上望ましくない運転状態である．まずステッピングモータが周期インパルス列で駆動される振り子と等価であることを導出し，第2章の結果を踏まえ，ポアンカレ写像の構成と分岐の解析を行なった．また，分岐を抑制する制御器の設計とその制御系の数値シミュレーションを行ない，提案した制御方法の有用性を示した．

以上本研究は，非線形力学の分岐解析とカオス制御に関する一般的手法を示すものであり，本論文は博士（工学）の学位授与に値するものと判定する．